TE WHARE WĀNANGA O TE ŪPOKO O TE IKA A MĀUI
VICTORIA
UNIVERSITY OF WELLINGTON

Impact of large volcanic events on the marine environment recorded in marine cores

Sophie Ellen Wilkinson

A thesis submitted to
Victoria University of Wellington
in partial fulfilment of the requirements for the degree of

Master of Science
in Geology

School of Geography, Environment and Earth Sciences
Victoria University of Wellington
2016

Contents

List of Figures

List of Tables

Acknowledgements

A huge thank you must first go to my supervisors Monica Handler and Helen Neil. Monica, your complete willingness to help whenever I needed it has been so appreciated. From talking over ideas, to helping me in the lab, sorting out the various admin tasks, your detailed and valuable feedback and not to mention your constantly immediate replies to any questions I had really helped me throughout the year. Helen, thank you for giving me the opportunity to study at NIWA for most of the year. It has allowed me to have some great experiences and meet a lot of new people. Also, thank you for your feedback, help with lab work and getting me to think outside the square, I think it has greatly improved my understanding of various aspects of my research.

Many people have contributed their time, knowledge and amazing kindness that have all helped the completion of this thesis. In no particular order, thank you to Lisa Northcote for all your help in the lab and teaching me about foraminifera. To Alan Orpin for teaching me to use the x-ray machine and for all the chats in the tea room. Richard Wysoczanski for giving me the amazing opportunity to experience life onboard the Tangaroa and learn so much in the process. To Helen Bostock, thank you for always being so helpful and kind, whether it was suggesting papers to read or generally taking the time to discuss and help with so many aspects of my research, especially all your feedback at the end, I really appreciate it.

At VUW, thank you to David Flynn for all your assistance with and knowledge about the SEM, I thoroughly enjoyed learning everything. To Gavin Dunbar for giving up your time to help me with my foraminiferal analyses and passing on your knowledge despite the amount of time you have invested in working out the most effective methods. To Dan Sinclair, the amount of time you spent helping with the LA-ICP-MS, and setting up the software to process the data, was amazing, thank you so much.

To the great people I got to spend most morning teas and lunchtimes with, and the occasional afternoon tea, it was a blast. Bryn, Ben, Rebecca and Zoe, you have

been there for most of my time at NIWA and made 10:30am the best time of day. Your constant support and conversation has made the past year so much more enjoyable. To all those that I met along the way, at football, touch or frisbee, it was a pleasure. To Martin and Penny, thank you for your advice.

Finally, to those that have always been there for me, thank you to my family. To mum for all your continual support and always listening to me when I needed to clarify things in my own head as well as reading through my thesis for me at the last minute. To dad and Timon for always being there and trying to help whenever you could. To my sister Genna, your amazing enthusiasm to read my entire thesis and correct the grammar was awesome. To my brother Reilly, for sharing my interest in science and actually being enthused when I talk about it. Most of all a huge thank you to Jo. You've supported me right from the start and have always been there with anything I needed, I can't thank you enough.

Abstract

Explosive silicic volcanic eruptions blanket widespread terrestrial and marine areas in ash, and have a profound effect on climate and local ecosystems. Short-term climate effects are caused by the dispersal of ash, but the injection of gas into the stratosphere, with sulphur being particularly important, drives a cooling of the climate that can last several years. These prolonged perturbations have been observed and recorded in recent decades, but despite the importance of the ocean in regulating global atmospheric climate, little is known about how and to what extent the climate signal produced by volcanic eruptions alters the oceanic environment. As the composition of foraminifera tests is highly sensitive to changes in the surrounding environment, a significant sea surface temperature decrease following a large silicic volcanic eruption may be recorded in the tests of live planktic foraminifera, now preserved in marine sediments. This study examines marine cores (and foraminifera within) that contain tephra units from three major volcanic events to determine if changes can be resolved in ocean temperature and/or foraminifera test morphology following large silicic eruptions.

The Holocene Taupo, Waimihia and Mamaku tephra units have been identified in a series of marine sediment cores collected from areas with high sedimentation rates off the east coast of North Island, New Zealand. The sources of these eruptions were from two calderas within the Taupo Volcanic Zone, one of the most active and important rhyolitic regions in the world. Sampling of sediment and foraminifera from these cores has been undertaken at 0.5 cm intervals above and below each tephra. This equates to varying sampling resolutions between cores of 5-30 years, with sufficient sampling taken to establish a stratigraphic record of >100 years either side of each tephra unit. A detailed stratigraphy was undertaken on the sediment surrounding all tephra units, including grain size and $CaCO_3$ analyses, to identify primary and secondary tephra deposits. One core, Tan0810-12 that contained solely Taupo tephra, was selected for foraminiferal analyses to determine changes in ocean temperature and foraminifera test morphology following this eruption. This core was selected based on the results of the stratigraphic analyses that identified the tephra as a primary deposit with minimal bioturbation above the ash layer and a

very high sedimentation rate that enabled sub-decadal scale sampling.

Scanning electron microscope imaging was employed to identify the presence of surface contaminants on and within the foraminifera tests and allowed observations of test morphology and size. The morphologies of planktic foraminifera species *Globigerinoides ruber* and *Globigerina bulloides* showed no obvious change following the Taupo eruption. The *Globigerinoides ruber* test sizes distinctly decreased for a period after the eruption, while *Globigerina bulloides* tests slightly increased in size, correlating well with a decrease in sea surface temperature after the eruption as these species prefer warmer and colder temperatures, respectively. This suggests there is potential for test size to be employed as a proxy for temperature change in conjunction with geochemical analyses. Mg/Ca temperature analyses were conducted in situ using laser ablation inductively coupled plasma mass spectrometry. Both species indicated a decrease in sea surface temperatures when comparing results from tests collected below the tephra deposit to those above. Further results indicate ocean temperature may not have recovered for more than 65 years after the eruption. Such a rapid change in the oceanic environment not only has drastic implications for marine ecosystems but also atmospheric climate, and therefore, terrestrial ecosystems. To reduce the margin of error and determine a more exact value of temperature change following the eruption a greater population of foraminifera is needed. Nonetheless, this study highlights the potential of this method in determining how the oceans are impacted by volcanism and how further research is needed to determine the effects of volcanic eruptions on past and future climate.

1 Introduction

Volcanic eruptions rapidly alter Earth's terrestrial climate (Robock, 2000), but our limited knowledge of how large volcanic eruptions influence the world's oceans places limitations on our understanding of the long-term role volcanism has played on the global climate system in the past. Climate change studies suggest the current global warming trend has been negatively offset by sulphate aerosols produced during volcanic eruptions and without these occurrences Earth's atmosphere would be even warmer than current observations (Solomon et al., 2011, Neely et al., 2013). However, most studies that incorporate volcanic eruptions into climate models, both future projections and those that estimate Earth's climate in the past, typically solely incorporate the effects of volcanism on the atmospheric climate. The oceans make up ∼71% of the Earth's surface (Costanza, 1999) and absorb 1,000 times more heat than the global atmosphere due to the high heat capacity of water (Levitus et al., 2005). The expected rise in atmospheric temperatures from increasing greenhouse gas concentrations predicted by climate models does not correlate with current atmospheric temperature readings. Atmospheric temperatures have not risen as expected from climate models because observations show the ocean has absorbed more than 90% of the heat caused by anthropogenic global warming (Levitus et al., 2005, Gleckler et al., 2016). These findings show the importance of the oceans in balancing the global climate system.

Volcanism has played an important role in reducing global warming from anthropogenic climate change over the past 30 years. Since 1980 two eruptions were large enough to noticeably impact Earth's climate. The 1982 El Chichón and 1991 Mt Pinatubo eruptions produced plinian columns that reached the stratosphere and contained sufficient sulphur gases to decrease the average temperature of the Northern Hemisphere by up to 0.6 and 1°C, repectively (Rampino and Self, 1984, Robock, 1984, 2000). These were relatively small eruptions when compared to the size of volcanic events that have occurred throughout Earth's history. Nonetheless, the sulphate aerosols formed from these eruptions, and smaller events prior, are enough to perturb the temperature of the atmosphere by up to 0.2°C when compared to the same atmosphere with the contribution of volcanic sulphate aerosols removed (Fig.

1; Solomon et al. (2011)).

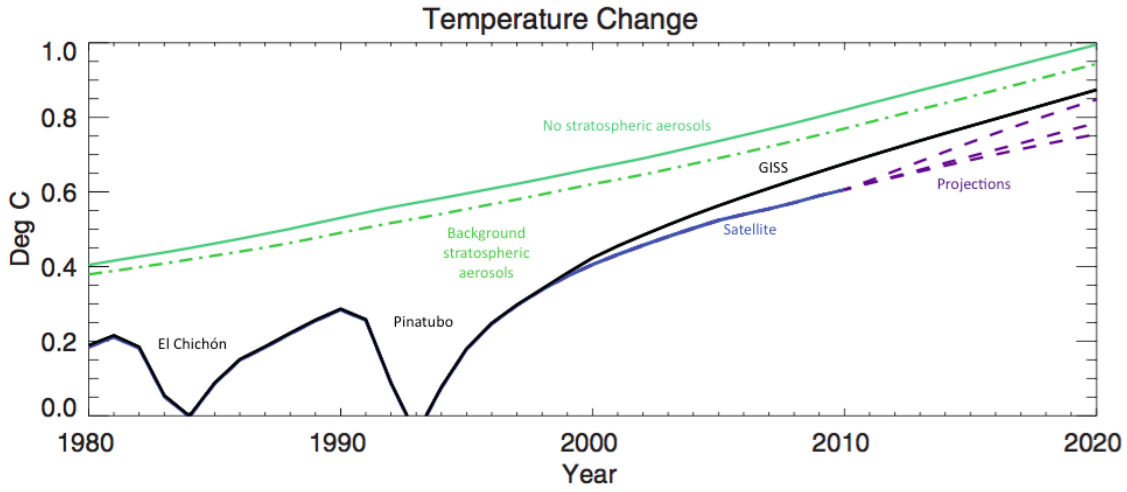

Figure 1: Change in atmospheric temperature (°C) since 1980. The green solid line represents an atmosphere without stratospheric aerosols, the green dashed line is what the temperature change in the atmosphere would be if only background stratospheric aerosols were present without aerosols from any volcanic activity. The black line is a climate model from the NASA Goddard Institute for Space Studies (GISS) that shows the natural atmosphere with all stratospheric aerosols included until 2000. Following this the GISS line models an atmosphere with no futher volcanic activity while the blue line shows the satellite observations of the atmosphere from 2000 with possible outcomes up to 2020 in purple. The top scenario is the outcome with a 5%/yr increase in aerosol forcing, the middle is an extension of the current trend and the bottom is if the aerosol forcing returned to levels prior to these two eruptions. Modified from Solomon et al. (2011).

While the importance of volcanic eruptions on the global climate system is well recognised, few studies have been conducted on the impacts of significantly large eruptions on the world's oceans. This is largely because the biggest eruption to occur since satellite observations began was the Mt Pinatubo eruption, and satellite data has been proven to be biased towards colder temperatures through contamination of the stratospheric aerosols (Reynolds, 1993). Several studies have shown the strong link between volcanic eruptions and rapid global cooling events (Huang et al., 2001, Rampino et al., 1979, Rampino and Self, 1992). While it is likely there is a link between the two, the difficulty in determining which is the cause and which is the effect lies largely in the uncertainty associated with age models. In many cases it appears the climate began shifting prior to the volcanic eruption, but whether the eruption intensified and prolonged the climate event by penetrating into the deep ocean layers is difficult to understand based on the limited knowledge of how long

the atmospheric climate is perturbed and whether it remains perturbed long enough to have a significant impact on the ocean.

Direct reconstructions of the impact of volcanic eruptions on the Earth's climate are essential in order to predict not only how volcanic eruptions will impact the Earth in the future but also to factor into climate models how eruptions have shaped the course of Earth's climate in the past. Climate models so far have not accurately estimated the change in climate following volcanic eruptions. Church et al. (2005) compared climate model predictions and observational data for the world's oceans, computed by Levitus et al. (2005), to determine how global ocean heat content and global mean sea level estimates compared to the global observation data during the period of the Agung, El Chichon and Mt. Pinatubo eruptions between 1960 and 2000. The climate model data often overestimated or underestimated the impacts of the eruptions and the length of time it took for the Earth's climate system to recover. The difficulty with climate model predictions is the lack of direct reconstructions of changes to the global climate following large volcanic events in the past.

Global anthropogenic climate change rapidly increased over the 20^{th} century, making short-term climate perturbations with periodicities on the scale of hundreds to thousands of years relevant and necessary to understand for the immediate future. Explosive silicic eruptions provide an opportunity to study short-term climate perturbations and observe how the oceans respond and are affected by rapid changes to the atmosphere.

This study aims to evaluate if foraminifera can be used to reconstruct a high-resolution sea surface temperature (SST) profile east of North Island, New Zealand before and after a major silicic eruption. The east coast of North Island, New Zealand provides a unique opportunity to observe marine sediment cores with very high sedimentation rates that allow for sub-decadal scale sampling. A detailed stratigraphy of these sediment cores allows us to determine how the temperature of the ocean responded to the eruption through time, on a sub-decadal scale. Past SSTs can be determined by analysing the Mg/Ca values of planktic foraminifera,

preserved in marine sediments and obtained by collecting marine sediment cores. Foraminifera are single-celled organisms that construct calcite shells (tests) incrementally during their life span. Planktic foraminifera species inhabit the upper layers of the ocean and incorporate the chemistry of the ocean into their tests during construction. After death, the tests sink to the bottom of the ocean where, if conditions are favourable, are preserved and buried in marine sediments. Analysing the chemical make-up of these tests provides information on the sea surface environment during the life span of the individual foraminifera. The abundance of foraminifera species across every region of the world's oceans (Fig. 2) make them particularly important in the marine food chain, but also as one of the most used sources of paleoceanography proxies (Kucera, 2007). Here we aim to use the Mg/Ca concentrations of planktic foraminifera to evaluate if they can be used to determine how SSTs changed after a large silicic eruption. If a change in ocean conditions occurred after the eruption, the extreme sensitivity of foraminifera to their surrounding environment would likely cause a change to the way they build their tests. In addition, comparing the size and morphology of foraminifera tests, and therefore any changes, before and after the eruption can also indicate changing ocean conditions and how an important part of the marine food web adapts to a rapidly changing environment.

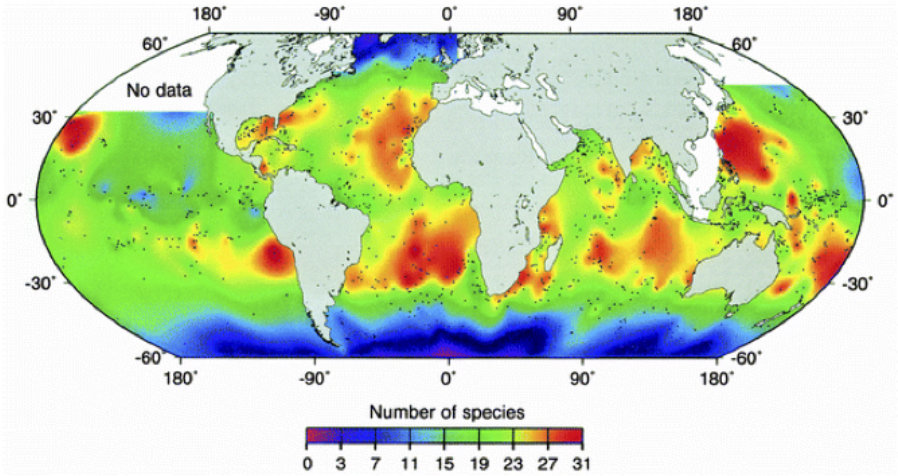

Figure 2: The global diversity of planktic foraminifera, determined from core-top samples by (Rutherford et al., 1999).

1.1 Thesis aims and format

The primary aims of this thesis are:

- To determine if a change in ocean SST following a large silicic volcanic eruption can be resolved by using geochemical analyses of foraminifera tests.
  - If a change in ocean temperature is present I also aim to determine how long this perturbation extends before temperatures return to background levels.
- To observe the morphology and size of foraminifera tests and determine if the volcanic eruption impacts either of these features. If the morphology or size of the tests are different following the eruption, can this be used alongside temperature measurements as a potential proxy for rapid ocean change?

These aims will be investigated via:

- Core stratigraphy
  - Characterisation of tephras and surrounding sediment
  - Age models and sedimentation rates
  - Grain size and $CaCO_3$ analyses
- High-resolution imaging of foraminifera tests
- Geochemical analyses of foraminifera tests

1.2 Volcanism and climate

Explosive silicic volcanic eruptions have the ability to alter Earth's climate through the injection of tephra and gas into the atmosphere. Tephra can temporarily block out sunlight but the density of ash results in most of it settling to the ground in a few days (Cole-Dai, 2010). Volcanic gases released during eruptions can impact the global climate if the eruption column is large enough for the gases to reach the stratosphere. In the troposphere, gas can be removed via wet or dry deposition (Langmann, 2013), but if it reaches the stratosphere advection transports it around

the Earth in 2-3 weeks. The volcanic gases released during eruptions are, in order of abundance, CO_2, H_2O and S, the latter present mostly as SO_2 but also as H_2S. The volumes of CO_2 and H_2O released are negligible compared to the amounts already present in the atmosphere (von Glasow et al., 2009). In comparison, S is considerably more damaging. Volcanic eruptions can produce several thousand times the normal background level of SO_2 in one explosive event (Oppenheimer et al., 1998). S released into the troposphere is usually insignificant, removed in a matter of days before it has time to oxidise. Tephra and gas that make it into the stratosphere, more than 20km high, cause the biggest impact on the Earth's climate.

Large flood basalts have occurred periodically throughout Earth's history. Studies have proposed the timing of these volcanic events correlate with global mass extinction episodes, most likely caused by periods of significant global climate change thought to occur from the large volumes of gas extruded during the series of eruptions (Rampino and Stothers, 1988, Hofmann et al., 1997, Courtillot and Renne, 2003). Flood basalts are incredibly important in Earth's geological history and highlight the potential of volcanism to severely alter the climate system. However, this study focuses on observing the impacts of large rhyolitic eruptions because of their presence in offshore marine cores and the very long periodicity of flood basalt events, estimated to be every $\sim$32 million years, with the most recent event occurring $\sim$17 million years ago (Rampino and Stothers, 1988).

The atmosphere, as opposed to volcanic gases, has a very high concentration of oxygen. Therefore, nearly all the SO_2 from eruptions that reach the stratosphere will react with OH and H_2O to form H_2SO_4 (Robock, 2000, Frölicher et al., 2011, Stenchikov et al., 2009). In approximately 2-3 weeks the sulphate aerosols are advected around the Earth, remaining in the stratosphere for 2 to 3 years (Fig. 3). Gradually the aerosols are removed by gravitational sedimentation and episodic transportations of stratospheric air into the troposphere (Frölicher et al., 2011). Aerosols scatter the incoming shortwave radiation from the sun, increasing the planetary albedo and causing a reduction of the Earth's surface temperature. To a lesser extent, the aerosols also absorb the outgoing longwave radiation from the Earth

causing a warming of the stratosphere (Cole-Dai, 2010, Robock, 2000). While these direct effects on the climate are well understood there are many potential effects that are in need of further research and many more that remain unknown.

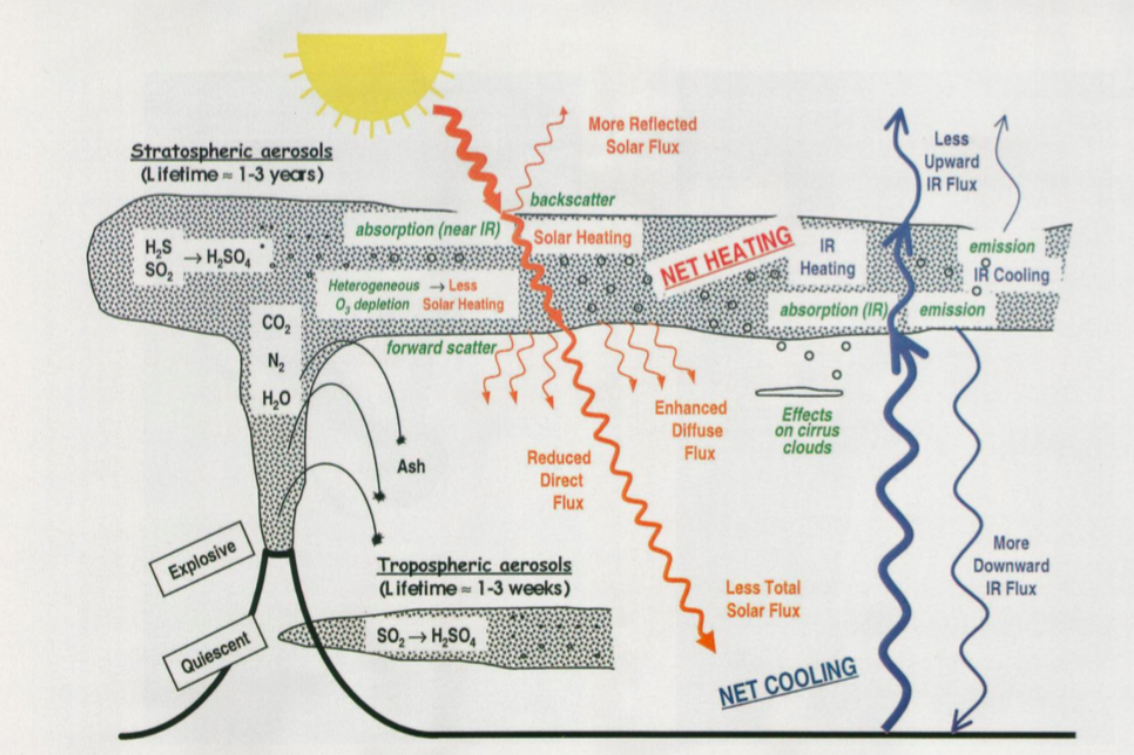

Figure 3: Schematic diagram of the effects of volcanic aerosols in the atmosphere from Robock (2000).

Trenberth and Dai (2007) studied the monsoon systems and the global hydrological cycle in the years following the 1991 Mt. Pinatubo eruption. They found the Asian and African monsoons and the global hydrological cycle were weaker the year immediately after the eruption. While patterns like this can be observed after the volcanic event they are difficult to predict based on the amount of variables involved in the eruption process. Variables such as the climate conditions prior to an eruption along with the location of the volcano can also impact how the climate will be affected following an eruption. Fischer et al. (2007) analysed previously collected multi-proxy reconstructions for Europe from 15 tropical volcanic eruptions over the past 500 years. In every case except one Europe experienced a cooler summer but a warmer, wetter winter in the 2 years following a major explosive eruption. The results from Fischer et al. (2007) strongly agree with previous studies (Robock and Mao, 1992,

Kelly et al., 1996) and suggest the warming is produced by a positive phase of the North Atlantic Oscillation (NAO). This in turn is caused by an enhanced stratospheric equator-to-pole temperature gradient from the warming of the stratosphere in the tropics. The tropics receive more direct sunlight so the radiative balance is perturbed more than at higher latitudes, resulting in a warmer stratosphere and an enhanced temperature gradient. Later climate models even suggest the NAO circulation could be offset up to a decade after a large eruption (Zanchettin et al., 2011)

Direct reconstructions of the impacts of volcanic eruptions on SSTs have been relatively inconclusive. Research conducted by Huang et al. (2001) on a marine core identified an SST cooling of $\sim$1°C in the South China Sea during the time of the Toba eruption, estimated to have occurred between $\sim$70 and 75 ka, however they could not attribute this cooling to the eruption with certainty and suggested further research was needed. Sutton and Chiswell (1996) used satellite data from the time of the Mt. Pinatubo eruption and found an SST cooling of $\sim$1°C around New Zealand. Sutton and Chiswell (1996) also could not discern whether this was a result of the Mt. Pinatubo eruption or a result of the Cerro Hudson eruption in Chile in 1991.

Climate model predictions have consistently shown that large volcanic eruptions should have perturbed the ocean temperature for decades after the event by penetrating deeper into the ocean's thermal structure. Rampino and Self (1992) hypothesise that the Toba eruption could have greatly accelerated the Earth's shift into glacial conditions, suggesting there could be an important feedback between climate change and volcanic eruptions. Gleckler et al. (2006) used 12 climate models to show that the 1883 Krakatoa eruption significantly reduced the warming of the deep ocean caused by anthropogenic sources over the past 120 years. Climate models reveal what could have happened during time periods where real-time monitoring instruments and observations were unavailable. However, while it is likely the impacts from volcanic aerosols extend well beyond the widely accepted short-term, transient climate perturbations, there are no direct measurements as yet to confirm these hypotheses.

1.3 TVZ eruptions

The Taupo Volcanic Zone (TVZ) is one of the most active rhyolitic volcanic regions in the world. This NE-SW trending volcanic arc is formed from the subduction of the Pacific Plate beneath the Australian Plate (Fig. 4a). On land it extends more than 200 km across North Island, New Zealand (Wilson et al., 1995). The southern and northern volcanoes are predominantly andesitic in composition but rhyolitic volcanism dominates the centre and makes up most of the volcanic activity that has occurred from the TVZ since its formation ca. 1.8 million years ago (Wilson et al., 1995, Milner et al., 2003). Many ash deposits from the TVZ are deposited and preserved in marine sediment to the east of North Island. The largest, most well-preserved tephra found in marine sediment cores east of New Zealand that erupted from the TVZ in the last 10,000 years include the Taupo, Waimihia and Mamaku deposits (Lowe et al., 2008).

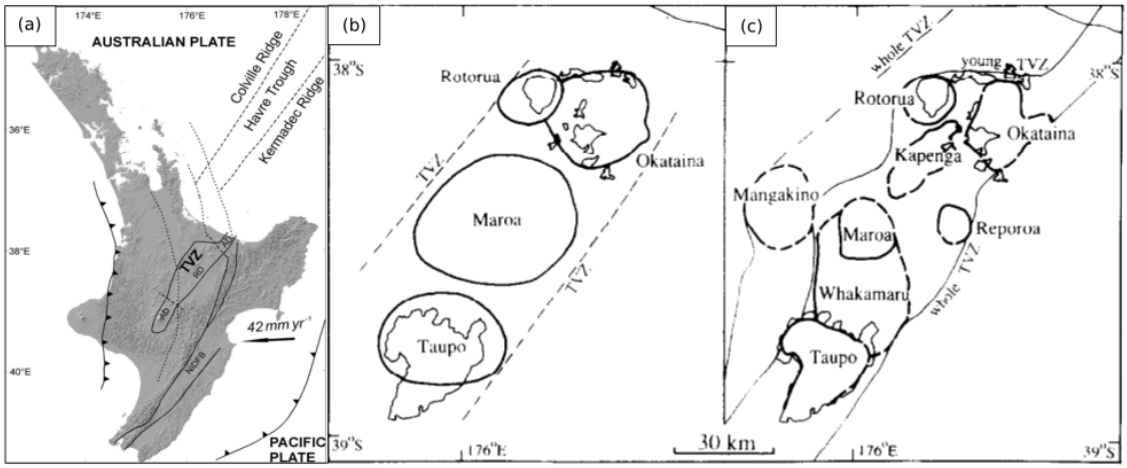

Figure 4: Map of the Taupo Volcanic Zone created by the subduction of the Pacific Plate beneath the Indo-Australian Plate (a) from Cole and Spinks (2009), with volcanism separated into andesite dominant (AD) and rhyolite dominant (RD) zones. Four volcanic centres (b), made up of eight rhyolitic calderas (c), make up the central TVZ. Adapted from Wilson et al. (1995).

1.3.1 Mamaku

The Mamaku eruption event occurred from a series of vents across the Okataina Volcanic Centre (OVC; Fig. 4b), one of four volcanic centres within the TVZ (Nairn, 1981). The Mamaku eruption style was mostly effusive with a lava volume of more than 12 km^3 identified from flow deposits (Smith et al., 2006). However, a minor

explosive episode occurred during the eruption that produced a plinian airfall deposit preserved in land and marine sediments to the east of OVC. The Mamaku event is estimated to have occurred 8005 ± 45 cal. yr BP based on radiocarbon dates collected from the Kaipo peat sequence by Lowe et al. (2008).

1.3.2 Waimihia

The Waimihia tephra deposit was erupted from a vent on the eastern side of Lake Taupo, a caldera located within the TVZ (Fig. 4c). Taupo is the most productive rhyolitic volcano in the world, exhibiting an average eruption rate of 0.2 m^3/s over the past 65 ka (Wilson et al., 1995). Lowe et al. (2008) also used stratigraphic wiggle-matching of ^{14}C dates obtained from the Kaipo bog to estimate an age of $3,410 \pm 40$ cal. yr BP for the Waimihia deposit. The eruption was dominated by a rhyolitic source with more than 92% of the erupted material composed of rhyolite and the remaining minor proportion comprising rhyodacite and andesite (Blake et al., 1992). The isopach map of tephra from the plinian eruption indicates a west to north-west wind direction, spreading the ash across Poverty Bay where it is preserved in marine sediments (Fig. 5). The total volume of the Waimihia plinian fall deposit has a large range of estimates from 5.10 km^3 up to 29 km^3 (Walker, 1981, Blake et al., 1992, Froggatt and Lowe, 1990, Carter et al., 1995, Lowe et al., 2008). While the total volume is still disputed it is nonetheless one of the largest plinian eruptions to occur in New Zealand over the past 10,000 years, closely following the Taupo eruption that occurred less than 2,000 years later.

1.3.3 Taupo

The Taupo eruption is the largest volcanic event on Earth to occur in the past 5,000 years. The eruption was also produced from a vent that is now submerged beneath Lake Taupo (Fig. 4c). The vent is believed to be situated at Horomatangi Reefs (Wilson and Walker, 1985), now nearly the deepest point of Lake Taupo. Several different units make up the eruptive sequence, likely spread out over a period of weeks to months and estimated to have a combined volume of more than 100 km^3, with at least 65 km^3 inferred from known deposits on land. The largest of the sequence was the second plinian eruption, one of the most widely dispersed deposits

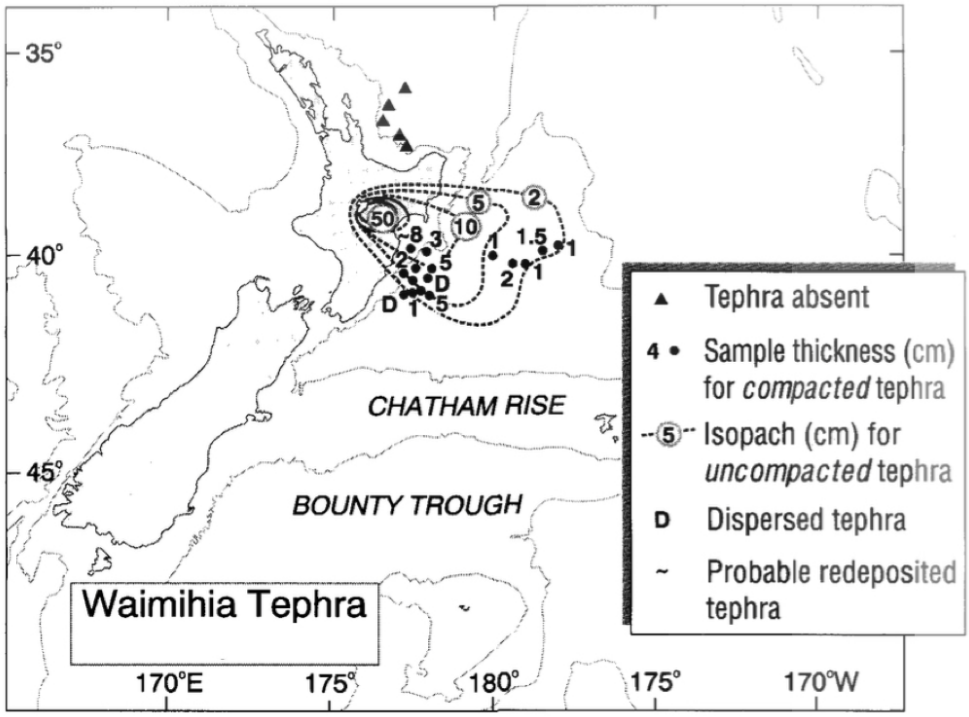

Figure 5: Estimated uncompacted Waimihia tephra isopach, adapted from Carter et al. (1995).

discovered, and is often referred to as ultraplinian, a rare class of eruption style (Walker, 1980).

The total volume of the ultraplinian event is estimated to be 23 km^3 based on the weight of crystals in the deposit. From this volume the eruption column could be expected to have only reached a height of approximately 25 km (Sigurdsson et al., 2015), however, at its maximum thickness the deposit is only 1.8 m with around 80% of the total volume deposited more than 220 km from the vent. Due to the prevailing westerly wind across Taupo the ash was dispersed to the east of North Island (Fig. 6). According to Walker (1980) "fall from a column less than about 50 km high would have required transport by wind with an implausibly high velocity", meaning it is likely the eruption reached as high as the mesosphere. Wilson and Walker (1985) suggested the required exceptional column height cannot be attributed to the power of the eruption alone, but was a combination of the rapid magma eruption rate and the high percentage (>75%) of very fine material, ∼16 μm in size. Small particles release heat rapidly that would have added constant momentum to boost the height of the column. Related to, and synchronous with, the ultraplinian eruption was a

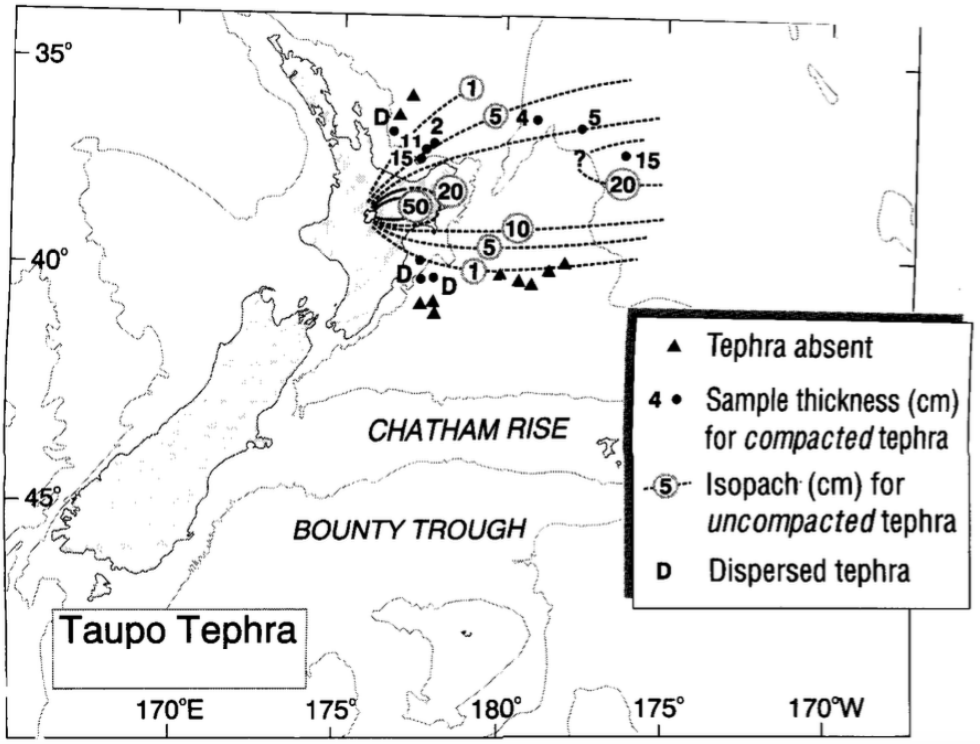

Figure 6: Estimated Taupo eruption isopach map for the dispersal of uncompacted tephra. Adapted from Carter et al. (1995).

smaller volume of ignimbrite activity. The volume and rate of magma release from this activity caused the vent to be unsupported and collapse. A widening of the vent then caused the eruption column to collapse. The combination of the column collapsing and a rapid change in eruption conditions unleashed a drastic change in eruption rate to produce an ignimbrite of >30 km^3 with a radius of 80 $\pm$ 10 km (Wilson and Walker, 1985). It is estimated the ignimbrite was erupted in 400 s at a rate of up to 300 m/s (Wilson and Walker, 1981), a climax that caused a complete collapse of the vent and ceased the last known significant activity from Lake Taupo.

The age of the eruption sequence has been a topic of debate with several different ages proposed. Wilson et al. (1980) proposed a date on, or just prior to, AD 186 based on Chinese and Roman literature. Each piece of literature describes abnormal colours in the sky during sunrise and sunset, similar to those seen after the 1883 Krakatoa eruption when blood red skies occurred in the morning and evening. At 50 km high the ash plume and aerosols would have reached the mesosphere, taking years to fall to lower atmospheric levels (Barry and Chorley, 2009). Wilson et al. (1980) suggested at heights greater than 30 km the fine particles would get caught

in the high level drift, to be easily transported around the globe and explaining the observations in China and Europe. Zielinski et al. (1994) also suggest the aerosols could have reached the Northern Hemisphere by attributing a spike in $SO_4{}^{2-}$ in the Greenland Ice Core GISP2 to the Taupo eruption at AD 181 ± 2. Radiocarbon dating of charcoal, wood, peat, lake sediment and seeds by Froggatt and Lowe (1990) produced multiple ages with a mean age of 1850 ± 10 yrs BP. From this a calendar age was estimated of AD 214 with a 1σ range of AD 138-230. Alternatively, Sparks et al. (1995) and Hogg et al. (2012) used ^{14}C analyses of tree rings from the Pureora forest, near Lake Taupo, which was buried by the eruption. The calendar ages produced by Sparks et al. (1995) and Hogg et al. (2012) were AD 232 ± 15 and AD 232 ± 5 (1718 ± 5 cal. yr BP) respectively. Sparks et al. (2008) later redefined the age of AD 232 ± 15 to AD 233 ± 13 (1717 ± 13 cal. yr BP) using further statistical analyses. This age was backed up by radiocarbon dating of the Kaipo bog sequence by Lowe et al. (2008) and is the age adopted throughout the rest of this study.

1.4 Regional setting

Seven marine sediment cores were used for this study. Four were collected during the 2006 *R.V. Marion Dufresne* voyage MD152 MATACORE, MD06-3003, MD06-3008, MD06-3009 and MD06-3017. The remaining three cores, Tan0810-3, Tan0810-11 and Tan0810-12, were obtained from the *R.V. Tangaroa* voyage TAN0810. All cores are from locations just offshore from East Cape, North Island, New Zealand, spanning from Poverty Bay around to the Bay of Plenty (Fig. 7).

The east coast of North Island is situated downwind of the Taupo Volcanic Zone (TVZ). The prevailing wind at this latitude is a strong westerly. The winds are caused by the temperature gradient from the equator to the poles, and the direction governed by the rotation of Earth. They flow relatively unimpeded due to the lack of landmasses surrounding New Zealand, building strength across the ocean before reaching land. Any volcanic material erupted from within the TVZ is therefore almost always deposited to the east (Carter et al., 1995, 2003).

Tephra is commonly well preserved in the sediments off East Cape due to the gener-

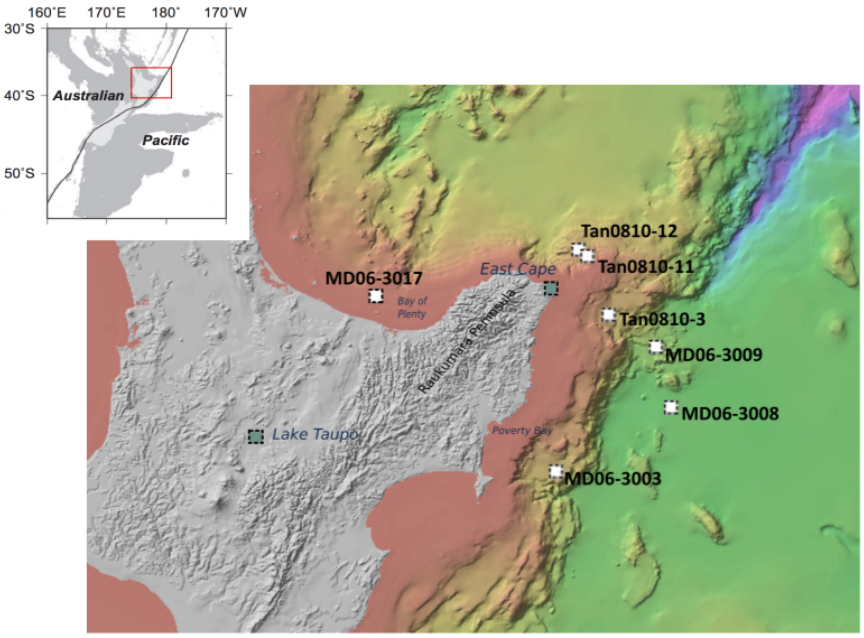

Figure 7: Map of North Island, New Zealand showing the locations of core sites used in this study imposed on the regional bathymetry. The inset map is modified from Townend et al. (2012) and shows the location of the core map relative to New Zealand.

ally high sedimentation rates off the continental shelf. The exposed nature of New Zealand's landmass lends itself to high erosion rates. The Raukumara Ranges lie across East Cape (Fig. 7), and deliver large amounts of sediment to surrounding rivers and streams. The suspended sediment yield (SSY) measured in rivers and streams around East Cape is approximately 20,000 t/km^2/yr, the highest across North Island (Fig. 8). The Waiapu and Waipaoa rivers alone deliver 35 Mt/yr and 15 Mt/yr, respectively, of suspended sediment to the continental shelf (Hicks et al., 2003, 2011). The high erosion rates are caused by the active subduction margin across New Zealand, the moderately high rainfall in the region and the easily eroded mudstone that makes up the dominant lithology of the Raukumara Ranges. Deforestation has also contributed to a rapid rise in the rate of erosion since European settlers arrived in New Zealand (Hicks et al., 2003).

The high sedimentation rates off the east coast of North Island enable high resolution analyses to be conducted on the marine cores. Sedimentation rates are necessary to determine how the stratigraphy within the cores has changed over time. In this

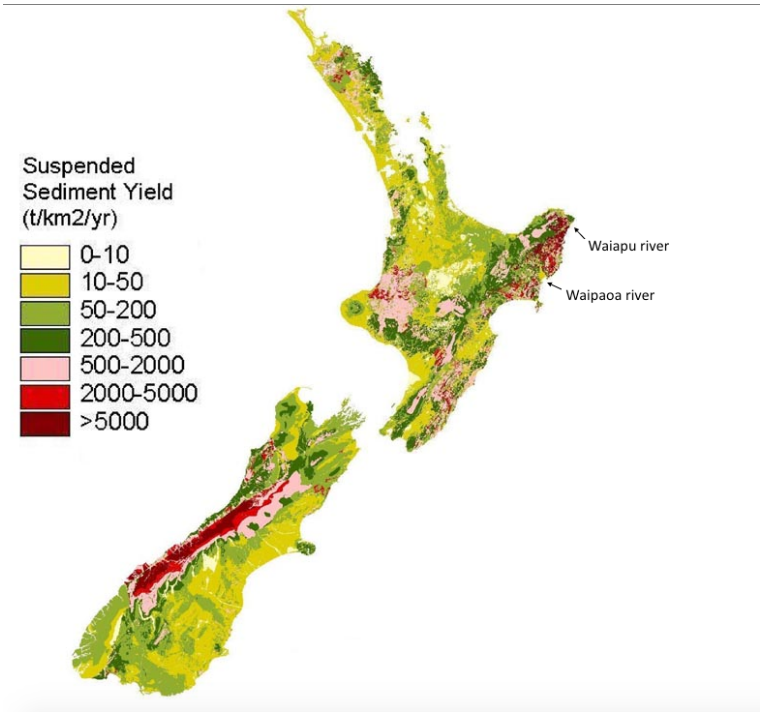

Figure 8: Map of New Zealand showing the suspended sediment yield into rivers and streams across the country. The colours from yellow to red indicate the amount of sediment, from lowest to highest respectively, measured in tonnes per square kilometre per year. Arrows indicate locations of the Waiapu and Waipaoa river mouths. Adapted from Hicks et al. (2003).

study the high sedimentation rates in the cores allow, in some cases, for sub-decadal scale sampling. This is fundamental because in order to observe how oceans respond to volcanism, an in depth understanding of the time it takes for the oceans to respond and how long the perturbation remains is necessary for the information to be used in climate models and/or to determine how deep the signal penetrates into the ocean.

1.5 Oceanography

New Zealand straddles two major surface water masses. The Subtropical Front (STF) is the boundary separating the warm water from the subtropics and the cool water from the subantarctic (Fig. 9). The STF moves across the Tasman Sea at ~43°S before migrating around the bottom of the South Island, back up to 43°S and continuing across the South Pacific Ocean (Chiswell et al., 2015). The warm Subtropical Water (STW) from the north is characterised by temperatures of >15°C, high salinity (>34.8 psu) and low nutrients, brought to New Zealand by the East

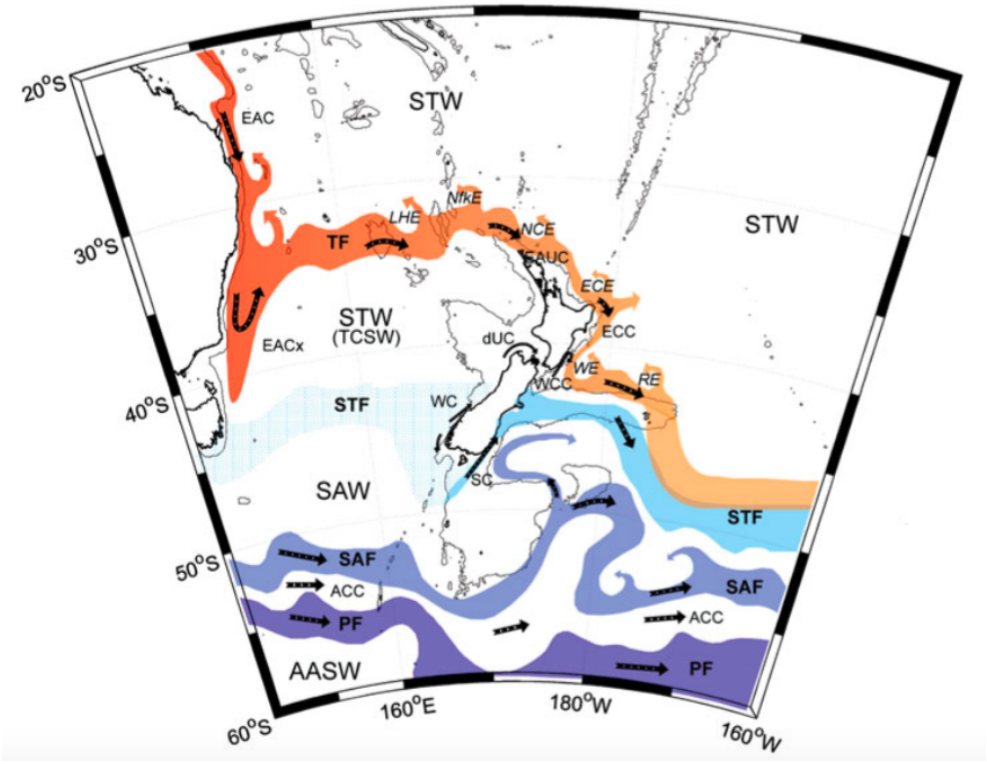

Figure 9: Map of New Zealand with ocean surface currents. Arrows indicate flow direction and colours are indicative of water temperature. The shading differences for the STF indicate a change in density. Water Masses are Subtropical Water (STW), Tasman Sea Central Water (TSCW), Subantarctic Water (SAW) and Antarctic Surface Water (AASW). Ocean fronts are Tasman Front (TF), Subtropical Front (STF), Subantarctic Front (SAF) and Polar Front (PF). Ocean currents are East Australia Current (EAC), East Australia Current extension (EACx), East Auckland Current (EAUC), East Cape Current (ECC), dUrville Current (dUC), Wairarapa Coastal Current (WCC), Westland Current (WC), Southland Current (SC) and Antarctic Circumpolar Current (ACC). Eddies are Lord Howe Eddy (LHE), Norfolk Eddy (NfkE), North Cape Eddy (NCE), East Cape Eddy (ECE), Wairarapa Eddy (WE) and Rekohu Eddy (RE) from Chiswell et al. (2015)

.

Australian Current (EAC) and the South Pacific subtropical gyre (Heath, 1985, Chiswell et al., 2015, Boyd et al., 1999).

The EAC is a major surface current in the South Pacific that flows south along the east coast of Australia. A section of the EAC splits from Australia and moves eastward towards New Zealand, known as the Tasman Front (TF; Tilburg et al., 2001). Surface water currents, driven by the Trade Winds, branch off the TF and bring warm, saline water to New Zealand. One branch of the TF is directed around the northern tip of North Island where it becomes the East Auckland Current (EAUC).

The EAUC follows the northeast coastline until it reaches East Cape where the East Cape Eddy (ECE) and East Cape Current (ECC) are formed. The warm water continues south until ∼43°S where it turns eastward just north of the Chatham Rise (Heath, 1985; Fig. 9).

Cool Subantarctic Water (SAW; 8 – 14°C) is the main surface water between the STF and the Subantarctic Front (SAF; Chiswell et al., 2015). Contrary to the STW, these waters are characterised by nutrient-rich, lower-salinity (<34.4 psu) water transported north by the westerly winds (Boyd et al., 1999, Heath, 1985).

All marine sediment cores examined in this study are located in STW with direct influence from the ECE and the ECC. The average annual SST, averaged over 20 years from 1993 to 2013, for core site MD06-3017 is ∼18-19°C (Fig. 10). For the rest of the core sites the average temperature is closer to ∼18°C. The average summer temperature around East Cape is 20°C, while in winter the average temperature reduces to 17°C (Bolton et al., 2011).

1.6 Ecology of foraminifera

Foraminifera are single-celled organisms that have existed since the early Cambrian. Planktic foraminifera possess a shell, or test, made up of a series of chambers. Test chambers are predominantly constructed incrementally, continually covering the aperture of the previous chamber while maintaining contact with the surrounding environment (Loeblich and Tappan, 1988). d'Orbigny (1826) first characterised the order Foraminifères from two Latin words, foramen and fer, meaning an 'opening' and to 'carry', respectively, referring to the apertures between chambers. Eventually, during its translation to English, Foraminifères became Foraminifera and its ranking was increased from order to class (Lipps et al., 2011). There are four main groups based on the composition of the shell. The first group of foraminifera possess tests made from organic material. Agglutinated tests (tests built from surrounding material) form a second group and a very small number of foraminifera are defined by tests made of opaline silica. This study focuses on foraminifera from the fourth group that possess tests composed of secreted $CaCO_3$ (Gupta and Barun, 1999).

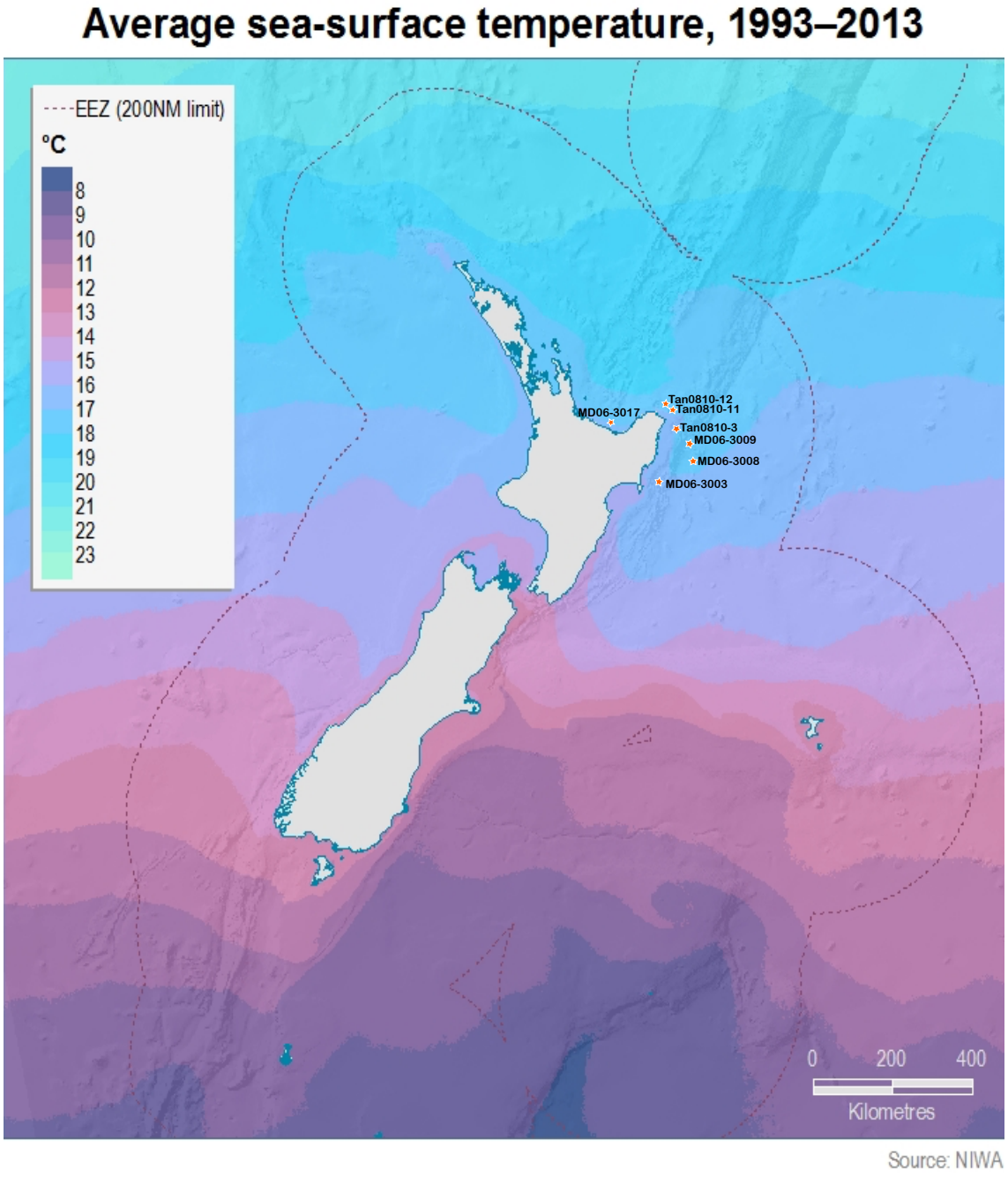

Figure 10: Averaged annual SSTs around New Zealand measured over 20 years between 1993 and 2013. Stars indicate the locations of the core sites. Dashed line represents the outer limit of the EEZ - Exclusive Economic Zone. Data collected by NIWA.

They are found throughout ocean basins across the world, from polar waters to the tropics. While they only make up a small portion of the global zooplankton population, their tests can dominate pelagic sediments, termed calcareous ooze (Hemleben et al., 1989). The tests of foraminifera sink to the seafloor and are preserved in the sediments if conditions are favourable.

Foraminifera that secrete $CaCO_3$ to form their tests also incorporate trace elements into the process. The tests are generally ∼99% $CaCO_3$ leaving ∼1% made up of trace elements (Lea, 1999). The complete process by which the tests are formed is not entirely understood. It is suggested that throughout their lifetime foraminifera migrate in the water column, releasing gametes at specific depths. Some foraminifera however, alternate between sexual reproduction and asexual reproduction most commonly through multiple fission (Goldstein, 1999). The first chamber formed is composed of organic material and is termed the primary organic membrane (Kucera, 2007). Calcite layers are then secreted on either side of the membrane. Erez (2003) suggested the first layer is formed from highly soluble calcium bound to the membrane that provides the initial surface to precipitate the $CaCO_3$ layer. Hemleben et al. (1989) propose a similar model; the primary organic membrane is the template for calcification and the cytoplasmic envelope may be involved in these initial stages. Following this the foraminifera is able to acquire calcite ions from the surrounding seawater, however, this initial layer is vital. To build their tests foraminifera incorporate seawater into their shells, a process known as vacuolization whereby vacuoles (storage bubbles) are used to store seawater and enables them to alter its physical and chemical properties. This occurs in order to make the conditions suitable for precipitating calcium carbonate. The basic equation for this process is given as:

$$Ca^{2+} + 2\,HCO^{3-} \rightleftharpoons CaCO_3 + H_2O + CO_2 \tag{1}$$

The ∼1% of trace elements in the shell are incorporated directly from the surrounding environment by substituting for the Ca^{2+} ion during precipitation. This process

is described by the equation:

$$CaCO_3 + TE^{2+} \rightleftharpoons TECO_3 + Ca^{2+} \quad (2)$$

Trace elements identified in foraminifera shells include Mg, Na, Sr, F, B, Al, Li, Mn, Zn, Ba, Fe, Cu, Nd, Cd, V and U (Lea, 1999). Their incorporation into the test are based on the composition of the seawater at the time of precipitation, providing important information on the oceanic environment in the past. Various trace elements can be used as indicators of specific parameters, such as nutrient availability, physical, chemical and diagenetic properties, of the ocean at the time of precipitation.

Elemental concentrations of foraminifera tests not only provide information on the ocean but also the depths and locations the foraminifera inhabited during their lifetime. This gives a unique insight into the life cycles of these organisms. Specific chambers are constructed at various times throughout their existence (Kucera, 2007). For example, for symbiont-bearing species such as *Globigerinoides ruber* their depth habitat remains relatively consistent, in the upper 50 m of the ocean, because of their reliance on photosynthesis (Hemleben et al., 1989). This is observed in the chemistry of their tests with the antepenultimate and penultimate chambers containing similar Mg/Ca concentrations (Bolton et al., 2011). Conversely, non-symbiont bearing species, such as *Globigerina bulloides*, have a distinctly more variable depth habitat, with this particular species inhabiting the upper 400 m of the water column. Such species change depths throughout their lifetime based on areas of upwelling and nutrient availability. This is also reflected in the Mg/Ca concentrations of their tests with each individual chamber exhibiting different concentrations (Marr et al., 2011).

The effects of life processes such as gametogenesis, the biological process of cell division, can be observed in the morphology and chemistry of foraminifera tests. Spinose species typically resorb their spines prior to gametogenesis. Many species such as *Globigerinoides sacculifer* also form a calcite crust immediately prior to gamete release (Ketten and Edmond, 1979, Caron et al., 1990), covering the outer surface of the test in a thick wall. Hemleben et al. (1989) suggest that during ga-

metogenesis species such as *G. sacculifer* and *Globorotalia truncatulinoides* sink in the water column, forming the calcite crust that is observed as a series of euhedral crystals commonly covered by a smooth layer (Fig. 11). Crystallinity is a sign the calcite was grown slowly, often representative of cooler waters. However, not all foraminifera will go through gametogenesis and those that do, will not always produce a calcite crust. Sinking during this reproductive period is often caused by a loss of buoyancy, if this does not occur it is unlikely that a crust will be produced (Hemleben et al., 1989).

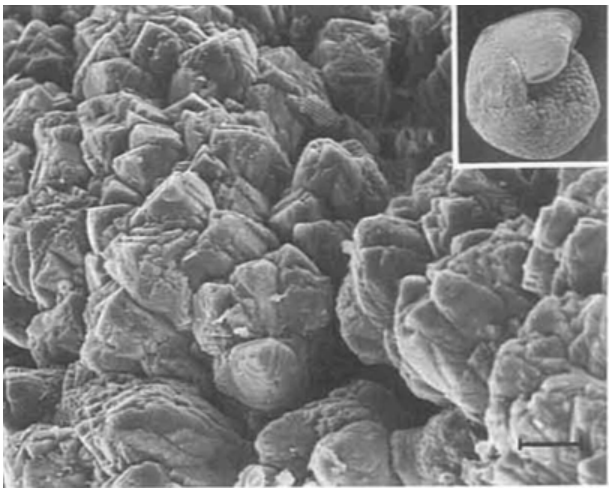

Figure 11: SEM image of a gametogenic calcite crust formed in situ on a foraminifera collected from a sediment trap deployed at 3200m water depth. The species is *Globorotalia truncatulinoides* with complete test view shown in the inset. Scale bar represents 10μm. From Hemleben et al. (1985).

In this study analyses are conducted on two species of foraminifera, *Globigerinoides ruber* and *Globigerina bulloides*. Both are common in STW around New Zealand and have shown robust calibrations with temperature (Bolton et al., 2011, Marr et al., 2011).

1.6.1 *Globigerinoides ruber* (d'Orbigny, 1839a)

Globigerinoides ruber is a surface-dwelling, symbiont-bearing species, restricting its depth habitat to the upper 50m of the ocean. These spinose planktic foraminifera have existed since Late Miocene times and are currently most abundant in equatorial to temperate waters (Saitō et al., 1981). Their preferred temperature range spans 14 to 30°C with peak productivity occurring from 21 to 29°C (Bé and Tolderlund,

1971). Two varieties of *G. ruber* are present in marine sediments. The pink variety is slightly bigger than the white and prefers warmer waters. According to Thompson et al. (1979) the pink form became extinct in the Indo-Pacific ∼120,000 BP, during the late Pleistocene, though it still exists in the Atlantic Ocean. Conversely, the white form of *G. ruber* is ubiquitous within modern subtropical waters (Bé and Tolderlund, 1971). The white variety of *G. ruber* can be defined by four various morphotypes. Three of these morphotypes, *Globigerinoides elongatus, Globigerinoides pyramidalis* and *Globigerinoides cyclostomus*, are known collectively as sensu lato (Fig. 12a) and the final morphotype, the normal form of *G. ruber*, as sensu stricto (Fig. 12b; Thirumalai et al., 2014). There is ongoing debate whether these two forms of white *G. ruber* are geochemically identical or distinct. For example, studies such as Steinke et al. (2005) and Sadekov (2008) found *G. ruber* sensu lato has distinctively lower Mg/Ca values than *G. ruber* sensu stricto. Alternatively, the results from studies by Thirumalai et al. (2014), Mohtadi et al. (2009) and Bolton (2011) suggest the two types are geochemically identical. A moderate flux of *G. ruber* occurs throughout the year with no apparent seasonal dependence. Peaks can occur during the year but these appear to happen during different seasons at different geographical locations and are not large enough to bias studies towards a particular season (Xiang et al., 2015, Thirumalai et al., 2014).

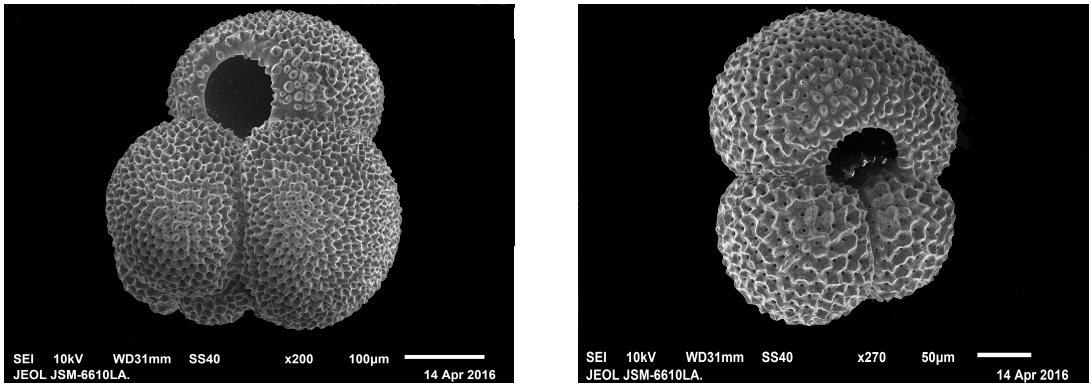

(a) *G. ruber* (W) sensu lato (b) *G. ruber* (W) sensu stricto

Figure 12: Scanning electron microscope images, from this study, of the two morphotypes of *Globigerinoides ruber* (white)

1.6.2 *Globigerina bulloides* (d'Orbigny, 1826)

Globigerina bulloides is a non-symbiotic, spinose species that has existed since Late Miocene times. It is currently found from subtropical to polar waters but dominates the planktic foraminifera population in subantarctic and subarctic waters (Saitō et al., 1981, Bé and Tolderlund, 1971). The depth habitat for *G. bulloides* is difficult to constrain because patterns suggest they are most abundant where phytoplankton blooms are in occurrence, usually due to upwelling (Mortyn and Charles, 2003). Hemleben et al. (1989) suggest a depth above 400m, but more specifically above the thermocline. Other studies such as Saraswat and Khare (2010) and Niebler et al. (1999) are in agreement with Hemleben et al. (1989) with estimates of 0-200m and 0-100m, respectively. This species is constrained by sea surface temperatures of 0 to 27°C with peak abundance occurring between 3 and 19°C (Bé and Tolderlund, 1971). The reliance of *G. bulloides* on phytoplankton blooms typically limits their annual flux to a particular season. During summer and autumn the oceans around New Zealand are typically stratified, limiting the cold, deep, nutrient-rich water from reaching shallower depths. In winter, this stratification begins to break down, allowing nutrients to rise towards the surface and causing an increase in primary productivity during the following spring (Northcote and Neil, 2005). Therefore, the highest flux of *G. bulloides* typically occurs during late spring with little to no production throughout the rest of the year (Northcote and Neil, 2005, King and Howard, 2001). Results of analyses on *G. bulloides* tests are therefore likely to be representative of late spring conditions.

1.7 The Mg/Ca ratio as a paleotemperature proxy

Mg^{2+} is one of the most abundant trace elements found in calcite shells (Lea, 2006). It can be substituted for Ca^{2+} during the formation of $CaCO_3$ and gives valuable information on SSTs at the time of precipitation. The reaction whereby Mg^{2+} is substituted for Ca^{2+} in the test lattice is endothermic. The ratio of Mg/Ca is therefore higher with warmer temperatures, given by the exponential equation:

$$\mathrm{Mg/Ca} = \mathrm{B} \times \mathrm{e}^{(\mathrm{AxT})} \tag{3}$$

Where T is the calcification temperature in °C and A and B are constants (Barker et al., 2005). Mg/Ca paleothermometry of foraminifera can be applied on a timescale of 0 - 100 million years (Lea, 2006). The advantage of this paleotemperature proxy comes from the relatively long oceanic residence times of Mg and Ca, 10^7 and 10^6 years, respectively. The ambient Mg/Ca ratio is therefore interpreted to have remained the same for millions of years (Barker et al., 2005).

For equilibrium calcite formation, a 3% increase in Mg/Ca corresponds to a 1°C temperature increase. However, for reasons not fully understood, foraminifera produce an increase in test Mg/Ca of 9 ± 1% per degree Celsius (Anand et al., 2003, Lea, 2006). This suggests the uptake of trace elements in foraminifera test construction is controlled internally, commonly referred to as a vital effect (Erez, 1978, Hemleben et al., 1989). Further complications arise from the knowledge that the uptake of Mg into the test lattice is not exclusively controlled by temperature and the concentration of these elements in the ocean. Other influences can include salinity, nutrient availability and carbonate saturation (Schmidt et al., 2004). Recent studies by Arbuszewski et al. (2010) and Mathien-Blard and Bassinot (2009) suggest increasing salinity can cause an increase in Mg/Ca of 15 and 27% respectively per practical salinity unit (psu). Others argue an increase of only 4-6% exists per psu (Nürnberg et al., 1996, Hönisch et al., 2013, Kısakürek et al., 2008).

Each species is adapted to a specific ecological niche and the exact process of test construction is a function of both internal and external factors, making it difficult to understand the complete test construction process. Carbonate supersaturation increases from the poles to the tropics because CO_2 is more soluble in colder waters. Higher carbonate supersaturation could therefore also influence the calcification process (Schmidt et al., 2004). Foraminifera from different species and regions are therefore likely to display slightly different elemental and morphological traits. For these reasons Mg/Ca calibrations for specific species and regions are crucial. Calibrations have been determined from live culturing, core-top sampling or by collecting foraminifera from the water column using sediment traps (Anand et al., 2003).

According to Hemleben et al. (1989), planktic foraminifera can only migrate vertically in the water column. With no form of propulsion they keep themselves buoyant by releasing gases or lipids that allow them to move vertically in the water column (Kucera, 2007). If they are transported out of their preferred environment by currents or upwelling, or their specific environment changes, they can exhibit stress. This is manifest in the morphology, size and geochemical make up of their tests. Test contruction can be a function of stress, providing a barrier to the changing environmental conditions (Marszalek et al., 1969). However, it is an action that also requires a substantial amount of energy (Weinkauf et al., 2016). Several studies have shown a strong relationship between test size and temperature with the largest average test sizes correlating positively to the species specific optimum calcification conditions (Hecht, 1976, Schmidt et al., 2003, 2004, Moller et al., 2013). The further the foraminifera were from their ideal growing environment the smaller the shell size for most species. Additionally, in most cases the smaller the test size the lower the Mg/Ca values, revealing temperature as the most significant cause of variation. Other factors can contribute to small test sizes in areas of upwelling, the northern and southern polar fronts and the subtropical frontal regions. However, these areas are characterised by turbulent waters and constantly changing environmental conditions, displacing and stressing species that may inhabit these areas (Schmidt et al., 2004). Gametogenic calcite also causes a large variation in shell size that can significantly alter the Mg/Ca concentrations (Ni et al., 2007). However, species such as *G. ruber* and *G. bulloides* are not known to exhibit gametogenic calcite crusts allowing reliable comparisons of test size and Mg/Ca values to be conducted (Hoogakker et al., 2009, Caron et al., 1990, Moy et al., 2009).

1.7.1 Preservation and contamination of tests

Secondary effects, alterations after death but prior to or during deposition, on foraminifera tests make it difficult to identify the ecological processes involved in calcification process. The world's sea surface waters are supersaturated with respect to calcite. As pressure increases and temperature decreases with depth in the ocean, the solubility of $CaCO_3$ increases, leaving the bottom waters undersaturated (Pälike et al., 2012, Bostock et al., 2011). The lysocline is the depth at which the

oceans become undersaturated with respect to $CaCO_3$ (Fig. 13). The point at which the rate of $CaCO_3$ supply equals the amount of loss, leaving no $CaCO_3$ preserved, is known as the calcite compensation depth (CCD).

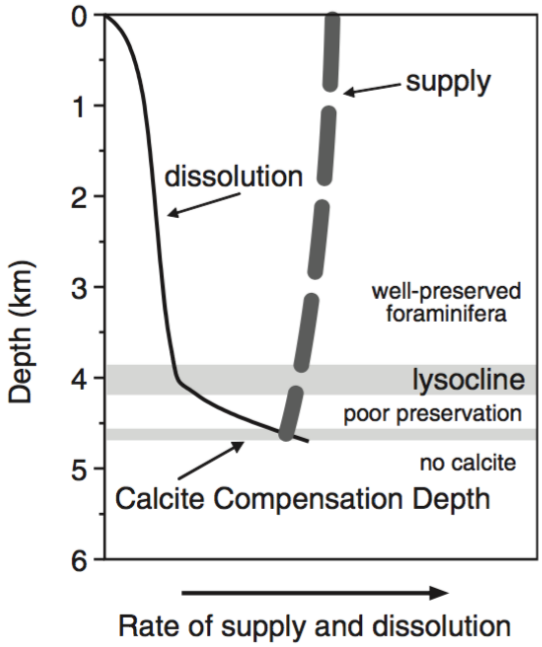

Figure 13: Simplified diagram to demonstrate the relationship between dissolution of foraminiferal calcite and the lysocline and CCD. From Kucera (2007).

The lysocline and CCD depths vary in different oceanic regions, dependent on a number of factors related to the depth and temperature of the ocean, the currents and the amount of biological productivity. NE of New Zealand the lysocline and the CCD depths are ∼4 km (Bostock et al., 2011).

It is known that dissolution preferentially dissolves the Mg-rich sections of the tests, which are usually the chambers formed closest to the sea surface and will therefore bias results of paleotemperature calculations towards colder temperatures (Hecht et al., 1975, Rosenthal et al., 2000, Dekens et al., 2002). Some studies have concluded that gametogenic calcite slows the rate of dissolution in foraminifera tests (Caron et al., 1990, Prasanna et al., 2016). While the rate at which it slows varies between species, it has been shown to decrease the rate of dissolution by up to five times for species such as *Orbulina universa* (Caron et al., 1990). However, gametogenic calcite crusts are themselves thought to bias Mg/Ca results towards colder

values because they are thought to form near the end of the foraminifera life cycle, as they begin to lose their buoyancy and sink to greater depths (Hemleben et al., 1989). There is no easy way to correct for dissolution but, if present, it can and should be accounted for in the uncertainty of the results (Lea, 2006).

Foraminifera tests can also be covered in surface contaminants that even in minor concentrations can affect the results of geochemical analyses. Cleaning the tests prior to performing the analyses can remove most of the surface contaminants but detrital material can adhere to the test or remain inside the chambers. Chemical processes such as diagenesis cause inorganic calcite growths on the tests and alter their geochemical make-up. Various elements can be used to detect contamination or diagenesis in samples that can then be removed from the results to ensure reliability.

When measuring foraminiferal element to calcium ratios, Al/Ca can be used to detect detrital material such as clay particles (Barker et al., 2003, Bender et al., 1975, Kraft et al., 2013). Typically Al/Ca values over 100 µmol/mol indicate high percentages of detrital material in the sample (Lear et al., 2015). Less commonly, Ti/Ca can also be used alongside Al/Ca to detect detrital contamination (G. Dunbar, pers. comm., 2016). High values of Mn/Ca can indicate the presence of a $MnCO_3$ diagenetic overgrowth or adhering material on the foraminifera test (Boyle, 1983, Bender et al., 1975, Regenberg et al., 2007, Marchitto, 2006). $MnCO_3$ has little impact on the composition of major elements in the shell, but it can considerably impact the trace element concentrations. These overgrowths are difficult to remove and can prevent sufficient cleaning of clay particles that lie beneath them (Boyle, 1983). The most efficient way to prevent contamination is to remove samples containing Mn/Ca values above 100 µmol/mol (Boyle, 1983, Marchitto et al., 2007, Lear et al., 2015). Contamination has a significant effect on Mg/Ca ratios but also to a lesser extent Sr/Ca. Mg/Ca can naturally vary highly in foraminifera tests, making it difficult to detect contaminants where the Mg/Ca ratio is not distinctly offset. Sr/Ca is relatively robust and constant in foraminiferal samples. Spikes in Sr/Ca can therefore also be used to indicate high levels of contamination or chemical coatings and in most cases suggest the Mg/Ca concentration will also have been

altered (G. Dunbar, pers. comm., 2016).

1.7.2 Analytical techniques

The most common technique for detecting elemental concentrations in foraminiferal calcite is through dissolving and analysing several individual foraminifera together in solution (Nürnberg et al., 1996, Lea et al., 1999, Lear et al., 2000, 2002). However, modern analytical techniques are becoming more sensitive making it possible to analyse individual chambers of foraminifera. Laser ablation inductively coupled plasma mass spectrometry (LA-ICP-MS) acquires in situ concentrations of trace elements in foraminifera tests. Both solution-based and laser ablation methods are considered accurate and have their advantages and disadvantages.

Solution-based techniques typically involve rigorous cleaning procedures of foraminifera tests before dissolving the bulk samples in solution (Barker et al., 2003). The advantages of this technique mostly come from the relatively rapid data processing following the analyses. However, cleaning procedures prior to the analyses can be significantly time consuming because without sufficient cleaning all contaminants are dissolved into the solution with the foraminifera, potentially causing artificial results without a way of determining the origin of contamination. Another disadvantage stems from dissolving the entire foraminifera test, leaving no ability to perform further analyses or decipher the different concentrations between chambers (Marr, 2009).

LA-ICP-MS provides a different approach to geochemical analyses. This technique obtains results from high spatial resolution (25-30 μm), allowing individual test chambers to be analysed, providing information about the various depths and environments the foraminifera inhabited during their lifetime. Significantly less cleaning is required when using LA-ICP-MS compared to solution-based techniques because contaminated areas can be avoided or sometimes identified in the results and their influence removed. Additionally, the minimal amount of material required for analysis leaves the remaining parts of the test available for further analyses. The main disadvantage with this technique is encountered during processing after the data

has been collected. This procedure can be time consuming because any signs of contamination in the data need to be identified in order to ensure the results are accurate.

1.8 Project overview

The overall aims of this project are:

- To determine if foraminifera records from marine cores can be used to identify if SSTs are altered following large silicic eruptions including, if present, the degree of change and how long the ocean surface is perturbed. Ideally a sub-decadal scale record could be produced to observe the change in temperature at a very high resolution.
- To determine if analysing the morphology and size of specific planktic foraminifera tests can indicate if and/or how their marine environment is altered following an explosive eruption.
  - This approach will provide insights on how foraminifera may adapt to a changing environment, whether their ability to precipitate $CaCO_3$ is compromised following a large silicic eruption and the length of time it may take for these species to adapt to a new environment.

These aims are addressed by:

1. Completing a detailed stratigraphy of seven marine sediment cores collected east of North Island, New Zealand, to identify the Taupo, Waimihia and Mamaku tephras and characterise the surrounding sediment. Age models for the cores are calculated to determine sedimentation rates and hence provide an indication of the time resolution of each stratigraphic record.
2. Performing grain size and $CaCO_3$ analyses on the sediment surrounding the tephra layers in order to identify the presence of any secondary deposits that could render the calculated sedimentation rates unreliable.

3. Using the outcomes of steps one and two to identify the cores with a primary tephra deposit, an undisturbed sedimentary record below and above the tephra and a high sedimentation rate (and therefore a high resolution) to use for further analyses.

4. Identifying, collecting and analysing specific planktic foraminifera species either side of the targeted tephra layer from the chosen cores. Analysing the size and morphology of the foraminifera tests using the scanning electron microscope (SEM) prior to performing geochemical analyses by LA-ICP-MS to obtain trace element compositions and calculate the SSTs before and after an eruption.

2 Core stratigraphy

The characterisation, structure and relative position of sedimentary features with respect to time defines the basis of stratigraphy. Superposition is one of the basic laws of stratigraphy and states that if a sedimentary layer is deposited on top of another layer, the layer on the bottom must be the oldest. Therefore, marine sediment cores are assumed to be in stratigraphic order from oldest at the base to youngest at the top and with ages taken throughout the core, the sediment in between can be assigned an age based on a constant sedimentation rate. However, this natural order of stratigraphy can be disturbed by sediment transportation after deposition, most commonly through sedimentary processes or biological activity. This disturbs the natural order of deposition and should not be included when characterising and dating sedimentary sequences based on sedimentation rates.

The cores used in this study were previously logged by Pouderoux (2011) and Zohrab et al. (2015). These core logs were used to identify the Taupo, Waimihia and Mamaku tephra layers (refer to section 1.3) in the cores. In this study we perform a detailed characterisation of the sediment surrounding these tephra layers in order to identify any sediment reworking, with an aim to identify sequences where the sediment is in stratigraphic order. This is necessary to define an accurate and reliable temporal resolution of the sediment either side of the tephra and observe how the oceanic environment has changed through time. Grain size and $CaCO_3$ analyses are useful stratigraphic tools for further identifying and categorising primary and secondary sedimentary deposits. These were performed following sediment characterisation in order to provide further information on the origin of the sediment surrounding the tephra deposits.

2.1 Core selection

Seven cores were selected for this study based on the presence of one or more of the Holocene tephra horizons: MD06-3003, MD06-3008, MD06-3009, MD06-3017 from the 2006 *Marion Dufresne* voyage and Tan0810-3, Tan0810-11 and Tan0810-12 from the 2008 *R.V. Tangaroa* voyage TAN0810. The Taupo, Waimihia and

Mamaku tephras had been previously identified in all cores, except MD06-3017, by Pouderoux (2011). Core MD06-3017 was logged and tephra identified by Zohrab et al. (2015).

All cores were from areas with a high sedimentation rate off East Cape, New Zealand (Fig. 7). MD06-3003 was collected from Poverty Bay in a water depth of approximately 1398 m and recovered a core length of 12.88 m. Around East Cape, MD06-3008 and MD06-3009 were obtained in water depths of 3520 m and 2940 m with recovered core lengths of 25.4 m and 20 m respectively. MD06-3017 was collected from the Bay of Plenty at a shallower water depth of 150 m and a recovered core length of 19.85 m, although only 12 m of the core is usable due to the barrel bending and breaking during coring (Pouderoux et al., 2012, Proust et al., 2006). Core Tan0810-3 was collected on the upper continental slope east of East Cape in a water depth of 1090 m with a recovered core length of 3.2 m. Tan0810-11 and Tan0810-12 were acquired from the Matakaoa submarine channel, northeast of East Cape from water depths of 1089 m and 1255 m with recovered core lengths of 2.6 m and 2.75 m, respectively (Pouderoux et al., 2012).

2.2 Methods

Based on the identification and ages of tephra in the marine cores determined by Pouderoux (2011) and Lowe et al. (2008), respectively, we constructed a detailed stratigraphy for the 5-15 cm of sediment either side of each of the Taupo, Waimihia and Mamaku tephra in every core. The extent of sediment characterisation around the tephra layers was dependent on the thickness and dispersal of the tephra in the cores. Using the calibrated ages of the Taupo, Waimihia and Mamaku tephra (Lowe et al., 2008), and the cumulative hemipelagite thicknesses of the cores determined by Pouderoux et al. (2012) we were able to calculate age models and sedimentation rates for every core. To further constrain the sedimentation rates the ages and depths of the Kaharoa, Whakatane, Rotoma and Waiohau tephra horizons in the marine cores were used with the depths determined by Pouderoux et al. (2014) and ages by Lowe et al. (2008). Radiocarbon dating of foraminifera by Pouderoux et al. (2012) provided further ages that were used for cores with few tephra deposits.

2.2.1 Core sampling

All seven marine sediment cores were sampled above and below identified Taupo, Waimihia and Mamaku tephra deposits. The surfaces of the split cores were first scraped to remove any contamination in the top layer of mud. Samples 0.5 cm thick were taken incrementally either side of each tephra from half of the split core. 0.5 cm is the smallest practical sampling limit that can be obtained for sediment cores and was therefore used to obtain the highest temporal resolution possible. The number of samples taken per core varied to ensure the samples covered a minimum time scale of 100 years above and below the tephra, and the final sample was far enough from the ash layer that there was little to no tephra remaining in the sediment. The minimum time scale of 100 years either side of the tephra was used because it was interpreted to be a sufficient amount of time to observe the impact of a volcanic eruption on SST but also provide background information about the ocean temperature before the eruption and how long it takes for the temperature to return to these background levels after the eruption. Additionally, in order to observe the effects of tephra, if any, on preserved foraminifera tests, the samples taken above the tephra horizons needed to be a sufficient distance up the core to ensure no ash remained and could therefore be compared with samples containing tephra. Care was taken to make sure the layer of mud touching the core barrel was left in the core because of contamination from mud sliding down the barrel during collection. The tephra were not sampled.

2.2.2 Grain size

Each sample was analysed for grain size in core MD06-3009 and every second sample analysed in the six other cores. Approximately 0.5 g from each sample was placed in a container with deionised water overnight to disaggregate the grains. The container was then placed in an ultrasonicator for 5 seconds at a time until the sample had completely disaggregated. The samples were analysed using the Beckman Coulter LS 13 320 laser diffraction particle size analyser coupled with an Aqueous Liquid Module (ALM). The purpose of the ALM is to send liquid samples to the sensor without influences such as air bubbles or thermal turbulence (Coulter, 2011). Prior to adding the sample, the analyser was left to warm up for at least 15 minutes before

rinsing, running a laser alignment and measuring offsets and background levels to ensure the sample would be measured with the highest accuracy. The sample was run for 60 seconds before a complete rinse and background measurement was completed and another sample could be run. Alignment and offset were measured every 30 minutes. Selected samples were run twice and always had reproducible results. The data produced by the laser diffraction particle size analyser was run through GRADISTAT, a computer program that calculates grain size statistics such as mean, mode, sorting and skewness (Blott and Pye, 2001).

2.2.3 $CaCO_3$

Consistent with the grain size analyses, $CaCO_3$ concentrations were analysed in each sample for MD06-3009 and every second sample for the remaining cores. Concentrations of $CaCO_3$ were measured using a vacuum gasometric system with a precision of $\pm 2\%$ (Jones and Kaiteris, 1983). Approximately 0.8 g of sample was left overnight to dry. It was then crushed using a mortar and pestle and dried in the oven at 100°C for a minimum of 6 hours. Once it was removed from the oven it was placed directly into a dessicator to prevent moisture affecting the sample while it was left to cool. 0.3 ± 0.009 g was weighed out from each sample and placed at the bottom of a reaction chamber with five drops of deionised water to reduce the size of the reaction when the acid was added. The side arm of the reaction chamber was then carefully filled with 5 ml of 70% orthophosphoric acid using a syringe to ensure no acid touched the sediment or side of the chamber. Rubber o-rings were coated with silicon and one positioned on top of each reaction chamber before the lids were clamped and tightened to completely seal the chamber.

The vacuum pump was turned on half an hour before use with valves B and C open (Fig. 14). The room temperature was recorded and the digital pressure gauge was turned on. Liquid nitrogen was added to the dewar, to trap any water vapour and prevent it from entering the pump, once the pressure had stabilised. The gauge was set to zero and the first reaction chamber was placed on the vacuum line with valves B and C open and the chamber lid closed. Once the pressure stabilised valves B and C were closed and the chamber lid opened to give the chamber/vacuum line

pressure reading. Valve C was then opened and the total pressure reading was recorded. Valve B was opened to evacuate the chamber and once the pressure was stable valve B and the chamber lid were closed simultaneously to give a start pressure that was also recorded. The reaction chamber was removed from the vaccum line and the acid was tipped from the side arm into the sample. This process was repeated for 19 samples at a time, plus a 100% $CaCO_3$ standard, a second temperature reading was taken and all samples were then left to react for $1\frac{1}{2}$ hours. A third temperature reading was taken after the samples had reacted. The vacuum was then left to pump down to ~0 with valve C closed and valve B open. Valve B was closed and the first reaction chamber was placed on the vacuum line. Valve B was opened again and left until the pressure had stabilised at which point valve B was closed and the chamber lid opened to give the end pressure. This process was also repeated with the remaining samples and the standard. This technique for determining the percentage of $CaCO_3$ in a sample is based on determining the original pressure within the reaction chamber and once the acid has reacted with the sample the $CaCO_3$ is dissolved and releases CO_2. The difference between the original pressure in the chamber and the pressure after the additional CO_2 has been released is a function of the volume of $CaCO_3$ in the sample.

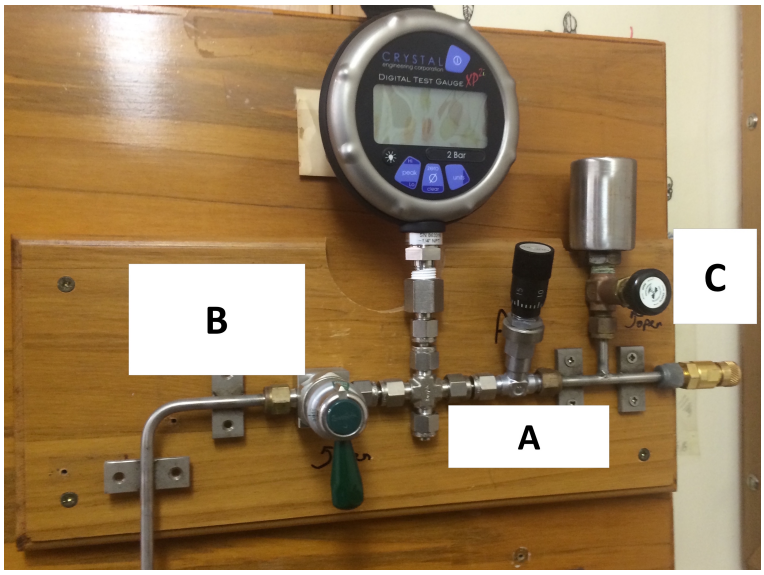

Figure 14: Vacuum line used for $CaCO_3$ analyses. The pressure gauge is in the centre with valves A, B and C labelled.

The data collected were entered into a NIWA-written Excel spreadsheet script where

the percentage of $CaCO_3$ in each sample was calculated based on the weight of the samples, the room temperature, the first and second pressure measurements and the start and end pressures. Any significant outliers seen in the data were discounted and the samples were run again.

2.3 Results

All cores exhibit an interlayering of hemipelagite and turbidites amongst the tephra deposits. The hemipelagite is olive-grey in colour compared to the similar but darker coloured turbidites. MD06-3009 and -3008 each contain Taupo, Waimihia and Mamaku tephra deposits (Figs. A1, A2). Taupo is consistently the thickest deposit followed by the Waimihia unit. MD06-3003 contains both the Taupo and Mamaku tephra but in each case there are two tephra units ∼10 cm apart (Fig. A3). The same sequence is observed in Tan0810-11 and MD06-3017 with two Taupo tephra deposits ∼10 cm apart in Tan0810-11 (Fig. A6), and three distinct ash layers for the Mamaku tephra in MD06-3017 (Fig. A4). The Taupo tephra within MD06-3017 is observed as a series of scattered blobs over a distance of 10-20 cm. Tan-0810-3 has a 9.5 cm thick Taupo tephra layer and a thin Waimihia layer (Fig. A5) and Tan0810-12 has a 3 cm thick Taupo deposit (Fig. 17). All tephras in Tan0810-3 and Tan0810-12 are surrounded by hemipelagite above and below. All tephras in these cores are concise with sharp basal contacts and minor to intense bioturbation above the units causing it to mix with the overlying hemipelagite.

2.3.1 Age model and sedimentation rates

The erosion rates around East Cape are the highest in North Island. The vast amount of sediment entering the ocean from the rivers and streams contributes to the high sedimentation rates seen in the cores collected from East Cape. The sedimentation rates were calculated using corrected depths, the amount of hemipelagite in the cores, determined by Pouderoux et al. (2012) by subtracting the turbidite and tephra thicknesses from the total thickness of the cores. Tan0810-11 and Tan0810-12 from the furthest position north show the highest average sedimentation rates of hemipelagite with 89 and 88 cm/kyrs respectively (Fig. 15). MD06-3003, MD06-3008, MD06-3009 and Tan0810-3 still have high sedimentation rates although signif-

icantly lower than Tan0810-11 and -12 with rates between 30 and 50 cm/kyrs. The average sedimentation rate in MD06-3017 is only slightly lower than Tan0810-11 and -12 at 70 cm/kyrs. The highest rates of 89 and 88 cm/kyrs equate to a 0.5 cm sample resolution of 5.6 to 5.7 years.

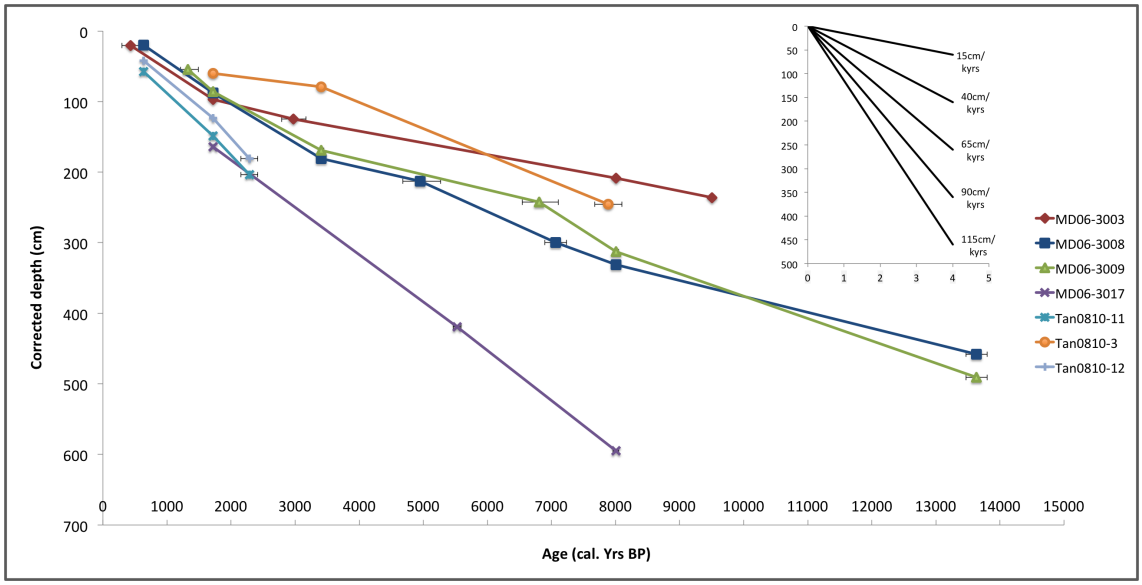

Figure 15: Age model for marine cores MD06-3003, -3008, -3009, -3017, Tan0810-3, -11, -12. The depth in core is the accumulated hemipelagite thickness. The ages in cal. Yrs BP are a combination of tephra ages from Lowe et al. (2008) and ^{14}C ages from Pouderoux et al. (2012). The inset is a comparison of calculated sedimentation rates.

2.3.2 Grain size

The laser diffraction particle size analyser used with the GRADISTAT program calculates the fraction of sand, silt and clay particles in each sample. Silt-sized particles dominate the grain size distributions across all cores, comprising 55-95% of each sample. The sand fraction varies between 0.5 and 42% in the samples while clay-sized particles remain relatively constant at <7% across all samples. The GRADISTAT program uses its own grain size scale (Table 1), based on those developed by Udden (1914), Wentworth (1922) and Friedman and Sanders (1978). The clay fraction is defined for grains <2 µm in size. Silt particles range from 2 µm to 63 µm and sand from 63 µm to 2 mm.

Grain size distributions measured for each core show two distinct patterns. The

Grain size		Descriptive terminology			
phi	mm/μm	Udden (1914) and Wentworth (1922)	Friedman and Sanders (1978)	GRADISTAT program	
			Very large boulders		
−11	2048 mm		Large boulders	Very large	
−10	1024		Medium boulders	Large	
−9	512	Cobbles	Small boulders	Medium	Boulders
−8	256		Large cobbles	Small	
−7	128		Small cobbles	Very small	
−6	64		Very coarse pebbles	Very coarse	
−5	32		Coarse pebbles	Coarse	
−4	16	Pebbles	Medium pebbles	Medium	Gravel
−3	8		Fine pebbles	Fine	
−2	4	Granules	Very fine pebbles	Very fine	
−1	2				
0	1	Very coarse sand	Very coarse sand	Very coarse	
1	500 μm	Coarse sand	Coarse sand	Coarse	
2	250	Medium sand	Medium sand	Medium	Sand
3	125	Fine sand	Fine sand	Fine	
4	63	Very fine sand	Very fine sand	Very fine	
5	31		Very coarse silt	Very coarse	
6	16	Silt	Coarse silt	Coarse	
7	8		Medium silt	Medium	Silt
8	4		Fine silt	Fine	
9	2	Clay	Very fine silt	Very fine	
			Clay	Clay	

Table 1: The grain size scale used in the GRADISTAT program compared to previous scales developed by Udden (1914), Wentworth (1922) and Friedman and Sanders (1978). Obtained from Blott and Pye (2001)

grain size distribution peaks at 8-10 μm with two significantly smaller peaks at 3 μm and 35 μm in cores MD06-3003, -3008 and -3009 (Fig. 16a). For the cores further north, MD06-3017, Tan0810-3, -11 and -12, the grain size is distinctly coarser with the main peak at 15 μm and a slightly smaller peak occurring at 35 μm (Fig. 16b). The three cores further south are therefore mostly composed of fine to medium silt while the other four cores show a distribution closer to medium to coarse silt.

The sand-sized fraction of the sediment cores increases in most cases in the samples directly above the tephra layers. Tephra typically has a larger grain size than hemipelagite. Bioturbation incorporates the tephra into the hemipelagite causing the samples closest to the tephra to have a higher percentage of sand derived from

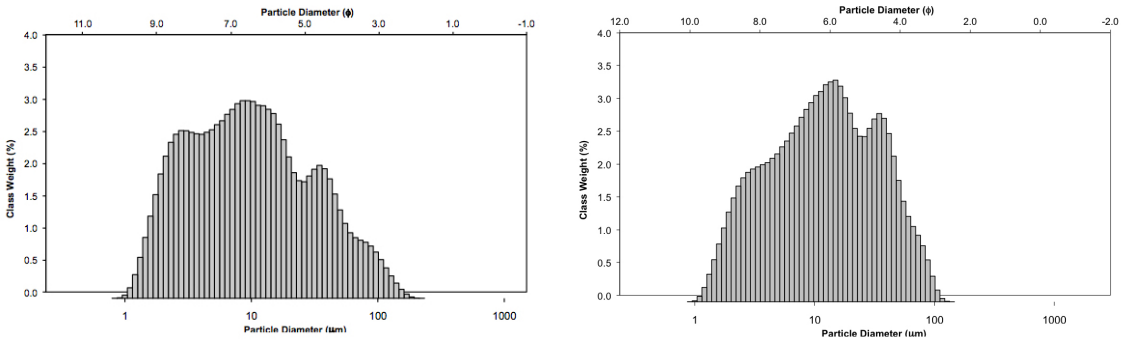

(a) MD06-3009 (b) Tan0810-12

Figure 16: Grain size distribution plots for all samples collected from cores MD06-3009 and Tan0810-12

the reworked tephra. Typically the grain size percentages return to the background levels seen below the tephra deposit after 1-2 cm. However, in some cases the grain size percentages do not return to normal and the sand-sized fraction remains high up to 10 cm above the tephra layer.

In core MD06-3008 the grain size distribution returns to background levels after the Mamaku tephra, but the sand-sized material remains well above the levels below the tephra following both the Waimihia and Taupo tephra deposits (Fig. A2). For MD06-3009 the sand fraction is significantly higher in all samples compared to the percentages seen in the other cores (Fig. A1). The grain size distribution for the samples surrounding the Mamaku deposit are relatively similar both before and after the tephra. The samples surrounding the Waimihia and Taupo tephras are similar to MD06-3008 with a prolonged period above the ash layers where the sand-sized fraction of material is distinctly higher than the background levels below. MD06-3017 and Tan0810-11 show very little change in grain size across all samples except for a brief section of increased sand-sized grains between two of the various Mamaku deposits in MD06-3017 (Figs. A4, A6). The samples immediately above the tephra deposits in MD06-3003 and Tan0810-12 have a high percentage of sand-sized material but this returns to the low background levels after less than 3 cm (Figs. A3, 17). Tan0810-3 shows the same pattern for the Taupo tephra with levels returning to normal relatively quickly however the sand-sized fraction remains higher than background levels for more than 5 cm above the Mamaku tephra (Fig. A5).

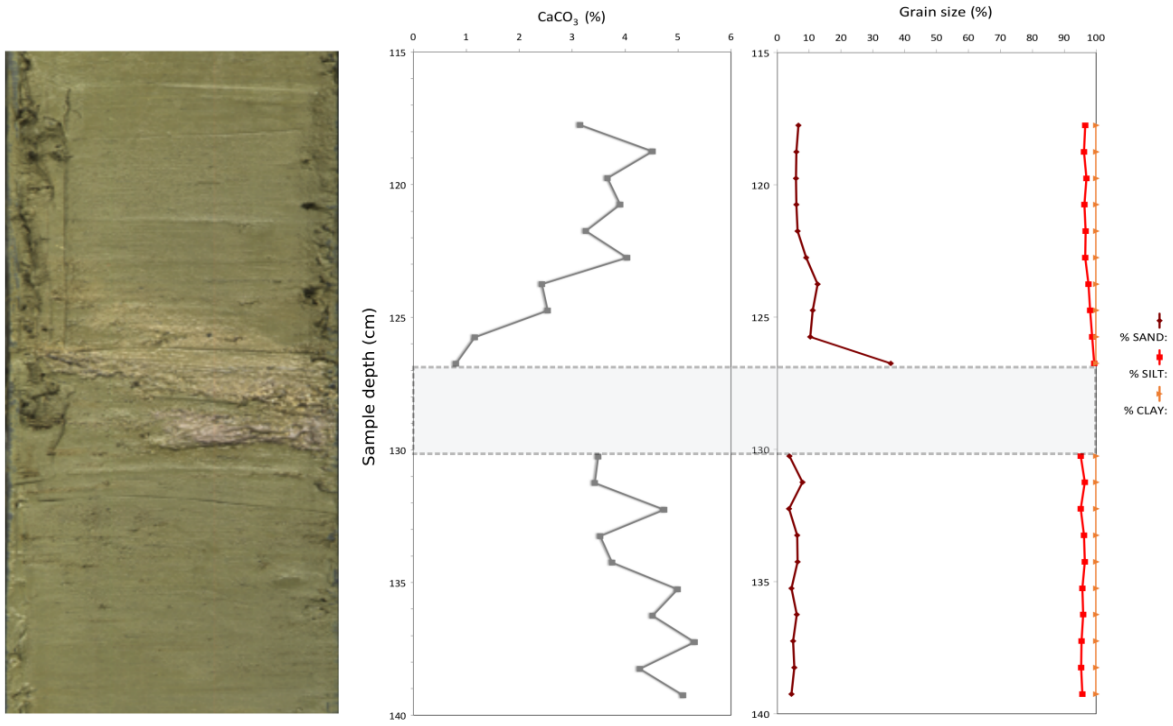

Figure 17: The results of grain size and $CaCO_3$ analyses on core Tan0810-12. Grain size values are 100% stacked and the grey boxes represent the Taupo tephra unit correlated to the core image.

2.3.3 $CaCO_3$

The $CaCO_3$ analyses performed on the marine sediment cores are a measure of the percentage of biogenic carbonate in each sample. All seven cores contained a consistently low percentage of $CaCO_3$ with less than 13% in each sample. The $CaCO_3$ content dropped by two to three percent directly above tephra horizons that are interpreted to be primary deposits. The samples above the tephra deposits in cores MD06-3003, MD06-3017 and Tan0810-11 show no significant difference in $CaCO_3$ content above the tephras compared to the samples below the tephra layers (Figs. A3, A4, A6), except for MD06-3017, which shows a 1% drop in $CaCO_3$ after the first Mamaku layer but no change after the upper two Mamaku layers. These cores are interpreted to contain tephras deposited by secondary depositional processes and contrast markedly with the $CaCO_3$ content observed in the cores with primary tephra deposits. The percentage of $CaCO_3$ in cores MD06-3009, -3008, Tan0810-3 and -12 is noticeably lower in the samples taken directly above each tephra deposit compared to the samples taken below (Figs. A1, A2, A5, 17).

The $CaCO_3$ content remains 2-3% lower for 1-2 cm above the tephra before returning to similar values as the samples collected below the tephra. The only exception is above the Mamaku tephra in core MD06-3009 where there is a 1-2% increase in the amount of $CaCO_3$ but here the tephra exists as a series of blobs, not a distinct layer.

2.4 Discussion

A detailed stratigraphy of the marine sediment cores is imperative for determining the depositional origins of the tephra deposits and surrounding sediment. Primary deposition in marine cores is the process of sediment settling through the water column and draping the ocean floor with no transportation once deposition has occurred. Conversely, secondary deposits are characterised by sediment transportation during or following deposition, often driven by gravity. The high sedimentation rates off the east coast of North Island are instrumental in preserving the tephra deposits in the marine cores. However, the large build up of sediment on the continental shelf can also cause large and frequent sediment gravity flows, most commonly turbidites, if a trigger or continental slope failure occurs. The most common triggers of turbidites are catastrophic floods and earthquakes. Less commonly, tsunamis, storm waves and large volcanic eruptions can also lead to sediment gravity flows (Pouderoux et al., 2012), the latter of which could have contributed to the multiple tephra layer deposits seen in cores MD06-3003, -3017 and Tan0810-11.

The Taupo and Mamaku tephras in MD06-3003 are both repeated approximately 10 cm apart. According to Pouderoux et al. (2012) the entire core is composed of 77% turbidite deposits. It is likely that either the upper tephra layer or both layers from the Taupo and Mamaku deposits were emplaced by a gravity-driven secondary depositional event (Lewis and Kohn, 1973). Either way the sediment above the tephras has been disturbed and the age of the hemipelagite relative to the tephra can not be considered reliable. In order to sample foraminifera on a sub-decadal timescale the sediment must be from a primary origin and the ages of the hemipelagite consistent. Tan0810-11 and MD06-3017 also contain tephra that are repeated in the core. In core Tan0810-11 the Taupo tephra is repeated once and in MD06-3017 the Mamaku tephra consists of three separate layers.

The remaining cores, MD06-3008, -3009, Tan0810-3 and -12, are interpreted to contain primary tephra deposits. The sharp basal contacts with the underlying sediment suggests a primary origin. Minor to heavy bioturbation in the overlying sediment distributes the tephra up the core, creating a generally gradational upper contact. Heavy bioturbation suggests hemipelagite is overlying the tephra, consistent with an interpretation of a primary tephra deposit. To confirm these interpretations grain size and $CaCO_3$ analyses were also performed on all sediment samples taken around the tephra horizons in each core.

The grain size and $CaCO_3$ analyses largely support the interpretations made from the stratigraphic observations of the marine cores and provide further information about the transportation and deposition of the tephra layers. Samples overlying the tephra layers in cores MD06-3008, -3009, Tan0810-3 and Tan0810-12 show a 2-3% drop in the percentage of $CaCO_3$ that remains for at least 2 cm above the tephra before steadily recovering to background levels. Results from Cobianchi et al. (2015) show a similar pattern, and suggest a rapid decrease in surface water pH could cause a period of increased dissolution of surface-dwelling organisms. Volcanic aerosols are highly acidic and their rapid dispersal across the surface of the ocean is interpreted to cause a short-term ocean acidification event (Cobianchi et al., 2015). Additionally, volcanic ash has been shown to cause a reduction in surface water pH through the release of acids but may also have the potential to increase primary productivity in surface-dwelling organisms through ocean fertilisation (Frogner et al., 2001, Jones and Gislason, 2008, Cobianchi et al., 2015). The reduction in $CaCO_3$ in the 2 cm above the tephra along with the gradual return to background levels agree with the findings of Cobianchi et al. (2015) that a decrease in surface water pH following the eruption could have increased dissolution rates for a period of time, reducing the amount of $CaCO_3$ reaching the ocean floor. However, there is no indication in our data that suggests an increase in primary productivity caused by the release of nutrients from the volcanic ash. Alternatively, or coeval with the dissolution, the lower percentages of $CaCO_3$ above the tephras interpreted to be primary in origin could be explained by bioturbation mixing the sediment overlying the tephra, extending

the dissolution affected sediment signal and in effect diluting the $CaCO_3$ signal.

Cores MD06-3003, -3017 and Tan0810-11 that showed characteristics of secondary depositional events in the stratigraphic analyses around and/or including the tephra deposits also display contrasting grain size and/or $CaCO_3$ results to the other cores. The absence of variation in $CaCO_3$ values across the tephra layers from MD06-3003 and Tan0810-11 agrees with the interpretation that the Taupo tephra in both cores and the Waimihia tephra in core MD06-3003 were emplaced by a secondary depositional process. The sediment overlying the tephra layers emplaced by secondary depositional processes could not be expected to show a change in $CaCO_3$ because the chronological order of the core has been disturbed. Cores MD06-3003 and Tan0810-11 were therefore discounted from further analyses because the sediment surrounding the tephra deposits is interpreted to have been disturbed, altering the stratigraphic order of the core.

Tephra deposits present in the form of dispersed blobs or non-distinct layers are also not surrounded by a variation in grain size or $CaCO_3$ percentage. The MD06-3009 Mamaku tephra deposit and the Taupo tephra in MD06-3017 appear in a section of the core but do not consist of a complete layer. The grain size results show no variation in grain size between the samples below the tephra and those above it. The $CaCO_3$ values also remain the same for MD06-3017 but show a slight increase after the tephra in MD06-3009. This suggests, that for volcanic ash to cause an increase in dissolution in the ocean surface, the tephra needs to be a distinct layer at least 1 cm thick in the core to have impacted the surface biota when it was dispersed into the ocean.

The increase in sand-sized grains immediately above the tephra horizons in cores MD06-3008, -3009, Tan0810-3 and -12 is likely caused by bioturbation. The Taupo tephra deposits from Tan0810-3 and -12 show a spike in grain size directly above the tephra deposit that gradually returns to background levels after 2-3 cm. Benthic fauna can burrow into the overlying sediment, reworking the substrata and causing a disruption of deposited layers. The presence of bioturbation above the tephra hori-

zons suggests the eruption did not produce a sufficient volume of ash to completely smother the benthic fauna. Hess and Kuhnt (1996) reveal a distinct absence of benthic fauna above areas where the tephra is 6 cm thick. Therefore, the tephra in these marine cores is unlikely to have been originally deposited more than 6 cm thick.

It is difficult to ascertain how much bioturbation has occurred above the Taupo tephra deposit in Tan0810-3. It is unlikely the tephra was originally deposited 9.5 cm thick based on the presence of bioturbation in the overlying sediment and the percentage of $CaCO_3$ being only approximately 1% lower above the tephra compared to below. If it was 9.5 cm thick when it was first deposited it would most likely have destroyed all benthic fauna for at least a few years after the eruption, preventing bioturbation (Hess and Kuhnt, 1996). Additionally, if this volume of ash was erupted and deposited on the surface of the ocean, a much larger drop in $CaCO_3$ would be expected based on our interpretation, from the Cobianchi et al. (2015) hypothesis, that the ash could cause a rapid drop in the pH of the surface of the ocean, dissolving the carbonate tests. The tephra also appears to contain hemipelagic silt, suggesting bioturbation has caused the tephra to be dispersed over a greater thickness.

Tephras in cores MD06-3008, -3009 and the Waimihia deposit in Tan0810-3 show an increase in sand-sized grains above the tephra horizon that do not return to background levels at the furthest extent of the samples. The samples above the Taupo tephra in MD06-3008 and -3009 were sieved to determine the composition of the >63 μm size fraction. The >63 μm fraction of all samples above the tephra was largely composed of tephra. The samples extend 6 cm above the tephra in core MD06-3008 and 12 cm in MD06-3009. The presence of ash up to 12 cm from the tephra deposit suggests either heavy bioturbation reworked a significant amount of tephra into the overlying sediment, a turbidite deposit emplaced ash-rich sediment above the tephra layer or a source of tephra in a surrounding area constantly fed into the sediment at the core location. In any case the overlying sediment has been significantly disturbed and therefore can not be used for Mg/Ca analyses of foraminifera. In Tan0810-12 the Taupo tephra is distinct, with grain size analyses

indicating minimal bioturbation.

2.4.1 Temporal resolution

The location of East Cape, adjacent to the active Hikurangi subduction margin, subjects the area to a large amount of tectonic activity. The subduction of the Pacific Plate beneath the Australian plate is uplifting the Raukumara Ranges at ∼3 mm/yr (Clark et al., 2010). This activity, combined with the moderately high rainfall in the area and easily eroded mudstone that dominates the lithology of the ranges, contributes to the high sedimentation rates observed in the marine sediment cores (Hicks et al., 2003, 2011). The rapid high discharge of sediment of the East Cape to Hawke Bay region, is instrumental in preserving the tephra layers in the cores and reducing the amount of bioturbation that distributes the tephra throughout the core. A high sedimentation rate is paramount in order to sample on the sub-decadal time scale necessary to observe the response of marine fauna to the volcanic event. 0.5 cm is the lowest practical sampling limit for these marine cores, restricting the time scale to rely on a high sedimentation rate to produce a high temporal resolution record. MD06-3009, -3017, Tan0810-11 and -12 have sufficient average sedimentation rates to be sampled at a decadal to sub-decadal resolution. However, with cores MD06-3009, -3017 and Tan0810-11 discounted from further analyses because the sedimentation rates of these cores can't be considered accurate, Tan0810-12 provides the best opportunity. Based on the sedimentation rates calculated for Tan0810-12, the 0.5 cm samples above the Taupo tephra correspond to a time frame of 6.6 years. Below the tephra deposit the samples equate to a resolution of 5 years.

2.5 Conclusion

Stratigraphy can provide information about the origin of a sedimentary sequence and how it has been altered post-deposition. The combination of stratigraphy and sedimentation rates within the core enable time to be applied to changes in the stratigraphic record. Grain size and $CaCO_3$ analyses can be used to make interpretations on the origin of sedimentary deposits. In this study, spikes in sand-sized particles above the tephra deposits are interpreted to be a factor of bioturbation. $CaCO_3$ analyses reveal a drop in the percentage of $CaCO_3$ directly above the tephra

deposits in various cores. This is interpreted to have been caused by the volcanic aerosols and ash falling on the surface of the ocean and rapidly reducing the pH of the sea surface, agreeing with the interpretations of Cobianchi et al. (2015). A drop in pH would lead to increasing dissolution of $CaCO_3$ and less accumulation on the ocean floor. Therefore, a tephra is determined to be primary in origin if the percentage of sand-sized sediment increases above the tephra and the percentage of $CaCO_3$ decreases. Cores containing repeated tephra layers with no change in grain size and/or the percentage of $CaCO_3$ above the tephra deposits suggest the stratigraphic order for the corresponding sections in those cores have been disturbed.

The sediment surrounding the tephra layers in cores MD06-3003, MD06-3017 and Tan0810-11 suggests these sections of the cores have been disturbed. The repetition of tephra layers and absence of change in grain size and/or $CaCO_3$ content above the tephra deposits discount these cores from further analyses because in order to understand if foraminifera can be used to determine changes in SST through time following a volcanic eruption, the stratigraphy of the core needs to remain in order of deposition. Cores MD06-3009 and MD06-3008 are also discounted from further analyses because grain size and $CaCO_3$ results indicate the sediment above the tephra deposits either do not reveal a drop in $CaCO_3$ content or the sediment remains significantly coarser than before the tephra and does not return to background levels, suggesting bioturbation has likely significantly disturbed the sediment. Sedimentation rates in core Tan0810-3 change dramatically throughout sections of the core and are too low to produce a temporal resolution on a sub-decadal scale. Between the Waimihia and Taupo tephra deposits the sedimentation rate suggests each 0.5 cm sample equates to $\sim$45 years and therefore discounts this core from further analyses. Core Tan0810-12 will be used for further analyses based on a high sedimentation rate that enables sub-decadal scale sampling, a distinct tephra layer 3cm thick and evidence of primary ash deposition from the brief increase and decrease in grain size and $CaCO_3$ content, respectively, directly above the tephra that then return to background levels suggesting minimal disturbance from biological activity. Core Tan0810-12 will be used for analyses of foraminifera tests from the sediment surrounding the Taupo tephra to determine if this method can be used to obtain a SST

record following this large silicic eruption.

3 Foraminiferal analyses

Analysing foraminifera tests either by solution-based geochemical methods or using a laser ablation in situ technique, can provide information about the chemistry of the ocean during the lifetime of the foraminifera. Species inhabit specific ecological zones in the ocean with each species preferring different environmental conditions that provide them with the most amount of energy to grow and reproduce. Rapid changes to these conditions cause stress and this can be observed in the number of individuals, morphology or size of the tests.

In this study, the chemistry of foraminifera tests is analysed in order to determine if foraminifera can be used to obtain a SST record following a large silicic volcanic eruption. In doing so, the population, morphology and size of the foraminifera tests are analysed to test if these features can indicate a change in the marine environment through the ability of the foraminifera to grow and reproduce. Additionally, the morphology and size of the tests aid the interpretation of the chemistry. SEM images were taken of the collected tests to categorise their size and shape. LA-ICP-MS was then used to investigate the Mg/Ca concentrations of the tests, and SSTs of the ocean before and after the Taupo tephra in marine core Tan0810-12.

3.1 Methods

3.1.1 Sieving and picking foraminifera

The sediment surrounding the Taupo tephra horizon in Tan0810-12 was prepared and picked for foraminifera tests. Approximately 2 g of sediment from each 0.5 cm sample was placed in a container with deionised water overnight to disaggregate the grains. The sample was then washed through a 63 μm sieve to separate the mud and sand-sized fractions. Deionised water in a spray bottle was used to clean the >63 μm sample fraction and wash through any remaining mud. The <63 μm size fraction was left to settle for 2-3 days before the water was siphoned off and the mud was left to dry. The >63 μm size fraction was placed in filter paper in a foil container and dried in an oven at 50°C overnight. Once dry, both size fractions were weighed separately, and values recorded to 3 decimal places, in order to determine

the foraminifera population densities in each sample.

The two planktic foraminifera species picked from Tan0810-12 were *G. bulloides* and *G. ruber*. These species were selected for trace element chemistry because they are common in waters NE of New Zealand and previous studies from Marr (2009) and Bolton (2011), who also used LA-ICP-MS methods, were able to determine Mg/Ca temperature calibrations for these species. Additionally, both species have a near-surface habitat and were the second most abundant in the samples. The most abundant species at this location was *Globoconella inflata*, however, Marr (2009) could not determine any correlation between Mg/Ca and temperature for this species. The temperature calibrations determined for these species are specific to New Zealand waters (Marr, 2009, Bolton, 2011). The dry >63 μm size fraction of each sample was placed on a tray and observed under a binocular microscope. All samples around the chosen tephra contained <8% $CaCO_3$ so every identified *G. bulloides* and *G. ruber* test was picked using a paintbrush dipped in deionised water. Between 0 and 14 foraminifera of each species were present in each sample.

3.1.2 Preparation for SEM and LA-ICP-MS

The cleaning of the picked foraminifera tests consisted of agitating each test in three rinses of Milli-Q to remove surface contaminants. Ultrasonication of foraminifera tests is a common cleaning method to remove detrital particles (Eggins et al., 2004, Numberger et al., 2009, Bolton, 2011, Sadekov, 2008). In this case the shells were too weak and ultrasonication caused the test specimens to break, therefore this technique was not used. Instead, the tests were placed in a container with Milli-Q and shaken vigorously. The foraminifera were then pipetted out of the container and on to a clean watch glass while the Milli-Q was discarded and the container refilled with clean Milli-Q. The same foraminifera tests were placed back in the container to agitate them again. This process was repeated three times. After the third rinse the excess Milli-Q was pipetted off and the foraminifera were placed on a clean watch glass to dry. Four strips of carbon tape were placed on each of two glass microscope slides and the foraminifera were transferred from the watch glass on to the tape. For *G. ruber* all specimens from each of the 20 0.5 cm samples were transferred on

to the carbon tape. For *G. bulloides* each specimen from 10 samples immediately either side of the tephra layer were used.

Three layers of carbon coating were applied to the slides to improve conductivity and image resolution on the SEM. The glass slides were attached to a stub and left in a vacuum desiccator for 40 hours to remove any moisture from the tape or samples. Each individual foraminifera from both species was imaged using a JEOL JSM-6610LA, housed in the School of Chemical and Physical Sciences at Victoria University of Wellington, using secondary electron imaging. Images were checked for evidence of dissolution and surface contaminants. Those that still showed a presence of detrital material on the test surfaces were removed from the carbon tape, agitated further in Milli-Q and remounted. Test size was also calculated using the SEM, determined by measuring the longest length from the top of the f chamber to the bottom of the f-1 or f-2 chamber for *G. ruber* (Fig. 18a) and from the top of the f chamber to the bottom of the f-2 chamber for *G. bulloides* (Fig. 18b).

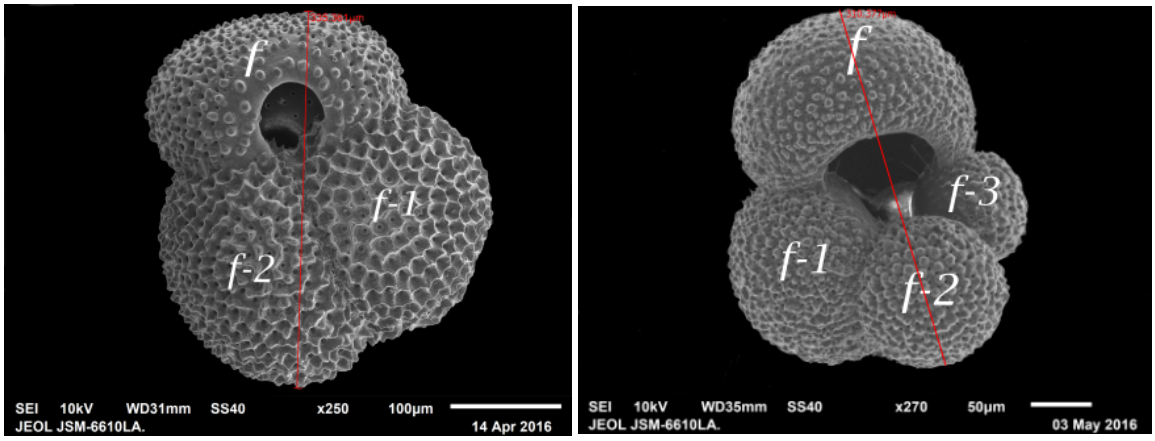

(a) *G. ruber* (b) *G. bulloides*

Figure 18: SEM test size measurements for (a) *G. ruber* and (b) *G. bulloides*. f is the final chamber, f-1 the penultimate, f-2 the antepenultimate and f-3 the preantepenultimate chamber.

The final chamber of each *G. ruber* was cracked off using a fine pointed scalpel before the glass slide was recoated with carbon and the foraminifera imaged a second time using the SEM. This was to observe the internal structure of the foraminifera test and to ensure the inside of the chamber was also free of detrital material that could cause contamination. It also exposes the inner surface of the test, allowing

the laser to ablate from the inside of the test outward to avoid the interference of surface topography (G. Dunbar, pers. comm., 2016). *G. bulloides* was not cracked open due to the fragility of their tests and were instead lasered from the outside in.

3.1.3 LA-ICP-MS trace element analysis

The trace element ratios of the foraminifera were measured using a Resonetics S155-SE, 193nm excimer laser ablation system coupled with an Agilent 7500CS ICP-MS from the School of Geography, Environment and Earth Sciences at Victoria University of Wellington. The final chamber was analysed on *G. ruber* by lasering from the inside of the chamber out and the f-2 chamber was analysed for *G. bulloides* by lasering from the outside in. The trace element masses measured were ^{11}B, ^{24}Mg, ^{25}Mg, ^{27}Al, ^{43}Ca, ^{44}Ca, ^{47}Ti, ^{49}Ti, ^{55}Mn, ^{66}Zn, ^{88}Sr and ^{138}Ba.

Prior to ablating the samples the laser was tuned using the National Institute of Standards and Technology (NIST)610 tuning standard and a NIST610 standard was run at the start and end of every analytical sequence and after every five foraminifera. The laser was set to ablate with a repetition rate of 1.5 Hz, 25% attenuation, a laser beam energy of 2 mJ and a 25 μm spot size. These were the lowest settings that could be used and still produce a good quality signal. The tests were very thin in places so low laser beam settings were used to prolong the signal in order to give the best possible results.

Prior to ablation, three cleaning pulses were fired on most tests, with a spot size of 35 μm, to remove any surface material that was present on the inside of the test chambers. Only one cleaning pulse was used for the foraminifera with thinner final chambers. A total of 1-4 spots were made on each foraminifera chamber. This value was dependant on the size and fragility of the chamber.

Following the LA-ICP-MS analyses, the data were processed through Iolite, a software package developed for analysing data obtained by laser ablation. The trace element data were background corrected and normalised to an internal standard. ^{43}Ca was used for the internal standard and ^{44}Ca was measured for internal monitoring.

Outliers greater than 3 SE are automatically discounted by the Iolite processing system. Once the trace element data had been background corrected and outliers were discounted, trace element to calcium ratios were calibrated using the NIST610 analyses and the most recently published elemental concentrations of NIST610 (Jochum et al., 2011). Samples containing abnormally high counts of ^{27}Al, ^{47}Ti, ^{88}Sr and ^{55}Mn were removed to ensure no contaminated samples were included with Al and Ti indicative of detrital material, Mn indicating the presence of most likely $MnCO_3$ and Sr, a robust element that if abnormal likely indicates the more easily affected Mg will be contaminated. The threshold values used to screen for contamination were adopted from Boyle (1983), Marchitto et al. (2007) and Lear et al. (2015) with samples containing Al/Ca and/or Mn/Ca values above 100 μmol/mol discounted.

The *G. ruber* Mg/Ca values, once standardised, were converted to temperature estimates using the southwest Pacific Ocean chamber specific calibration determined by Bolton et al. (2011). The calibration for the final chamber of *G. ruber* is Mg/Ca (mmol/mol) = $0.590e^{0.072T}$. For *G. bulloides* the temperature calibration for the *f*-2 chamber, Mg/Ca (mmol/mol) = $0.955e^{0.068T}$, was used, adopted from Marr et al. (2011). The results obtained for each individual spot were averaged over every chamber and the chamber results were then averaged for each sample.

3.2 Results

3.2.1 Species population

The total number of individual foraminifera per total weight of each sample was calculated for *G. ruber* and *G. bulloides* from Tan0810-12 to determine an unbiased population count. Every identifiable foraminifera was collected and counted from these species for the portion of every sample above the 63 μm size fraction. Below the Taupo tephra horizon *G. ruber* and *G. bulloides* follow a similar population trend. *G. ruber* shows a highly fluctuating pattern but there is no overall increasing or decreasing trend observed (Fig. 19a). *G. bulloides* has a similar fluctuating pattern but has overall a very slight decreasing trend from the bottom of the core towards the tephra (Fig. 19c). Above the ash layer the population trends change significantly. The two samples immediately above the tephra contain neither *G.*

ruber nor *G. bulloides* and the third and fourth samples contain no *G. bulloides* and *G. ruber*, respectively. From these points, both species follow a similar continuously fluctuating pattern but overall increasing trend, particularly for *G. bulloides*. However, ∼85 years above the tephra horizon *G. ruber* begins a decreasing trend that continues until the end of the samples while the number of *G. bulloides* continues to increase (Figs. 19a, c). The total number of specimens of *G. ruber* in the 20 samples above the tephra horizon (55) is almost half of the number in the 20 samples below the tephra (109). The opposite occurs for *G. bulloides*, there are approximately 20% more specimens above the tephra horizon than there are below it.

3.2.2 Foraminifera test size

The size of the foraminifera tests for both species were measured using the SEM as the distance from the top of the final chamber to the bottom of the f-1 or f-2 chamber for *G. ruber* and the bottom of the f-2 chamber for *G. bulloides*. Every foraminifera from all 40 samples was measured for *G. ruber* while the foraminifera from only 20 samples, 10 above the tephra and 10 below, were measured for *G. bulloides*. The test sizes measured for individual foraminifera were averaged per sample to determine any change in test size through the core. *G. ruber* tests fluctuate between 190 and 323 μm in size below the tephra and similarly above the tephra with sizes between 187 and 323 μm (Fig. 19b). The test sizes directly above the tephra horizon are the only samples that show any variation from the average trend. The samples above the Taupo tephra show a prolonged trend of small test sizes, with sample averages between 187 and 223 μm, compared to the rest of the core where the sizes fluctuate. The sizes remain small until ∼60 years after the eruption before they return to similar values to those seen below the tephra.

G. bulloides shows a different trend in test size to *G. ruber*. Only 20 samples were analysed for *G. bulloides* using the SEM, resulting in half the number of test size values than *G. ruber*. A total of 64 individual *G. bulloides* tests were measured, and averages taken for each sample. The *G. bulloides* tests begin very slightly below pre-eruption sizes before a rapidly increasing trend occurs in size ending in larger test sizes than those observed below the tephra, an opposite trend to *G. ruber* tests

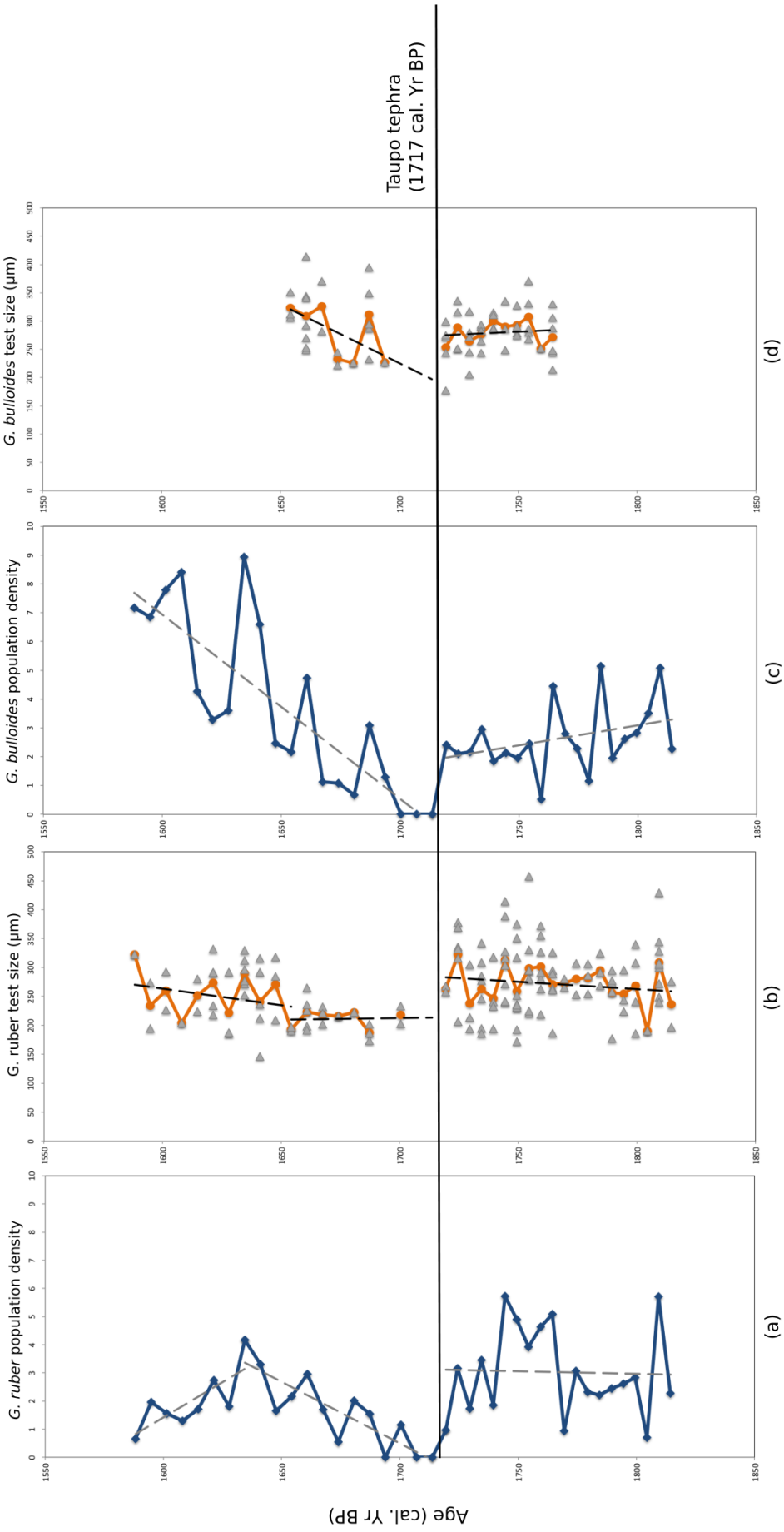

Figure 19: Population densities and test sizes of *G. bulloides* and G. ruber around the Taupo tephra in core Tan0810-12. (a) and (c) are the population densities, respectively, for *G. ruber* and *G. bulloides*. The population densities are compared to the test sizes for (b) *G. ruber* and (d) *G. bulloides*. Test sizes (µm) were measured using the SEM for (a) *G. ruber* and (b) *G. bulloides*. The grey triangles are the individual measurements for every foraminifera. The orange line connects the average test sizes determined by averaging the individual foraminifera values for each sample. Grey and black dashed lines represent the data trends before and after the Taupo eruption.

(Fig. 19d). When comparing each individual foraminifera, before the sample average, the tests below the tephra vary between 177 and 371 μm. Above the tephra the test size values are between 221 and 414 μm.

3.2.3 Test morphology

The morphology of foraminifera tests was analysed in conjunction with trace element geochemistry to ensure the Mg/Ca analyses would not be affected by abnormal test morphologies and to assess any impact of proximity to tephra on *G. ruber* and *G. bulloides* test morphology. The SEM images of *G. ruber* tests reveal various morphologies throughout the core, both on chamber surfaces and within the chambers. *G. bulloides* however, did not appear to display any abnormal morphologies anywhere in the sampled core section. Eight *G. ruber* tests were coated with a surface layer of euhedral crystals (Fig. 20). This microcrystalline surface texture caused a thickening of the test wall in all cases, and appears to cover many of the pore holes on the outside of the chambers, observed by comparing the test surface to a 'normal' test (Fig. 20). The distribution of the foraminifera with this morphology appears to be random throughout the core, suggesting the cause is unlikely to be related to the tephra deposit.

The *G. ruber* tests coated in euhedral crystals showed variable and abnormal element/Ca concentrations. The presence of this microcrystalline texture on the surface of the tests was used to exclude the tests from the Mg/Ca temperature calculations. However, conversely, the laser ablation analyses can provide information on the origin of this morphological feature because of the direct in situ nature of this analytical technique. Two out of the eight tests containing euhedral crystals displayed what would be expected from an $MnCO_3$ coating, high Mg/Ca values, Mn/Ca values over 100 μmol/mol and slightly abnormal Sr/Ca concentrations. However, of the remaining six, two disintegrated when broken open and four showed distinctly different elemental concentrations. Three of these were very high in Mg/Ca with values up to 3000 μmol/mol but contained low to average Mn/Ca values around 10-20 μmol/mol and standard Sr/Ca values. The final test varied extensively between laser spots, displaying Mg/Ca values under 1000 μmol/mol and over 2500

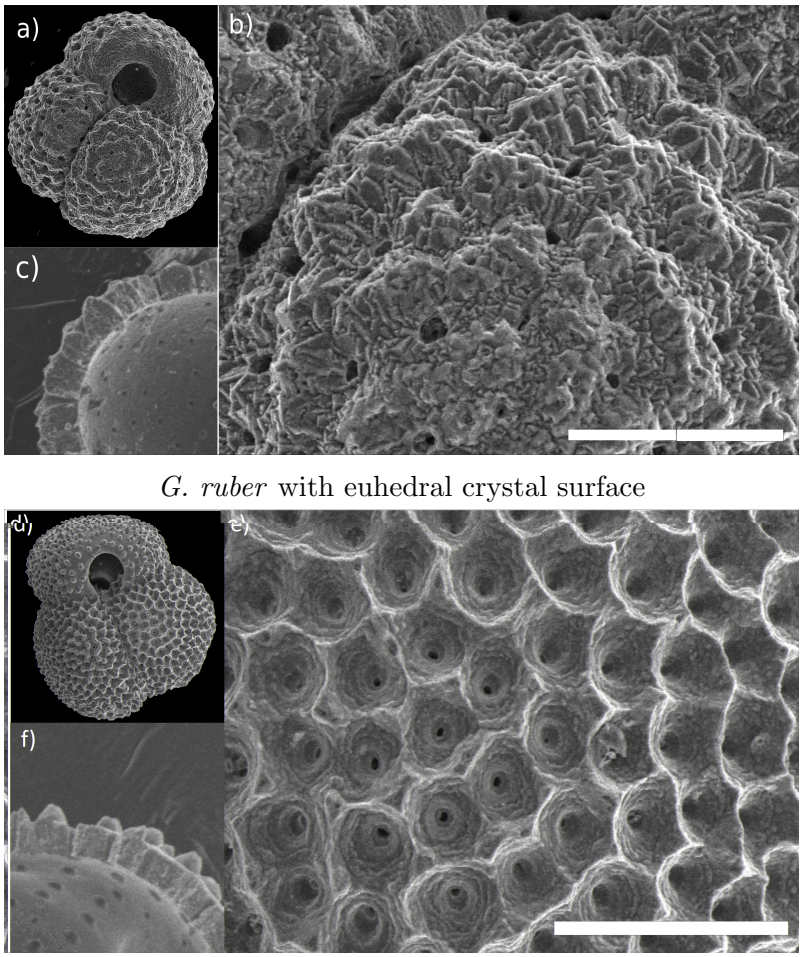

G. ruber with euhedral crystal surface

G. ruber 'normal' test surface

Figure 20: SEM image of a *G. ruber* test coated with euhedral crystals compared to a *G. ruber* with a 'normal' test surface. a) and d) are the SEM images of the outside of the foraminifera with b) and e) close-up views of the test surfaces. c) and f) are taken from the SEM images of the same foraminifera with the final chambers broken open and show the slight thickening of the test wall for the test displaying euhedral crystals. b) scale bar represents 20 µm. e) scale bar represents 50 µm.

µmol/mol and low Mn/Ca values for both. The presence of high-Mg calcite on the surface of these tests highlights the importance of identifying and removing these tests prior to performing geochemical analyses using Mg/Ca as a temperature proxy.

Several of the *G. ruber* tests also appeared to contain kummerforms, a term used to describe diminutive chambers that form, for this species, on the external test surface (Fig. 21). Seven foraminifera displaying a kummerform chamber were distributed randomly throughout the core, also suggesting the tephra event did not contribute to their formation.

Laser ablation geochemical analyses were completed on the tests containing kummer-

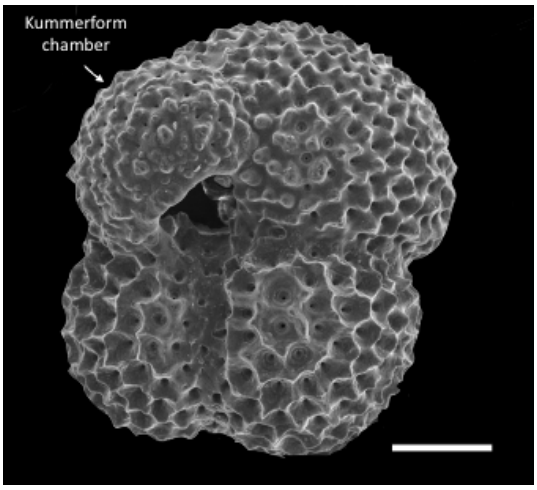

Figure 21: SEM image of a *G. ruber* test containing a kummerform. Scale bar represents 50μm.

forms to determine the origin of this morphology, but were also not included in the Mg/Ca temperature calculations. The aim for the kummerform bearing foraminifera was to detach the small chamber and laser it from the inside out. In many cases the kummerforms did not produce a determinable signal but in three cases data were able to be collected. Additionally, the final normal-sized chambers were analysed, even where data could not be obtained for the kummerform. The three kummerform chambers contained low Mg/Ca values between 800 and 1300 μmol/mol. Low Mg/Ca values for the kummerform could be explained by the chamber forming in colder waters, found deeper in the water column. Conversely, the final normal-sized chambers from the same specimens produced higher Mg/Ca concentrations than the final chambers of the normal-form foraminifera, around 1800-2500 μmol/mol compared to ∼1000-1600 μmol/mol, suggesting the kummerform chambers are likely to be the final chamber that has most likely not formed to true size.

3.2.4 Mg/Ca temperatures

G. ruber and *G. bulloides* were analysed for Mg/Ca concentrations using the LA-ICP-MS for every sample collected from Tan0810-12. Every foraminifera was analysed in the samples including those with abnormal morphologies. These abnormal foraminifera were not included in the final Mg/Ca temperature results but were still analysed in order to provide information on the origin of these morphologies. The test sizes of *G. ruber* and *G. bulloides* were compared to the Mg/Ca results to ensure

the Mg/Ca ratios were not biased based on the conclusions reached by Elderfield et al. (2002) that an increase in test size is correlated with an increase in Mg/Ca concentrations within the tests.

A total of 112 individual *G. ruber* tests produced stable signals with 33 of these above the Taupo tephra and 79 below. The Mg/Ca values ranged from 814 μmol/mol to 3571 μmol/mol, indicating various tests contained significant contamination or dissolution. Once the samples containing elevated concentrations of Al/Ca, Ti/Ca, Mn/Ca and Sr/Ca were removed, to exclude contaminated specimens, only 11 individual foraminifera remained above the tephra horizon from six different samples. Below the tephra there was sigificantly less contamination with 50 foraminifera considered reliable from 15 different samples (Fig. 22a). No reliable results could be calculated on *G. ruber* tests in the ∼50 years directly after the Taupo eruption. The tests were either coated in the euhedral crystals, full of foreign material with high Al/Ca and/or Mn/Ca values within the chambers or they appeared brittle and crushed easily when broken open.

The tests directly above the tephra deposit that appeared brittle and often disintegrated in parts during the attempt to break the final chamber open contained abnormally high concentrations of Mg/Ca, ∼2500-3000 μmol/mol compared to the average concentrations of uncontaminated tests that were ∼1300 μmol/mol. The Al/Ca concentrations were below 100 μmol/mol for most samples but approximately four showed very high values of 400-5000 μmol/mol. Mn/Ca concentrations were also slightly high around 50-100 μmol/mol. One of the benefits of LA-ICP-MS is the ability to still obtain uncontaminated results from tests that may only be contaminated in small areas. However, for the tests directly above the tephra, all three laser ablated spots on the chambers produced results indicating the presence of contamination. The high Mg/Ca, Al/Ca and Mn/Ca values are unlikely to be caused by contamination from the tephra because of its rhyolitic composition, meaning it contains very low concentrations of Mg and Mn compared to basalt so it would not significantly elevate the concentrations of these values in the foraminifera tests. Rhyolite is high in Al but only four of the tests revealed high Al/Ca values. This

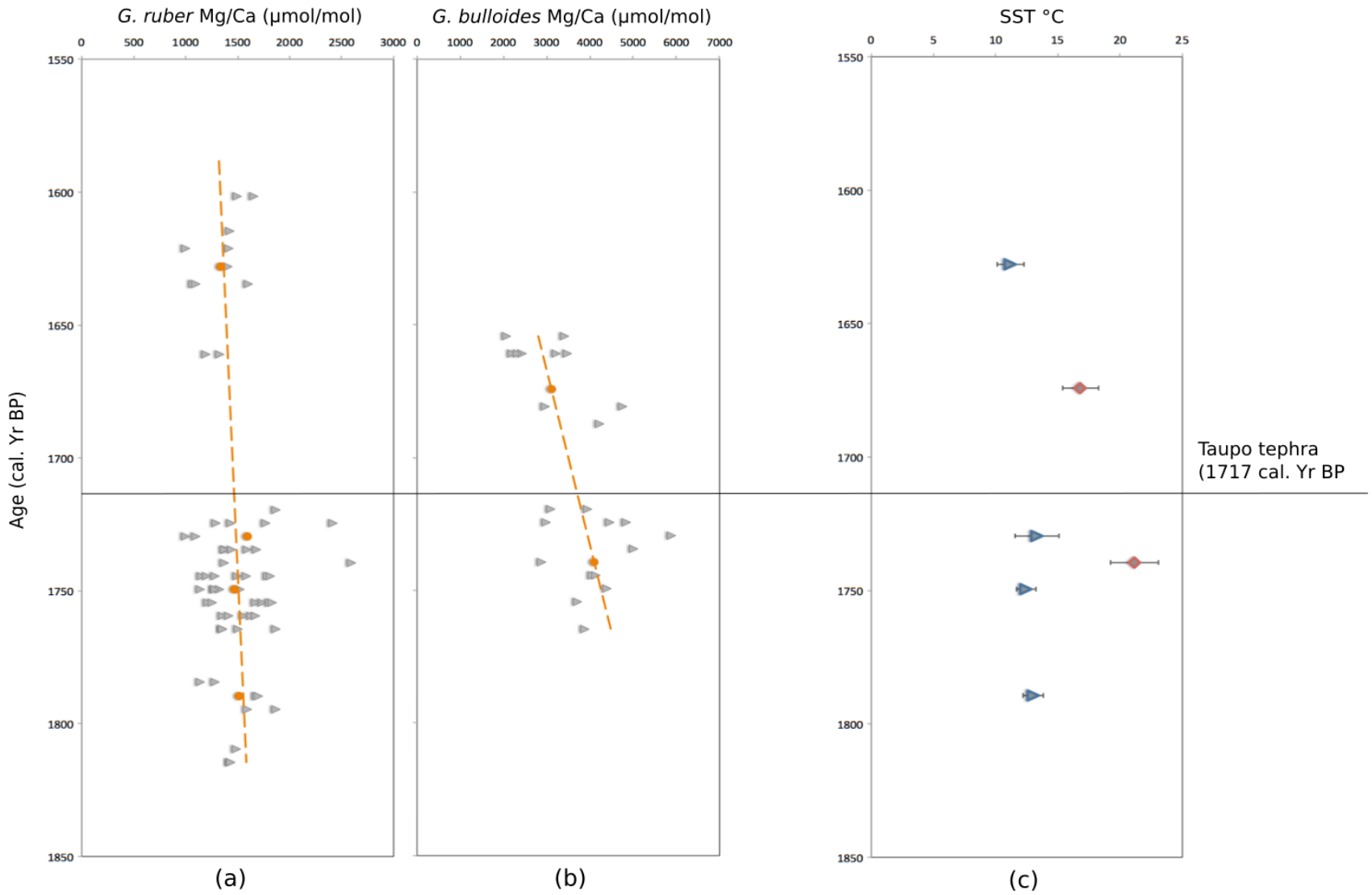

Figure 22: Mg/Ca ratios in µmol/mol for (a) *G. ruber* and (b) *G. bulloides* from Tan0810-12. Grey triangles represent Mg/Ca ratios for the individual foraminifera from Tan0810-12 samples. The orange circles are the averages of the Mg/Ca ratios of the collective individual foraminifera. (c) SSTs derived from the average Mg/Ca ratios for *G. ruber* (blue) and *G. bulloides* (red).

is contrary to the hypotheses of Lea et al. (2005) that suggest volcanic shards can cause elevated Mg/Ca and trace element values. However, the study area used by Lea et al. (2005) contains basaltic volcanic debris, which is high in Mg and Mn but low in Al. Dissolution is also unlikely to be the primary cause of test fragility in this case because it typically dissolves the Mg-rich areas of the tests first, leading to abnormally low Mg/Ca values (Hecht, 1976, Rosenthal et al., 2000). These samples were removed from the final results because without a known exact cause of contamination, and due to the entire chamber indicating the presence of contamination, it is not possible to remove the contaminated signal and reproduce the real Mg/Ca concentration and estimate SST.

Mg/Ca analyses of *G. bulloides* were only conducted on 10 samples above and below the tephra. The 10 samples above the tephra contained 17 individual *G. bulloides* tests while there were 28 tests in the 10 samples below. Mg/Ca values for *G. bulloides* were substantially higher than *G. ruber* with the minimum and maximum concentrations of 1437 and 8735 μmol/mol respectively, prior to the removal of contaminated tests (Fig. 22b). The same procedure for removing contaminated samples was used for *G. bulloides* as *G. ruber* with the ablated spots containing Al/Ca and/or Mn/Ca values above 100 μmol/mol discarded. Samples with elevated Sr/Ca and Ti/Ca were also monitored but these usually coincided with high Al/Ca or Mn/Ca values. Once the foraminifera considered to be contaminated were removed, 10 reliable *G. bulloides* tests remained above the tephra and 13 tests below (Fig. 22b). This shows an opposite trend to *G. ruber* where distinctly more samples were removed above the tephra than below, particularly directly above the tephra horizon. For *G. bulloides* more samples were removed from below the tephra, while those directly above did not seem to be impacted by the tephra in the way the *G. ruber* tests were. This further suggests the tephra did not contribute to the elevated Mg/Ca values observed in the *G. ruber* tests directly above the tephra because it is unlikely only the *G. ruber* tests would be altered.

The temperature calibrations adopted for *G. ruber* and *G. bulloides* are both chamber specific for these species and regionally specific to the southwest Pacific Ocean

(Marr, 2009, Bolton, 2011). Ideally at least 20 individual foraminifera would be used to calculate each temperature value from Mg/Ca concentrations in order to reduce the error and account for seasonal change (Sadekov, 2008). In this case, based on the availability of reliable foraminifera, Mg/Ca analyses for 10 to 18 foraminifera were averaged to determine temperatures above and below the Taupo tephra horizon. For *G. ruber* three temperatures could be determined below the tephra based on the 50 reliable foraminifera present. The three average Mg/Ca values, 1516, 1465 and 1593 µmol/mol, were converted to mmol/mol and calibrated using the equation Mg/Ca (mmol/mol) = $0.590e^{0.072T}$. The SSTs produced were 13.0 ± 0.8°C, 12.4 ± 0.8°C and 13.3 ± 1.8°C, respectively (Fig. 22c). Above the tephra deposit the average Mg/Ca value for the 11 *G. ruber* tests was 1335 µmol/mol that was calibrated using the same equation to produce an SST of 11.2 ± 1.1°C.

G. bulloides shows a similar trend to *G. ruber*. Two temperatures were able to be determined, one below and one above the tephra, from the 25 *G. bulloides* tests. The average Mg/Ca values were 4100 µmol/mol and 3106 µmol/mol for all samples below and above the tephra, respectively (Fig. 22b). Using the calibration determined by Marr et al. (2011), where Mg/Ca (mmol/mol) = $0.955e^{0.068T}$, the Mg/Ca values were converted to SSTs and produced temperatures of 21.1 ± 1.5°C and 16.8 ± 1.9°C below and above the tephra, respectively (Fig. 22c). A drop in temperature above the tephra occurs for both *G. ruber* and *G. bulloides*, however, the *G. bulloides* values are significantly higher than *G. ruber*. This could be caused by a number of factors related to their different ecological habitats and biological responses to temperature.

Test size was not an influencing factor in the temperature results throughout the core. Studies have shown a strong response of increasing Mg/Ca values, and therefore temperature, with increasing test size (Elderfield et al., 2002). This can cause a bias if the test sizes vary extensively across the data. In this case every *G. ruber* and *G. bulloides* test used for Mg/Ca temperature analysis was compared with its correlating test size to ensure there was no trend in the data that suggested the results could be biased based on this relationship. Both *G. ruber* (Fig. 23a) and *G.*

bulloides (Fig. 23b) show a very slight negative trend, suggesting, that if anything, the larger tests were displaying slightly lower temperatures than the smaller tests, opposite to the findings of most studies for these species. However, the test sizes used in this study are within a relatively narrow margin, meaning they would not be expected to show a distinct trend, which correlates with the data as the negative trend is effectively negligible.

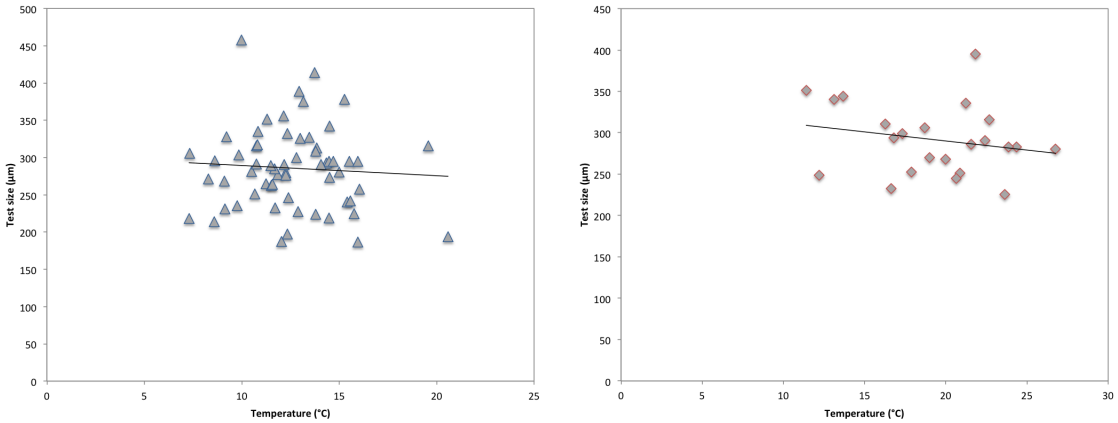

(a) *G. ruber* (b) *G. bulloides*

Figure 23: SEM test size measurements for (a) *G. ruber* and (b) *G. bulloides* versus sea surface temperature.

3.3 Discussion

Recent studies conducted on the impacts of volcanic eruptions on ocean temperatures are largely dominated by climate modelling. Few studies directly measure the changes in ocean temperature after a volcanic event, causing a major blind spot in how volcanism is factored into climate models and the role volcanism will play on Earth's climate in the future. Core Tan0810-12 potentially provides a unique, high temporal resolution insight into whether the effects of large-scale volcanic eruptions on sea surface temperatures can be measured in the preserved tests of specific foraminifera species. Observations of foraminifera tests also provide insight into the responses of these species to a changing environment and the preservation effects of volcanic ash on the foraminifera tests. Various morphological features discovered on several of the *G. ruber* tests also contribute to developing a more robust understanding of these organisms in order to further constrain and understand Mg/Ca as a paleothermometer.

3.3.1 Species population

The measured population densities of *G. ruber* and *G. bulloides* in Tan0810-12 are both distinctly different before and after the Taupo tephra and between the two species. Below the tephra horizon both *G. ruber* and *G. bulloides* are present in relatively similar abundances. The 2 cm (∼26 years of deposition) immediately above the tephra contains only 2 individual foraminifera of each species. Above this section, *G. ruber* numbers increase to nearly the same levels seen below the tephra before gradually decreasing again. However, the number of *G. bulloides* tests per sample continuously increases in a fluctuating pattern to levels above those seen below the tephra deposit.

The ∼26 years of deposition above the tephra deposit that contains little to no foraminifera is likely barren due to the strong acidity of volcanic ash causing fragility and dissolution of the carbonate tests (Cobianchi et al., 2015). Above this point dissolution does not appear to have any impact on test preservation based on the rapid increase in the populations of *G. ruber* and *G. bulloides* and the percentage of $CaCO_3$ in each sample, returning to background levels after ∼50 years after the eruption. Dissolution after the initial deposition of tephra through the water column should not be an issue based on the depth of the core at 1255 m, well above the lysocline and the CCD, estimated to be at a depth of around 4000 m NE of New Zealand (Bostock et al., 2011). The opposite responses of *G. ruber* and *G. bulloides* populations above the volcanic ash deposit suggest the sparsity of *G. ruber* is unlikely to be related to preservation issues in the 10 cm sampled section of the core above the tephra. The increasing and decreasing population densities for *G. bulloides* and *G. ruber*, respectively, may therefore be caused by the differing responses of these species to a change in their surrounding environment.

The impacts of large volcanic eruptions on the atmospheric climate are well-known. At the ocean-atmosphere interface, there is a strong interaction between the troposphere and the upper ocean, constantly transferring heat, water and momentum (Manabe et al., 1991). Changing the atmospheric climate by way of a large volcanic eruption is therefore likely to impact the surface temperature of the ocean,

and potentially deeper layers over time. Foraminifera are extremely sensitive to changes in their local habitats, primarily controlling their abilities to reproduce and grow effectively. Peak productivity for *G. ruber* occurs at temperatures between 21 and 29°C while *G. bulloides* prefers distinctly colder temperatures from 3 to 19°C (Bé and Tolderlund, 1971). The modern average annual temperature at core site Tan0810-12 is ∼18°C with the seasonal variation extending to 17°C in winter and 20°C in summer, and has likely been within 2°C of these temperatures for at least the past 2000 years (Loehle, 2007). 18°C is already below the peak productivity temperature for *G. ruber*, reflected by the relatively low abundance of this species in the record. Volcanic eruptions are known to reduce the amount of radiation reaching the Earth's surface, cooling the temperature of the troposphere for several years (Cole-Dai, 2010, Robock, 2000). Based on the constant transfer of heat between the atmosphere and the ocean, at least a minor reduction in local SSTs would be expected following a significant volcanic eruption. If annual temperatures reduced below 18°C, *G. ruber* is pushed further from its optimal habitat whereas *G. bulloides* moves closer to optimal temperatures for productivity.

The initial increase in population density for *G. ruber* does not correlate with a decrease in temperature. However, there are half the number of *G. ruber* tests present in the samples above the tephra deposit than there are below it. The overall trend is a decrease in population that can be explained by a decreasing temperature pushing *G. ruber* further from its preferred temperature range. A decrease in temperature also correlates well with *G. bulloides* dramatically increasing in population as conditions become more favourable for its preferred habitat. However, the increase then sharp decrease in the *G. ruber* population suggests further research is needed into impacts of changing ocean conditions on this species and highlights the complexity of foraminifera ecology. The hypothesis of a decrease in SST following the Taupo eruption is considered further in the following sections, regarding test size and chemistry.

3.3.2 Foraminifera test size

Test sizes of foraminifera have been strongly correlated to specific optimal growing conditions for most species. The largest test sizes are found to be most commonly produced where the species is growing in a constant environment, most importantly within their preferred temperature range (Hecht, 1976, Schmidt et al., 2003, 2004, Moller et al., 2013). Test construction requires a substantial amount of energy. If a foraminifera is not in an ideal environment, or the environment rapidly changes without time to adjust, they exhibit stress, primarily affecting their ability to construct chambers of their tests.

Interrelated with species productivity, at 18°C *G. ruber* is not in optimal temperatures for test construction, causing smaller test sizes than those observed in warmer waters. In a study of the size distributions of planktic foraminifera, Schmidt et al. (2003) found the largest test sizes for *G. ruber* occurred at temperatures of 27.5°C. At this temperature, tests grew to sizes of 974 μm, compared to the maximum size in our samples of 458 μm. While *G. ruber* are known to still calcify in temperatures below 15°C, the relative abundance of *G. ruber* is known to significantly decrease along with test size (Schmidt et al., 2003). If SSTs decreased following the Taupo eruption, the test sizes for *G. ruber* would therefore be expected to also decrease.

A significant and prolonged decrease in test size for *G. ruber* is observed for ∼65 years after the Taupo eruption. There is a natural fluctuation in test sizes, between 172 and 458 μm, before the eruption that then continues in the top ∼65 years of the sampled section of Tan0810-12. However, in between these background levels the ∼65 years of deposition directly above the tephra contains a mostly continual level of smaller test sizes between 173 and 265 μm. Studies conducted by Hecht (1976), Schmidt et al. (2003, 2004) and Moller et al. (2013) all concluded that the most significant control on foraminifera test size was temperature. In our data the test sizes do not return to background levels for ∼65 years. If a decrease in temperature was the primary cause for the smaller test sizes it would be expected that the population of *G. ruber* would follow the same trend. The initial increase in the population of *G. ruber* suggests the population of this species is not solely controlled by temper-

ature and could be influenced by other factors. Nonetheless, the reduction in the size of *G. ruber* tests above the tephra deposit indicates a decrease in atmospheric temperatures caused a temporary decrease in SST around core site Tan0810-12 that could have persisted for up to ∼65 years after the eruption.

The test sizes of *G. bulloides* in the samples above the tephra deposit support the interpretation of a decrease in SSTs indicated by *G. ruber* tests. In previous studies, *G. bulloides* test size assemblage also indicates a strong relationship to temperature (Schmidt et al., 2003, Kucera, 2007). This relationship is often defined as a negative correlation however, because the preferred growth temperature for *G. bulloides* is significantly colder than species such as *G. ruber*. Schmidt et al. (2003) found the largest test size for *G. bulloides* of 718 μm occurred at temperatures of 10.5°C. This suggests a decrease in SSTs following the Taupo eruption would lead to an increase in test sizes for *G. bulloides*. This is observed in Tan0810-12 above the tephra horizon. *G. bulloides* tests show a slight increase in size compared to levels observed below the tephra deposit. However, because *G. bulloides* tests were only collected in the 5 cm above the tephra, it is not possible to determine if or when the test sizes returned to background levels. The depth habitat for *G. bulloides* is interpreted to be variable but usually deeper than *G. ruber* because it is a non-symbiotic species and does therefore not need to remain in the photic zone in order for its symbionts to photosynthesize. The increase in test size for *G. bulloides* therefore suggests the change in atmospheric temperature caused by the Taupo eruption may have propagated into deeper ocean layers. With further sampling, *G. bulloides* could provide an important insight into how the change in surface temperature may have extended into the mixed layer.

3.3.3 Test morphology

The presence of micro euhedral crystals and kummerforms on several of the *G. ruber* tests highlights the importance of SEM imaging prior to undertaking geochemical analyses. Abnormal morphologies present on the external and/or internal surfaces of foraminifera test walls can severely bias or alter the results of Mg/Ca paleothermometry and should be identified and removed prior to laser ablation or

solution-based analyses. In this case, the *G. ruber* tests containing euhedral crystals or a kummerform chamber were identified from the SEM images and excluded from the Mg/Ca analyses for paleothermometry. However, they were laser ablated separately to provide further information about their origins and the influence these irregularities can have on Mg/Ca concentrations in samples.

The euhedral crystals on the surface of several *G. ruber* tests contained anomalous, independent element/Ca ratios. Only one of the 8 foraminifera tests coated in crystals exhibited a distinctly high (>100µmol/mol) Mn/Ca concentration. This suggests the coating was caused by an Mn-bearing diagenetic overgrowth, formed post-deposition. $MnCO_3$ precipitates on the test surfaces of foraminifera and can often contain high concentrations of various trace elements (Boyle, 1983). Generally, foraminifera incorporate very little Mn into their tests during calcite precipitation. This indicates that samples containing high concentrations of Mn/Ca have likely been contaminated by an $MnCO_3$ overgrowth (Boyle, 1983). Isotopic analyses are not thought to be significantly effected by Mn. However, trace element analyses can not be considered reliable if high concentrations of Mn/Ca are detected in a sample because of the amounts of various trace elements often contained in the overgrowth. Studies have suggested ways to remove the contaminant but only a very minor concentration of a trace element needs to be present to significantly bias the results of the analyses. The most effective way to remove the suspected contamination is to discount the sample from the analyses.

The remaining tests containing a euhedral crystallite texture reveal high Mg/Ca coupled with low Mn/Ca values. The crystals of these tests appeared very similar to the shells coated in a diagenetic Mn overgrowth but contained no element/Ca concentrations that suggested contamination was present except the anomalously high Mg/Ca ratio. The euhedral crystals appear similar in shape to those formed during gametogenesis on species such as *G. truncatulinoides*. However, *G. ruber* has not been known to produce a calcite crust or exhibit any amount of test wall thickening prior to the release of gametes (Caron et al., 1990, Hoogakker et al., 2009). Additionally, gametogenic crusts are generally formed deeper in the ocean,

often caused by a loss of buoyancy during gamete release, and therefore produce noticeably lower Mg/Ca concentrations (Hemleben et al., 1989). It is likely the euhedral crystallinity on the surfaces of these tests was caused by a high-Mg secondary inorganic precipitate. The concentrations of Mg/Ca were significantly higher than values observed in normal tests suggesting a similar surface coating to the Mn overgrowth that contains a minor percentage of trace elements, contaminating the natural abundances of these elements incorporated during test construction. This agrees with the findings of Regenberg et al. (2007) and Kontakiotis et al. (2011), that inorganic diagenetic crusts are often composed of euhedral crystals and form post-deposition, with particularly high concentrations of Mg that largely bias the results of Mg/Ca paleothermometry.

The formation of kummerform chambers varies for individual species, making it difficult to understand their cause. For *G. ruber* kummerforms are generally believed to form after the growth of the penultimate chamber has been completed. The kummerform may represent the final chamber of the test that has not been able to grow to full size, most likely because of physical or biological stress (Hecht and Savin, 1970). The geochemical results of the *G. ruber* kummerforms in our samples indicate low Mg/Ca concentrations in all cases. This agrees with Hecht and Savin (1970) that found lower oxygen isotope values for the kummerform chamber. Hecht and Savin (1970) suggest these diminutive chambers could be caused by temperature stress, where the foraminifera is in deeper, colder water or warmer, shallower water than their optimal conditions. Caron et al. (1990) conducted gametogenic laboratory-based analyses on various species of foraminifera and found that for *G. ruber* some of the foraminifera seemed to produce kummerforms. Whether or not this was related to gametogenesis was not investigated. While *G. ruber* is generally not known to sink and produce a calcite crust during gametogenesis, it is possible some may lose partial buoyancy and descend through the water column prior to gamete release. This would cause stress and reduce the amount of energy available to construct their final chamber. Additionally, if the chamber is formed deeper in the ocean it explains the low Mg/Ca and oxygen isotope values of the kummerforms. The higher concentrations of Mg/Ca observed in the final normal-sized chambers

of the kummerform-bearing foraminifera suggests the kummerform chambers are in fact the final chamber that has not grown to full size. Higher concentrations of Mg/Ca are expected in the penultimate and antepenultimate chambers of normal-form *G. ruber* tests compared to the final chambers that are interpreted to form closer to the end of their life cycle (Bolton et al., 2011). Premature death could also explain the presence of the kummerform chambers but this would require the foraminifera to begin building this final chamber significantly deeper than normal.

3.3.4 Mg/Ca temperatures

Mg/Ca temperatures calculated from *G. ruber* and *G. bulloides* tests below and above the Taupo tephra in core Tan0810-12 reveal a distinct decrease in temperature. SSTs calculated using an LA-ICP-MS method indicate temperatures dropped by up to 1°C following the Taupo eruption. The Taupo eruption was hugely significant not just for the volume of erupted material but the height of the plinian column (Wilson et al., 1980). If the Taupo eruption reached the mesosphere it is likely the aerosols remained in the atmosphere for a longer period of time than 2-3 years. Perturbation of the Earth's climate, and more specifically the temperature of the troposphere, for more than 3 years would almost certainly have altered the surface temperatures of the world's ocean basins.

Previous Mg/Ca studies conducted on *G. ruber* and *G. bulloides* have shown a strong exponential correlation with temperature exists for these species (Anand et al., 2003, Marr et al., 2011, Bolton et al., 2011, Rosenthal and Lohmann, 2002, Kısakürek et al., 2008). These foraminifera species were picked below and above the Taupo tephra in Tan0810-12 and cleaned using several rinses of Milli-Q. For reasons unknown, ultrasonicating in order to remove adhered contaminants caused the tests to burst in less than one second, even for tests taken well below the tephra. Therefore, rigorous cleaning methods were not explored but SEM images revealed very little surface contamination, and where present, the tests were rinsed again thoroughly. Samples that presented any signs of contamination, based on abnormal Al/Ca, Mn/Ca and Sr/Ca ratios, were removed from the Mg/Ca results.

G. ruber tests revealed consistently lower Mg/Ca ratios than would be expected. The global climate has remained relatively stable for the past 2000 years, suggesting the SSTs around New Zealand at the time of the Taupo eruption were unlikely to have been more than 2°C above or below the current temperature of ∼18°C (Loehle, 2007). However, these results agree with Bolton et al. (2011) who found distinctly lower Mg/Ca ratios for the final chamber of *G. ruber*. While it is possible this anomaly could be explained by the final chamber of the test forming near the end of their life cycle, as they begin to sink in the water column and therefore would precipitate the chamber in colder waters, Bolton et al. (2011) found the same anomaly in live tests collected near the surface. This suggests the formation of this chamber in deeper water is unlikely to be the primary cause of the low Mg/Ca values. Marr (2009) and Anand and Elderfield (2005) also found lower Mg/Ca concentrations in the final chamber of *G. bulloides*, suggesting it does not appear to be a species specific irregularity or caused by environmental conditions. Our interpretation agrees with the hypothesis of Bolton et al. (2011) that the lower Mg/Ca concentrations in both *G. ruber* and *G. bulloides* tests is most likely controlled by some internal biological system. Whether or not the same biological processes affect the Mg/Ca signature for each individual foraminifera of a species is unknown. If it does, the final chamber of *G. ruber* and *G. bulloides* tests could still be used for Mg/Ca analyses to determine changes in temperature but in order to calculate exact temperature values further research is needed into the cause and effect of this irregularity.

G. bulloides on the other hand appears to show temperature estimates well within modern SSTs, suggesting the f-2 chambers were likely constructed close to the ocean surface. Accounting for maximum and minimum errors, the Mg/Ca values for *G. bulloides* estimate a minimum SST cooling of 1°C after the Taupo eruption. Nearly the entire annual shell flux for *G. bulloides* is known to occur during spring (Northcote and Neil, 2005, King and Howard, 2001). The temperatures calculated for this species are therefore more than likely to be indicative of spring temperatures. Around East Cape, these are currently between 19 and 20°C, very similar to the temperature calculated on *G. bulloides* tests prior to the eruption. However, *G. bulloides* are generally known to inhabit the mixed layer of the ocean, suggesting

Mg/Ca concentrations of this species should represent the temperature of the ocean at greater depths. At core site Tan0810-12 there is direct influence from the ECE (Fig. 9). Eddies cause turbulent mixing of the ocean, beneficial for *G. bulloides* because nutrients are brought up from deeper, colder waters. Marr (2009) found *G. bulloides* collected from sites near the Wairarapa Eddy (WE; Fig. 9) inhabited significantly shallower depths, around 50 m, compared to other sites where they were found mostly at around 125 m. Therefore, around core site Tan0810-12 *G. bulloides* depth habitat could be influenced by the ECE, meaning the temperature estimates calculated before and after the eruption are likely to reflect the temperature at the surface of the ocean, not the mixed layer.

The SST cooling of at least 1°C estimated by our Mg/Ca analyses is in direct agreement with previous SST estimates following the Toba and Mt. Pinatubo eruptions studied by Huang et al. (2001) and Sutton and Chiswell (1996), respectively. These studies used long-chain ketone analyses and satellite-derived SST data, respectively, to estimate changes in ocean temperature following these eruptions but suggested further work was needed to accurately determine the change in climate because their data was inconclusive. Reynolds (1993) suggests satellite data used to estimate changes following volcanic eruptions could be biased towards colder temperatures by the influence of the large increase in stratospheric aerosols. Although most data agrees with a decrease in temperature following a large volcanic eruption, the interpretation of satellite-derived data by Reynolds (1993) should be further investigated to ensure when a large eruption happens in the future, the satellite data can be used to accurately observe changes to the Earth's terrestrial and marine biospheres.

Rampino et al. (1979) collected age and SST data produced from radiolarian assemblages over the past 8000 years in order to link the ages of large volcanic events to periods of rapid SST reductions. For the Taupo eruption, Rampino et al. (1979) estimate a SST decrease of ∼1-2°C occurred in the Santa Barbara Basin, located off the coast of southern California, immediately afterwards (Fig. 24). This study agrees with our data and suggests the decrease in SST after the Taupo eruption

could have also occurred in the Northern Hemisphere. The global distribution of sulphate aerosols is dependent on the distance of the volcano from the equator. Self (2006) estimates volcanoes located more than 30° north or south of the equator are unlikely to spread significant amounts of sulphate aerosols into the opposite hemisphere. However, if the results of Rampino et al. (1979) are accurate, our study suggests nearly the same decrease in SST occurred in both the Northern and Southern Hemispheres, despite the Taupo eruption vent being located at 38°S. This could be due to the abnormal height of the eruption column and/or the aerosols remaining in the atmosphere for longer than previously estimated for large volcanic eruptions.

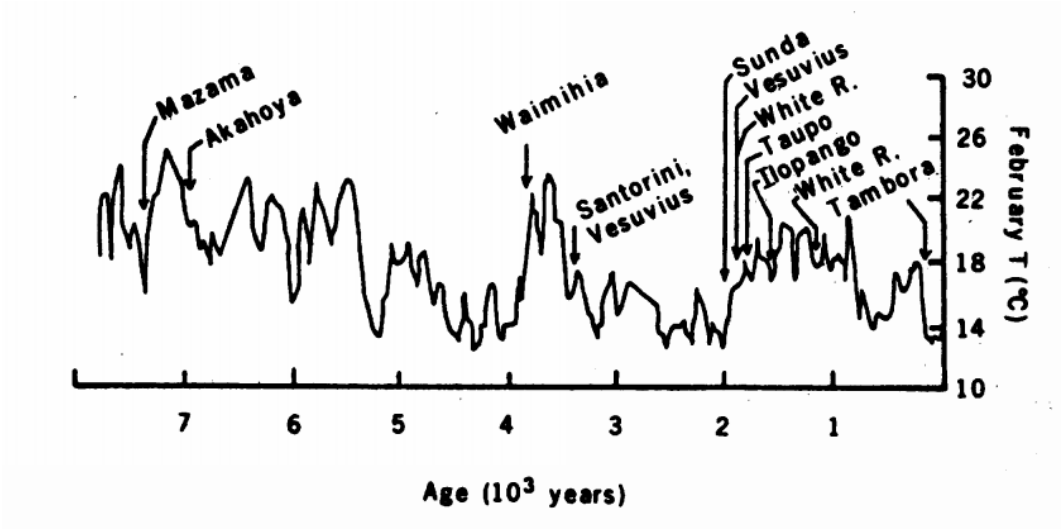

Figure 24: SST estimates over the past 8000 years determined from deep-sea cores collected from the Santa Barbara Basin, northeast Pacific, and compared with the ages of large volcanic eruptions (>10km^3) from Rampino et al. (1979).

The Mg/Ca values calculated from the *G. bulloides* tests above the Taupo tephra horizon do not begin increasing even at the furthest extent of our samples, ∼65 years after the eruption. Further sampling of the core above the tephra is needed to determine the full extent of this climate perturbation, however, this is already significantly longer than the recovery rate observed for the Mt. Pinatubo eruption. According to Church et al. (2005) global ocean heat content and global mean sea level returned to pre-eruption values after approximately 10 years. The Mt. Pinatubo eruption is significant in recent history because it is the largest volcanic event to occur since direct global satellite and atmospheric measurement data has been readily

collected. The eruption produced ∼5 km^3 of volcanic material and global atmospheric temperature data showed a tropospheric cooling of 0.5°C (Self, 2006). An eruption of this size perturbing SSTs for 10 years would suggest our estimate of at least a 65 year SST perturbation following the Taupo eruption (23 km^3) is plausible.

Volcanic eruptions are incredibly difficult to factor into climate modelling. Models have shown that the season or climate state prior to the eruption can have a large impact on the dispersal of gases in the stratosphere (Timmreck and Graf, 2006, Jones and Kaiteris, 1983). Additionally, and more importantly, the volume of SO_2 released during the eruption and the height of the eruption column will heavily influence how the climate is altered post-eruption (Self, 2006). Short-term climate change can be devastating to the human population by causing crop failure, starvation and destructive weather phenomena. However, the atmospheric climate appears to recover relatively quickly, it is the long-term changes to ocean temperature that need a distinct understanding in order to predict the full impacts of volcanism on Earth's climate. Our estimates of a SST cooling of 1°C for at least 65 years after the Taupo eruption determined from Mg/Ca concentrations of foraminifera tests, provides an insight into the potential impacts of volcanism on the oceans and suggests this method can used to observe rapid changes in the oceanic environment.

4 Conclusions

This study predominantly aimed to determine whether a timeline of ocean temperatures before and after a major silicic volcanic eruption could be constructed by using Mg/Ca concentrations of foraminifera collected from marine sediment cores. Core Tan0810-12 provides a unique opportunity to understand the impacts of volcanism on the physical and biological environment of the ocean at a very high temporal resolution. Sediment characterisation and grain size and $CaCO_3$ analyses indicate the Taupo tephra and surrounding sediment in this core are primary in origin with only minor bioturbation above the tephra. The stratigraphic order of this section of the core is therefore interpreted to be intact, allowing the age model and sedimentation rates to be used to determine changes in the oceanic record through time on a sub-decadal scale. Based on the sedimentation rates in this section of the core, each 0.5 cm sample below the tephra correlates to 5 years of deposition while above the tephra each sample represents 6.6 years of deposition.

This study used SEM imaging to determine the morphology and size of two planktic species of foraminifera, *G. ruber* and *G. bulloides*, collected from 0.5 cm samples above and below the Taupo tephra, representing ∼100 years of deposition before and after the eruption. While most species can survive outside their optimal growth conditions, rapid changes in their surrounding oceanic environment can cause stress that limits their ability to grow a normal test. *G. ruber* inhabits subtropical waters, preferring temperatures between 21 and 29°C. Above the Taupo tephra horizon the number of individual *G. ruber* tests show an overall decreasing trend but an increase for ∼65 years after the eruption before a rapid decrease. Schmidt et al. (2003) found a strong correlation between foraminiferal abundance, test size and temperature. The sizes of the *G. ruber* tests are smaller for ∼65 years after the Taupo eruption. This correlates with the decrease in temperature determined by Mg/Ca concentrations because this species would be pushed further from their optimum growing conditions but suggests the abundance of *G. ruber* tests are not controlled solely by temperature.

The increase in test sizes and individual *G. bulloides* tests above the tephra horizon

also agrees with a decrease in ocean temperature and suggests temperature may have more control on the abundance of *G. bulloides* tests than *G. ruber*. *G. bulloides* is a subpolar species, preferring colder waters than those found around New Zealand. A decrease in temperature would enhance the ability of *G. bulloides* to grow and reproduce. Analyses of *G. ruber* and *G. bulloides* tests indicate temperature is one of the most important controlling factors on test size, with the largest sizes correlating with the individual species optimal temperature range. The morphologies of both *G. ruber* and *G. bulloides* tests do not change above the tephra suggesting no correlation exists here between a rapid change in oceanic environment and change in test morphology.

LA-ICP-MS analyses were conducted on *G. ruber* and *G. bulloides* tests to determine the Mg/Ca concentrations and, by proxy, ocean temperature change following the Taupo eruption. Al/Ca, Mn/Ca, Ti/Ca and Sr/Ca concentrations were also determined alongside Mg/Ca in order to monitor foraminifera tests for contamination of detrital material, diagenetic coatings or possible impacts of tephra on carbonate tests. The final chamber of the *G. ruber* tests was analysed by LA-ICP-MS but revealed distinctly low values of Mg/Ca throughout the sampled section except for a period of distinctly high Mg/Ca concentrations in tests found in the first $\sim$50 years of deposition following the Taupo eruption. The high Mg/Ca concentrations found in the *G. ruber* tests directly above the tephra horizon are unlikely to be caused by contamination from the tephra. Rhyolite is compositionally low in Mg and Mn so would not be expected to greatly elevate Mg/Ca values. Additionally, *G. bulloides* tests do not show any indication of significant contamination above the tephra, further suggesting tephra is not the cause of contamination in the *G. ruber* tests. The low Mg/Ca concentrations in the final chambers of *G. ruber* tests were also observed by Bolton et al. (2011) in live foraminifera collected at shallow depths, suggesting the low values are not caused by the final chamber forming in deeper, colder water. Marr (2009) and Anand and Elderfield (2005) also found low Mg/Ca concentrations in the final chambers of *G. bulloides* tests that indicates the cause of irregularity is likely biological.

The *f*-2 chamber of *G. bulloides* revealed a decrease in Mg/Ca values that calibrated to a minimum decrease in temperature of 1°C when taking errors into consideration. The *G. bulloides* tests indicate a SST of 21.1 ± 1.5°C prior to the Taupo eruption that decreased to 16.8 ± 1.9°C following this volcanic event. While a 1°C temperature decrease is a conservative estimate, a greater number of *G. bulloides* tests are needed to reduce the error and further constrain the exact temperature difference. Nonetheless, this species provides a strong basis for calculating changes in ocean temperature in the past. The temperature values produced by Mg/Ca analyses of the *G. bulloides* tests are likely to be representative of spring temperatures because this species is largely reliant on phytoplankton blooms, that occur predominantly during spring (Northcote and Neil, 2005). Additionally, the Tan0810-12 core site is directly influenced by the ECE, likely causing mixing and reduced stratification at this location. Cold, deeper water is able to penetrate to the ocean surface, bringing nutrients and therefore *G. bulloides* higher in the water column. Therefore, our data are interpreted to represent spring SSTs, that are very similar to modern values and show the strong potential for this species as a paleotemperature proxy.

The SST change of 1°C determined from *G. bulloides* tests is directly in line with previous studies. This suggests a minimum case scenario for a silicic volcanic event on the scale of the Taupo eruption in the future would be a SST reduction of at least 1°C. The stratigraphy of marine cores is also significantly important and by using stratigraphic analyses on Tan0810-12, this study provides a unique insight into the length of time the oceanic environment remained perturbed following the Taupo eruption. The age model calculated for this core allowed a sedimentation rate to be determined and applied, revealing it is likely SSTs around East Cape remained low for at least 65 years after the Taupo eruption. Further sampling throughout the core is needed to determine how long the signal extends in the record, but the very high temporal resolution and undisturbed stratigraphic order of Tan0810-12 allows this minimum time frame to be applied.

This study has determined that stratigraphic and foraminiferal analyses can aid our understanding of the impacts of volcanism on the oceanic environment. Further

research is needed to better constrain the impacts of rapid climate change caused by volcanic eruptions on the marine environment in order to factor this information into climate models and better predict how both the terrestrial and marine environments may be impacted in the future.

5 Future work

To investigate further, Tan0810-12 could be sampled over longer timescales to get a better idea of the extent of change following the Taupo eruption. This could be aided by simply sampling more than one quarter of the core to obtain larger samples and therefore more foraminifera. Alternatively, obtaining cores in either colder waters, where there is likely to be a greater population of *G. bulloides* tests, or warmer waters to increase the number of *G. ruber* tests would provide greater populations to analyse. Until the cause of low Mg/Ca values in the final tests of *G. ruber* and *G. bulloides* is determined, further Mg/Ca studies should be conducted on the penultimate or antepenultimate chambers of these species. Mg/Ca ratios could be combined with oxygen isotope analyses to provide another proxy for temperature change. Alternative SST proxies could also be adopted including alkenones from coccolithophores or dinoflagellates. Additionally, more ages calculated for the cores would give a more accurate sedimentation rate and contribute to determining how the temperature has changed through time. It would also be beneficial, as volcanic eruption ages are becoming more accurate, to correlate a long-term SST record with large volcanic eruption ages to better determine if a pattern exists between volcanism and rapid climate change events.

The impacts of volcanic ash on the pH of the surface of the ocean and the dissolution of carbonate tests should also be investigated further. While it is suggested that volcanic ash could cause dissolution in the surface of the ocean, it would be beneficial to understand the extent of contamination. Dissolution of planktic and benthic fauna could be studied further by analysing foraminiferal assemblages before and after a large volcanic tephra in a marine sediment core to observe if the assemblages change in the number of total planktic or benthic foraminifera or the number of individual foraminifera of certain species. Alternatively, a useful method would be to sample and analyse the foraminifera in the marine cores containing a tephra layer just a few mm thick or present as a series of blobs. This would provide a comparison to observe the chemical changes caused by tephra and ensure there is no bias in the temperature record.

References

Anand, P. and Elderfield, H. (2005). Variability of Mg/Ca and Sr/Ca between and within the planktonic foraminifers *Globigerina bulloides* and *Globorotalia truncatulinoides*. *Geochemistry, Geophysics, Geosystems*, 6(11).

Anand, P., Elderfield, H., and Conte, M. H. (2003). Calibration of Mg/Ca thermometry in planktonic foraminifera from a sediment trap time series. *Paleoceanography*, 18(2).

Arbuszewski, J., deMenocal, P., Kaplan, A., Farmer, E. C., et al. (2010). On the fidelity of shell-derived $\delta^{18}O$ seawater estimates. *Earth and Planetary Science Letters*, 300(3):185–196.

Barker, S., Cacho, I., Benway, H., and Tachikawa, K. (2005). Planktonic foraminiferal Mg/Ca as a proxy for past oceanic temperatures: a methodological overview and data compilation for the Last Glacial Maximum. *Quaternary Science Reviews*, 24(7):821–834.

Barker, S., Greaves, M., and Elderfield, H. (2003). A study of cleaning procedures used for foraminiferal Mg/Ca paleothermometry. *Geochemistry, Geophysics, Geosystems*, 4(9).

Barry, R. G. and Chorley, R. J. (2009). *Atmosphere, weather and climate*. Routledge.

Bé, A. and Tolderlund, D. (1971). Distribution and ecology of living planktonic foraminifera in surface waters of the Atlantic and Indian Oceans. *The micropaleontology of oceans*, pages 105–149.

Bender, M. L., Lorens, R. B., and Williams, D. F. (1975). Sodium, magnesium and strontium in the tests of planktonic foraminifera. *Micropaleontology*, 21(4):448–459.

Blake, S., Wilson, C., Smith, I., and Walker, G. (1992). Petrology and dynamics of the Waimihia mixed magma eruption, Taupo Volcano, New Zealand. *Journal of the Geological Society*, 149(2):193–207.

Blott, S. J. and Pye, K. (2001). GRADISTAT: a grain size distribution and statistics package for the analysis of unconsolidated sediments. *Earth surface processes and Landforms*, 26(11):1237–1248.

Bolton, A. (2011). *LA-ICP-MS trace element analysis of planktonic foraminifera and application to Marine Isotope Stage 31 in the southwest Pacific Ocean*. PhD thesis, Victoria University of Wellington.

Bolton, A., Baker, J. A., Dunbar, G. B., Carter, L., Smith, E. G., and Neil, H. L. (2011). Environmental versus biological controls on Mg/Ca variability in *Globigerinoides ruber* (white) from core top and plankton tow samples in the southwest Pacific Ocean. *Paleoceanography*, 26(2).

Bostock, H. C., Hayward, B. W., Neil, H. L., Currie, K. I., and Dunbar, G. B. (2011). Deep-water carbonate concentrations in the southwest Pacific. *Deep Sea Research Part I: Oceanographic Research Papers*, 58(1):72–85.

Boyd, P., LaRoche, J., Gall, M., Frew, R., and McKay, R. M. L. (1999). Role of iron, light, and silicate in controlling algal biomass in subantarctic waters SE of New Zealand. *Journal of Geophysical Research: Oceans*, 104(C6):13395–13408.

Boyle, E. A. (1983). Manganese carbonate overgrowths on foraminifera tests. *Geochimica et Cosmochimica Acta*, 47(10):1815–1819.

Caron, D. A., Anderson, O. R., Lindsey, J. L., Faber, W. W., and Lim, E. L. (1990). Effects of gametogenesis on test structure and dissolution of some spinose planktonic foraminifera and implications for test preservation. *Marine Micropaleontology*, 16(1-2):93–116.

Carter, L., Nelson, C. S., Neil, H. L., and Froggatt, P. C. (1995). Correlation, dispersal, and preservation of the Kawakawa tephra and other late Quaternary tephra layers in the southwest Pacific Ocean. *New Zealand Journal of Geology and Geophysics*, 38(1):29–46.

Carter, L., Shane, P., Alloway, B., Hall, I. R., Harris, S. E., and Westgate, J. A. (2003). Demise of one volcanic zone and birth of another a 12 m.y. marine record of major rhyolitic eruptions from New Zealand. *Geology*, 31(6):493–496.

Chiswell, S. M., Bostock, H. C., Sutton, P. J., and Williams, M. J. (2015). Physical oceanography of the deep seas around New Zealand: a review. *New Zealand Journal of Marine and Freshwater Research*, 49(2):286–317.

Church, J. A., White, N. J., and Arblaster, J. M. (2005). Significant decadal-scale impact of volcanic eruptions on sea level and ocean heat content. *Nature*, 438(7064):74–77.

Clark, K., Berryman, K., Litchfield, N., Cochran, U., and Little, T. (2010). Evaluating the coastal deformation mechanisms of the Raukumara Peninsula, northern Hikurangi subduction margin, New Zealand and insights into forearc uplift processes. *New Zealand Journal of Geology and Geophysics*, 53(4):341–358.

Cobianchi, M., Mancin, N., Lupi, C., Bordiga, M., and Bostock, H. (2015). Effects of oceanic circulation and volcanic ash-fall on calcite dissolution in bathyal sediments from the SW Pacific Ocean over the last 550ka. *Palaeogeography, Palaeoclimatology, Palaeoecology*, 429:72–82.

Cole, J. and Spinks, K. (2009). Caldera volcanism and rift structure in the Taupo Volcanic Zone, New Zealand. *Geological Society, London, Special Publications*, 327(1):9–29.

Cole-Dai, J. (2010). Volcanoes and climate. *Wiley Interdisciplinary Reviews: Climate Change*, 1(6):824–839.

Costanza, R. (1999). The ecological, economic, and social importance of the oceans. *Ecological economics*, 31(2):199–213.

Coulter, B. (2011). LS 13 320 laser diffraction particle size analyzer instructions for use. *Beckman Coulter Inc*, 11800.

Courtillot, V. E. and Renne, P. R. (2003). On the ages of flood basalt events. *Comptes Rendus Geoscience*, 335(1):113–140.

Dekens, P. S., Lea, D. W., Pak, D. K., and Spero, H. J. (2002). Core top calibration of Mg/Ca in tropical foraminifera: refining paleotemperature estimation. *Geochemistry, Geophysics, Geosystems*, 3(4):1–29.

d'Orbigny, A. D. (1826). *Tableau méthodique de la classe des Céphalopodes*. Crochard.

Eggins, S. M., Sadekov, A., and Deckker, P. D. (2004). Modulation and daily banding of Mg/Ca in *Orbulina universa* tests by symbiont photosynthesis and respiration: a complication for seawater thermometry? *Earth and Planetary Science Letters*, 225(3-4):411–419.

Elderfield, H., Vautravers, M., and Cooper, M. (2002). The relationship between shell size and Mg/Ca, Sr/Ca, δ^{18}O, and δ^{13}C of species of planktonic foraminifera. *Geochemistry, Geophysics, Geosystems*, 3(8):1–13.

Erez, J. (1978). Vital effect on stable-isotope composition seen in foraminifera and coral skeletons. *Nature*, 273:199–202.

Erez, J. (2003). The source of ions for biomineralization in foraminifera and their implications for paleoceanographic proxies. *Reviews in mineralogy and geochemistry*, 54(1):115–149.

Fischer, E. M., Luterbacher, J., Zorita, E., Tett, S. F. B., Casty, C., and Wanner, H. (2007). European climate response to tropical volcanic eruptions over the last half millennium. *Geophysical Research Letters*, 34(5).

Friedman, G. M. and Sanders, J. E. (1978). *Principles of sedimentology*. Wiley.

Froggatt, P. C. and Lowe, D. J. (1990). A review of late Quaternary silicic and some other tephra formations from New Zealand: their stratigraphy, nomenclature, distribution, volume, and age. *New Zealand journal of geology and geophysics*, 33(1):89–109.

Frogner, P., Gíslason, S. R., and Óskarsson, N. (2001). Fertilizing potential of volcanic ash in ocean surface water. *Geology*, 29(6):487–490.

Frölicher, T., Joos, F., and Raible, C. (2011). Sensitivity of atmospheric CO_2 and climate to explosive volcanic eruptions. *Biogeosciences*, 8(8):2317–2339.

Gleckler, P., Wigley, T., Santer, B., Gregory, J., AchutaRao, K., and Taylor, K. (2006). Volcanoes and climate: Krakatoa's signature persists in the ocean. *Nature*, 439(7077):675–675.

Gleckler, P. J., Durack, P. J., Stouffer, R. J., Johnson, G. C., and Forest, C. E. (2016). Industrial-era global ocean heat uptake doubles in recent decades. *Nature Climate Change*, 6(7077):394–398.

Goldstein, S. T. (1999). Foraminifera: a biological overview. In *Modern Foraminifera*, pages 37–55. Springer.

Gupta, B. K. S. and Barun, K. (1999). *Modern foraminifera*. Springer.

Heath, R. (1985). A review of the physical oceanography of the seas around New Zealand 1982. *New Zealand journal of marine and freshwater research*, 19(1):79–124.

Hecht, A., Eslinger, E., and Garmon, L. (1975). Experimental studies on the dissolution of planktonic foraminifera. In *Dissolution of Deep-Sea Carbonates*, pages 59–69. Cushman Foundation for Foraminiferal Research.

Hecht, A. D. (1976). An ecologic model for test size variation in Recent planktonic foraminifera; applications to the fossil record. *The Journal of Foraminiferal Research*, 6(4):295–311.

Hecht, A. D. and Savin, S. M. (1970). Oxygen-18 studies of recent planktonic Foraminifera: comparisons of phenotypes and of test parts. *Science*, 170(3953):69–71.

Hemleben, C., Spindler, M., and Anderson, O. (1989). *Modern Planktonic Foraminifera*. Springer-Verlag.

Hemleben, C., Spindler, M., Breitinger, I., and Deuser, W. G. (1985). Field and laboratory studies on the ontogeny and ecology of some globorotaliid species from the Sargasso Sea off Bermuda. *The Journal of Foraminiferal Research*, 15(4):254–272.

Hess, S. and Kuhnt, W. (1996). Deep-sea benthic foraminiferal recolonization of the 1991 Mt. Pinatubo ash layer in the South China Sea. *Marine Micropaleontology*, 28(2):171–197.

Hicks, D. M., Shankar, U., McKerchar, A. I., Basher, L., Lynn, I., Page, M., and Jessen, M. (2011). Suspended sediment yields from New Zealand rivers. *Journal of Hydrology*, 50(1):81–142.

Hicks, M., Shankar, U., and McKerchar, A. (2003). Sediment yield estimates: a GIS tool. *science*, 11(1):24–25.

Hofmann, C., Courtillot, V., Feraud, G., Rochette, P., Yirgu, G., Ketefo, E., and Pik, R. (1997). Timing of the Ethiopian flood basalt event and implications for plume birth and global change. *Nature*, 389(6653):838–841.

Hogg, A., Lowe, D. J., Palmer, J., Boswijk, G., and Ramsey, C. B. (2012). Revised calendar date for the Taupo eruption derived by ^{14}C wiggle-matching using a New Zealand kauri ^{14}C calibration data set. *The Holocene*, 22(4):439–449.

Hönisch, B., Allen, K. A., Lea, D. W., Spero, H. J., Eggins, S. M., Arbuszewski, J., deMenocal, P., Rosenthal, Y., Russell, A. D., and Elderfield, H. (2013). The influence of salinity on Mg/Ca in planktic foraminifers: evidence from cultures, core-top sediments and complementary δ^{18}O. *Geochimica et Cosmochimica Acta*, 121:196–213.

Hoogakker, B. A., Klinkhammer, G. P., Elderfield, H., Rohling, E. J., and Hayward, C. (2009). Mg/Ca paleothermometry in high salinity environments. *Earth and Planetary Science Letters*, 284(3):583–589.

Huang, C.-Y., Zhao, M., Wang, C.-C., and Wei, G. (2001). Cooling of the South China Sea by the Toba eruption and correlation with other climate proxies ∼71,000 years ago. *Geophysical Research Letters*, 28(20):3915–3918.

Jochum, K. P., Weis, U., Stoll, B., Kuzmin, D., Yang, Q., Raczek, I., Jacob, D. E., Stracke, A., Birbaum, K., Frick, D. A., Günther, D., and Enzweiler, J. (2011). Determination of reference values for NIST SRM 610-617 glasses following ISO guidelines. *Geostandards and Geoanalytical Research*, 35(4):397–429.

Jones, G. A. and Kaiteris, P. (1983). A vacuum-gasometric technique for rapid and precise analysis of calcium carbonate in sediments and soils: RESEARCH-METHOD PAPER. *Journal of Sedimentary Research*, 53(2):655–660.

Jones, M. T. and Gislason, S. R. (2008). Rapid releases of metal salts and nutrients following the deposition of volcanic ash into aqueous environments. *Geochimica et Cosmochimica Acta*, 72(15):3661–3680.

Kelly, P. M., Jia, P., and Jones, P. (1996). The spatial response of the climate system to explosive volcanic eruptions. *International Journal of Climatology*, 16(5):537–550.

Ketten, D. R. and Edmond, J. M. (1979). Gametogenesis and calcification of planktonic foraminifera. *Nature*, 278(5704):546–548.

King, A. L. and Howard, W. R. (2001). Seasonality of foraminiferal flux in sediment traps at Chatham Rise, SW Pacific: implications for paleotemperature estimates. *Deep Sea Research Part I: Oceanographic Research Papers*, 48(7):1687–1708.

Kısakürek, B., Eisenhauer, A., Böhm, F., Garbe-Schönberg, D., and Erez, J. (2008). Controls on shell Mg/Ca and Sr/Ca in cultured planktonic foraminiferan, *Globigerinoides ruber* (white). *Earth and Planetary Science Letters*, 273(34):260–269.

Kontakiotis, G., Mortyn, P. G., Antonarakou, A., Martínez-Botí, M. A., and Triantaphyllou, M. V. (2011). Field-based validation of a diagenetic effect on *G. ruber* Mg/Ca paleothermometry: core top results from the Aegean Sea (eastern Mediterranean). *Geochemistry, Geophysics, Geosystems*, 12(9).

Kraft, S., Frank, M., Hathorne, E. C., and Weldeab, S. (2013). Assessment of seawater Nd isotope signatures extracted from foraminiferal shells and authigenic phases of Gulf of Guinea sediments. *Geochimica et Cosmochimica Acta*, 121:414–435.

Kucera, M. (2007). Planktonic foraminifera as tracers of past oceanic environments. *Developments in marine geology*, 1(6):213–262.

Langmann, B. (2013). Volcanic ash versus mineral dust: atmospheric processing and environmental and climate impacts. *ISRN Atmospheric Sciences*, 2013.

Lea, D. W. (1999). Trace elements in foraminiferal calcite. In *Modern Foraminifera*, pages 259–277. Springer Netherlands, Dordrecht.

Lea, D. W. (2006). Elemental and isotopic proxies. *Oceans Mar. Geochem.*, 6:1–26.

Lea, D. W., Mashiotta, T. A., and Spero, H. J. (1999). Controls on magnesium and strontium uptake in planktonic foraminifera determined by live culturing. *Geochimica et Cosmochimica Acta*, 63(16):2369–2379.

Lea, D. W., Pak, D. K., and Paradis, G. (2005). Influence of volcanic shards on foraminiferal Mg/Ca in a core from the Galápagos region. *Geochemistry, Geophysics, Geosystems*, 6(11).

Lear, C. H., Coxall, H. K., Foster, G. L., Lunt, D. J., Mawbey, E. M., Rosenthal, Y., Sosdian, S. M., Thomas, E., and Wilson, P. A. (2015). Neogene ice volume and ocean temperatures: insights from infaunal foraminiferal Mg/Ca paleothermometry. *Paleoceanography*, 30(11):1437–1454.

Lear, C. H., Elderfield, H., and Wilson, P. (2000). Cenozoic deep-sea temperatures and global ice volumes from Mg/Ca in benthic foraminiferal calcite. *Science*, 287(5451):269–272.

Lear, C. H., Rosenthal, Y., and Slowey, N. (2002). Benthic foraminiferal Mg/Ca-paleothermometry: a revised core-top calibration. *Geochimica et Cosmochimica Acta*, 66(19):3375–3387.

Levitus, S., Antonov, J., and Boyer, T. (2005). Warming of the world ocean, 1955-2003. *Geophysical Research Letters*, 32(2).

Lewis, K. and Kohn, B. (1973). Ashes, turbidites, and rates of sedimentation on the continental slope off Hawkes Bay. *New Zealand journal of geology and geophysics*, 16(3):439–454.

Lipps, J. H., Finger, K. L., and Walker, S. E. (2011). What should we call the Foraminifera? *The Journal of Foraminiferal Research*, 41(4):309–313.

Loeblich, A. and Tappan, H. (1988). *Foraminiferal Genera and Their Classification*. Springer US.

Loehle, C. (2007). A 2000-year global temperature reconstruction based on non-treering proxies. *Energy & Environment*, 18(7):1049–1058.

Lowe, D. J., Shane, P. A., Alloway, B. V., and Newnham, R. M. (2008). Fingerprints and age models for widespread New Zealand tephra marker beds erupted since 30,000 years ago: a framework for NZ-INTIMATE. *Quaternary Science Reviews*, 27(1):95–126.

Manabe, S., Stouffer, R., Spelman, M., and Bryan, K. (1991). Transient responses of a coupled ocean-atmosphere model to gradual changes of atmospheric CO_2. part I. annual mean response. *Journal of Climate*, 4(8):785–818.

Marchitto, T., Bryan, S., Curry, W., and McCorkle, D. (2007). Mg/Ca temperature calibration for the benthic foraminifer *Cibicidoides pachyderma*. *Paleoceanography*, 22(1).

Marchitto, T. M. (2006). Precise multielemental ratios in small foraminiferal samples determined by sector field ICP-MS. *Geochemistry, Geophysics, Geosystems*, 7(5).

Marr, J. (2009). Ecological, oceanographic and temperature controls on the incorporation of trace elements into *Globigerina bulloides* and *Globoconella inflata* in the southwest Pacific Ocean. Master's thesis, Victoria University of Wellington.

Marr, J. P., Baker, J. A., Carter, L., Allan, A. S., Dunbar, G. B., and Bostock, H. C. (2011). Ecological and temperature controls on Mg/Ca ratios of *Globigerina bulloides* from the southwest Pacific Ocean. *Paleoceanography*, 26(2).

Marszalek, D. S., Wright, R. C., and Hay, W. W. (1969). Function of the test in foraminifera. *Trans Gulf Coast Assoc Geol Soc*, 19:341–352.

Mathien-Blard, E. and Bassinot, F. (2009). Salinity bias on the foraminifera Mg/Ca thermometry: correction procedure and implications for past ocean hydrographic reconstructions. *Geochemistry, Geophysics, Geosystems*, 10(12).

Milner, D., Cole, J., and Wood, C. (2003). Mamaku ignimbrite: A caldera-forming ignimbrite erupted from a compositionally zoned magma chamber in Taupo Volcanic Zone, New Zealand. *Journal of Volcanology and Geothermal Research*, 122(3):243–264.

Mohtadi, M., Steinke, S., Groeneveld, J., Fink, H. G., Rixen, T., Hebbeln, D., Donner, B., and Herunadi, B. (2009). Low-latitude control on seasonal and interannual changes in planktonic foraminiferal flux and shell geochemistry off south Java: a sediment trap study. *Paleoceanography*, 24(1).

Moller, T., Schulz, H., and Kucera, M. (2013). The effect of sea surface properties on shell morphology and size of the planktonic foraminifer *Neogloboquadrina pachyderma* in the North Atlantic. *Palaeogeography, Palaeoclimatology, Palaeoecology*, 391:34–48.

Mortyn, P. G. and Charles, C. D. (2003). Planktonic foraminiferal depth habitat and $\delta^{18}O$ calibrations: plankton tow results from the Atlantic sector of the Southern Ocean. *Paleoceanography*, 18(2).

Moy, A. D., Howard, W. R., Bray, S. G., and Trull, T. W. (2009). Reduced calcification in modern Southern Ocean planktonic foraminifera. *Nature Geoscience*, 2(4):276–280.

Nairn, I. A. (1981). *Some studies of the geology, volcanic history, and geothermal resources of the Okataina Volcanic Centre, Taupo Volcanic Zone, New Zealand*. PhD thesis, Victoria University of Wellington.

Neely, R., Toon, O., Solomon, S., Vernier, J.-P., Alvarez, C., English, J., Rosenlof, K., Mills, M., Bardeen, C., Daniel, J., and Thayer, J. P. (2013). Recent anthropogenic increases in SO_2 from Asia have minimal impact on stratospheric aerosol. *Geophysical Research Letters*, 40(5):999–1004.

Ni, Y., Foster, G. L., Bailey, T., Elliott, T., Schmidt, D. N., Pearson, P., Haley, B., and Coath, C. (2007). A core top assessment of proxies for the ocean carbonate system in surface-dwelling foraminifers. *Paleoceanography*, 22(3).

Niebler, H.-S., Hubberten, H.-W., and Gersonde, R. (1999). Oxygen isotope values of planktic foraminifera: a tool for the reconstruction of surface water stratification. In *Use of Proxies in Paleoceanography*, pages 165–189. Springer.

Northcote, L. C. and Neil, H. L. (2005). Seasonal variations in foraminiferal flux in

the Southern Ocean, Campbell Plateau, New Zealand. *Marine Micropaleontology*, 56(3):122–137.

Numberger, L., Hemleben, C., Hoffmann, R., Mackensen, A., Schulz, H., Wunderlich, J.-M., and Kucera, M. (2009). Habitats, abundance patterns and isotopic signals of morphotypes of the planktonic foraminifer *Globigerinoides ruber* (d'Orbigny) in the eastern Mediterranean Sea since the Marine Isotopic Stage 12. *Marine Micropaleontology*, 73(1):90–104.

Nürnberg, D., Bijma, J., and Hemleben, C. (1996). Assessing the reliability of magnesium in foraminiferal calcite as a proxy for water mass temperatures. *Geochimica et Cosmochimica Acta*, 60(5):803 – 814.

Oppenheimer, C., Francis, P., Burton, M., Maciejewski, A., and Boardman, L. (1998). Remote measurement of volcanic gases by Fourier transform infrared spectroscopy. *Applied Physics B: Lasers and Optics*, 67(4):505–515.

Pälike, H., Lyle, M. W., Nishi, H., Raffi, I., Ridgwell, A., Gamage, K., Klaus, A., Acton, G., Anderson, L., Backman, J., Baldauf, J., Beltran, C., Bohaty, S. M., BownPaul, Busch, W., Channell, J. E. T., Chun, C. O. J., Delaney, M., Dewangan, P., Dunkley Jones, T., Edgar, K. M., Evans, H., Fitch, P., Foster, G. L., Gussone, N., Hasegawa, H., Hathorne, E. C., Hayashi, H., Herrle, J. O., Holbourn, A., Hovan, S., Hyeong, K., Iijima, K., Ito, T., Kamikuri, S.-i., Kimoto, K., Kuroda, J., Leon-Rodriguez, L., Malinverno, A., Moore Jr, T. C., Murphy, B. H., Murphy, D. P., Nakamura, H., Ogane, K., Ohneiser, C., Richter, C., Robinson, R., Rohling, E. J., Romero, O., Sawada, K., Scher, H., Schneider, L., Sluijs, A., Takata, H., Tian, J., Tsujimoto, A., Wade, B. S., Westerhold, T., Wilkens, R., Williams, T., Wilson, P. A., Yamamoto, Y., Yamamoto, S., Yamazaki, T., and Zeebe, R. E. (2012). A Cenozoic record of the equatorial Pacific carbonate compensation depth. *Nature*, 488(7413):609–614.

Pouderoux, H. (2011). *Gravity flow sedimentation and active margin paleoseismicity : the example of the Hikurangi subduction margin of New Zealand*. PhD thesis, Université Rennes 1. Mémoire de Géosciences-Rennes n°142. ISBN : 2-914375-83-2.

Pouderoux, H., Proust, J.-N., and Lamarche, G. (2014). Submarine paleoseismology of the northern Hikurangi subduction margin of New Zealand as deduced from turbidite record since 16 ka. *Quaternary Science Reviews*, 84:116–131.

Pouderoux, H., Proust, J.-N., Lamarche, G., Orpin, A., and Neil, H. (2012). Post-glacial (after 18 ka) deep-sea sedimentation along the Hikurangi subduction margin (New Zealand): characterisation, timing and origin of turbidites. *Marine Geology*, 295 - 298:51 – 76.

Prasanna, K., Ghosh, P., Bhattacharya, S., Mohan, K., and Anilkumar, N. (2016). Isotopic disequilibrium in *Globigerina bulloides* and carbon isotope response to productivity increase in Southern Ocean. *Scientific reports*, 6(21533).

Proust, J., Lamarche, G., Migeon, S., Neil, H., and Shipboard, P. (2006). MD152/MATACORE tectonic and climate controls on sediment budget. *Les rapports de campagnes à la mer, Institut Paul Emile Victor*.

Rampino, M. R. and Self, S. (1984). Sulphur-rich volcanic eruptions and stratospheric aerosols. *Nature*, 310:677–679.

Rampino, M. R. and Self, S. (1992). Volcanic winter and accelerated glaciation following the Toba super-eruption. *Nature*, 359(6390):50–52.

Rampino, M. R., Self, S., and Fairbridge, R. W. (1979). Can rapid climatic change cause volcanic eruptions? *Science*, 206(4420):826–829.

Rampino, M. R. and Stothers, R. B. (1988). Flood basalt volcanism during the past 250 million years. *Science*, 241(4866):663.

Regenberg, M., Nürnberg, D., Schönfeld, J., and Reichart, G.-J. (2007). Early diagenetic overprint in Caribbean sediment cores and its effect on the geochemical composition of planktonic foraminifera. *Biogeosciences*, 4(6):957–973.

Reynolds, R. W. (1993). Impact of Mount Pinatubo aerosols on satellite-derived sea surface temperatures. *Journal of climate*, 6(4):768–774.

Robock, A. (1984). Climate model simulations of the effects of the El Chichón eruption. *Geofisica Internacional*, 23(3).

Robock, A. (2000). Volcanic eruptions and climate. *Reviews of Geophysics*, 38(2):191–219.

Robock, A. and Mao, J. (1992). Winter warming from large volcanic eruptions. *Geophysical Research Letters*, 19(24):2405–2408.

Rosenthal, Y. and Lohmann, G. P. (2002). Accurate estimation of sea surface temperatures using dissolution-corrected calibrations for Mg/Ca paleothermometry. *Paleoceanography*, 17(3).

Rosenthal, Y., Lohmann, G. P., Lohmann, K. C., and Sherrell, R. M. (2000). Incorporation and preservation of Mg in *Globigerinoides sacculifer*: implications for reconstructing the temperature and $^{18}O/^{16}O$ of seawater. *Paleoceanography*, 15(1):135–145.

Rutherford, S., D'Hondt, S., and Prell, W. (1999). Environmental controls on the geographic distribution of zooplankton diversity. *Nature*, 400(6746):749–753.

Sadekov, A. Y. (2008). *Advancing planktonic foraminifera Mg/Ca thermometry: a microanalytical perspective*. PhD thesis, The Australian National University.

Saitō, T., Thompson, P., and Breger, D. (1981). *Systematic index of Recent and Pleistocene planktonic foraminifera*. University of Tokyo Press.

Saraswat, R. and Khare, N. (2010). Deciphering the modern calcification depth of *Globigerina bulloides* in the southwestern Indian Ocean from its oxygen isotopic composition. *The Journal of Foraminiferal Research*, 40(3):220–230.

Schmidt, D. N., Renaud, S., and Bollmann, J. (2003). Response of planktic foraminiferal size to late Quaternary climate change. *Paleoceanography*, 18(2).

Schmidt, D. N., Renaud, S., Bollmann, J., Schiebel, R., and Thierstein, H. R. (2004). Size distribution of Holocene planktic foraminifer assemblages: biogeography, ecology and adaptation. *Marine Micropaleontology*, 50(3):319–338.

Self, S. (2006). The effects and consequences of very large explosive volcanic eruptions. *Philosophical Transactions of the Royal Society of London A: Mathematical, Physical and Engineering Sciences*, 364(1845):2073–2097.

Sigurdsson, H., Houghton, B., McNutt, S., Rymer, H., and Stix, J. (2015). *The encyclopedia of volcanoes*. Elsevier.

Smith, V. C., Shane, P., Nairn, I. A., and Williams, C. M. (2006). Geochemistry and magmatic properties of eruption episodes from Haroharo linear vent zone, Okataina Volcanic Centre, New Zealand during the last 10 kyr. *Bulletin of Volcanology*, 69(1):57–88.

Solomon, S., Daniel, J. S., Neely, R. R., Vernier, J.-P., Dutton, E. G., and Thomason, L. W. (2011). The persistently variable background stratospheric aerosol layer and global climate change. *Science*, 333(6044):866–870.

Sparks, R., Graham, I., and Morgenstern, U. (2008). Cosmic chronometers. *Graham IJ (chief ed.) A continent on the move: New Zealand geoscience into the 21st Century. Geological Society of New Zealand Miscellaneous Publication*, 124:64–67.

Sparks, R. J., Melhuish, W., McKee, J., Ogden, J., Palmer, J., and Molloy, B. (1995). ^{14}C calibration in the Southern Hemisphere and the date of the last Taupo eruption; evidence from tree-ring sequences. *Radiocarbon*, 37(2):155–163.

Steinke, S., Chiu, H.-Y., Yu, P.-S., Shen, C.-C., Löwemark, L., Mii, H.-S., and Chen, M.-T. (2005). Mg/Ca ratios of two *Globigerinoides ruber* (white) morphotypes: implications for reconstructing past tropical/subtropical surface water conditions. *Geochemistry, Geophysics, Geosystems*, 6(11).

Stenchikov, G., Delworth, T. L., Ramaswamy, V., Stouffer, R. J., Wittenberg, A., and Zeng, F. (2009). Volcanic signals in oceans. *Journal of Geophysical Research: Atmospheres*, 114(D16).

Sutton, P. J. H. and Chiswell, S. M. (1996). Effect of volcanic aerosols on satellite-derived sea surface temperatures around New Zealand. *New Zealand Journal of Marine and Freshwater Research*, 30(1):105–113.

Thirumalai, K., Richey, J. N., Quinn, T. M., and Poore, R. Z. (2014). *Globigerinoides ruber* morphotypes in the Gulf of Mexico: a test of null hypothesis. *Scientific reports*, 4.

Thompson, P. R., Bé, A. W., Duplessy, J.-C., and Shackleton, N. J. (1979). Disappearance of pink-pigmented *Globigerinoides ruber* at 120,000 yr BP in the Indian and Pacific Oceans.

Tilburg, C. E., Hurlburt, H. E., O'Brien, J. J., and Shriver, J. F. (2001). The dynamics of the East Australian current system: the Tasman front, the East Auckland current, and the East Cape current. *Journal of Physical Oceanography*, 31(10):2917–2943.

Timmreck, C. and Graf, H.-F. (2006). The initial dispersal and radiative forcing of a Northern Hemisphere mid-latitude super volcano: a model study. *Atmospheric Chemistry and Physics*, 6(1):35–49.

Townend, J., Sherburn, S., Arnold, R., Boese, C., and Woods, L. (2012). Three-dimensional variations in present-day tectonic stress along the Australia-Pacific plate boundary in New Zealand. *Earth and Planetary Science Letters*, 353:47–59.

Trenberth, K. E. and Dai, A. (2007). Effects of Mount Pinatubo volcanic eruption on the hydrological cycle as an analog of geoengineering. *Geophysical Research Letters*, 34(15).

Udden, J. A. (1914). Mechanical composition of clastic sediments. *Geological Society of America Bulletin*, 25(1):655–744.

von Glasow, R., Bobrowski, N., and Kern, C. (2009). The effects of volcanic eruptions on atmospheric chemistry. *Chemical Geology*, 263(1-4):131–142.

Walker, G. (1980). The Taupo pumice: product of the most powerful known (ultraplinian) eruption? *Journal of Volcanology and Geothermal Research*, 8(1):69 – 94.

Walker, G. (1981). The Waimihia and Hatepe plinian deposits from the rhyolitic Taupo Volcanic Centre. *New Zealand journal of geology and geophysics*, 24(3):305–324.

Weinkauf, M. F., Kunze, J. G., Waniek, J. J., and Kučera, M. (2016). Seasonal variation in shell calcification of planktonic foraminifera in the NE Atlantic re-

veals species-specific response to temperature, productivity, and optimum growth conditions. *PloS one*, 11(2).

Wentworth, C. K. (1922). A scale of grade and class terms for clastic sediments. *The Journal of Geology*, 30(5):377–392.

Wilson, C., Ambraseys, N., Bradley, J., and Walker, G. (1980). A new date for the Taupo eruption, New Zealand. *Nature*, 288:252–253.

Wilson, C., Houghton, B., McWilliams, M., Lanphere, M., Weaver, S., and Briggs, R. (1995). Volcanic and structural evolution of Taupo Volcanic Zone, New Zealand: a review. *Journal of volcanology and geothermal research*, 68(1):1–28.

Wilson, C. J. N. and Walker, G. P. L. (1981). *Tephra Studies: Proceedings of the NATO Advanced Study Institute "Tephra Studies as a Tool in Quaternary Research", held in Laugarvatn and Reykjavík, Iceland, June 18–29, 1980*, chapter Violence in Pyroclastic Flow Eruptions, pages 441–448. Springer Netherlands, Dordrecht.

Wilson, C. J. N. and Walker, G. P. L. (1985). The Taupo eruption, New Zealand I. General aspects. *Philosophical Transactions of the Royal Society of London A: Mathematical, Physical and Engineering Sciences*, 314(1529):199–228.

Xiang, R., Liu, J., Wang, D., Chen, M., Han, C., Chen, Z., Yan, W., and Tang, S. (2015). Seasonal flux variability of planktonic foraminifera during 2009-2011 in a sediment trap from Xisha Trough, South China Sea. *Aquatic Ecosystem Health & Management*, 18(4):403–413.

Zanchettin, D., Timmreck, C., Graf, H. F., Rubino, A., Lorenz, S., Lohmann, K., Krüger, K., and Jungclaus, J. H. (2011). Bi-decadal variability excited in the coupled ocean-atmosphere system by strong tropical volcanic eruptions. *Climate Dynamics*, 39(1):419–444.

Zielinski, G. A., Mayewski, P. A., Meeker, L. D., Whitlow, S., Twickler, M. S., Morrison, M., Meese, D. A., Gow, A. J., and Alley, R. B. (1994). Record of volcanism since 7000 B.C. from the GISP2 Greenland ice core and implications for the volcano-climate system. *Science*, 264(5161):948–952.

Zohrab, A., Wysoczanski, R. J., Orpin, A., Neil, H., Kent, A., Tepley, F., and Handler, M. R. (2015). The Holocene tephra record of marine core MD06-3017. Unpublished raw data.